University of Dundee

University of Dundee

DOCTOR OF PHILOSOPHY

Pre-operative Risk Factors for Arteriovenous Fistula Failure in the Haemodialysis Population

Macdonald, Conor

Award date:
2019

Link to publication

General rights
Copyright and moral rights for the publications made accessible in the public portal are retained by the authors and/or other copyright owners and it is a condition of accessing publications that users recognise and abide by the legal requirements associated with these rights.

- Users may download and print one copy of any publication from the public portal for the purpose of private study or research.
- You may not further distribute the material or use it for any profit-making activity or commercial gain
- You may freely distribute the URL identifying the publication in the public portal

Take down policy
If you believe that this document breaches copyright please contact us providing details, and we will remove access to the work immediately and investigate your claim.

Download date: 04. May. 2023

Pre-operative Risk Factors for Arteriovenous Fistula Failure in the Haemodialysis Population

Conor James MacDonald

Thesis submitted for the degree of Doctor of Philosophy

The University of Dundee

June 2019

Contents

List of Figures

List of Tables

Acknowledgements

Firstly, I would like to express my gratitude to Prof. Graeme Houston, for, allowing me to pursue this research project, providing the generous funding to do so, and for his valuable input into all aspects of this study. I would also like to thank Dr. Rose Ross for hours of patience, advice and support throughout this project.

This PhD project is a result of the Renal Dialysis Vascular Access (ReDVA, redva.eu) project, and I would like to thank all members of the consortium for their academic input, advice and friendship. In particular, thanks go to Dr. Eoin Murphy, for lightening up long days in the office, Dr. Rudolf Hellmuth for his humour, and academic rigour, and Dr. Shona Matthew for invaluable help during the project.

Finally, I would like to thank my family: my mother, Elaine MacDonald, and my grandparents, James and Margaret MacDonald. They have offered me unconditional support throughout my life, regardless of the route I chose. Without that, it would have been impossible to see the completion of this project.

Declaration of originality

I hereby declare that I am the author of this thesis; that, unless otherwise stated, all references have been cited by myself; the work of which this thesis is a record has been done by myself except due acknowledgement is made; and that it has not been previously accepted for a higher degree.

Conor MacDonald

Declarations of others contributions

The following contributions were made to this thesis: In chapter 3, the standard pre and post-operative US assessments for patients were performed by Dr. Rose Ross, of the hospitals vascular laboratory. In chapter 4, patient recruitment was undertaken primarily by Dr. Shona Matthew, project manager of the ReDVA project. MRI scanning was performed under the supervision of Dr. Stephen Gandy, a member of the hospitals medical physics team. In chapter 5, MRI scanning of the phantoms was assisted by Mr. Lukasz Prisba, a member of the hospitals medical physics team. Vessel segmentations were performed by an experienced cardiovascular engineer, Dr. Eoin Murphy, also of the ReDVA project. Finally, CFD simulations were performed by another experienced cardiovascular engineer, Dr. Rudolf Hellmuth of Vascular Flow Technologies.

Supervisor's declaration

This is to clarify that Conor MacDonald has done this research under my supervision and that I have read this thesis. Also, to certify that he has fulfilled the conditions of Ordinance 39 and relevant regulations of the University of Dundee, so that he is qualified to submit for the degree of Doctor of Philosophy.

Acronyms and abbreviations

ACR - Albumin creatinine ratio

ADMA - Asymmetric Dimethylarginine

AS - Arterial Stiffness

AVF - Arteriovenous fistula

AVG - Arteriovenous Graft

BB - Brachio-Basilic

BC - Brachio-Cephalic

BMI - Body Mass Index

CE - Contrast Enhanced

CFD - Computational Fluid Dynamics

CKD - Chronic Kidney Disease

CoV - Coefficient of Variance

CRP - C-Reactive Protein

CT - Computed Tomography

CVC - Central Venous Catheter

DSA - Digital Subtraction Angiography

eGFR - Estimated Glomerular Filtration Rate

EoSRES - East of Scotland Research Ethics Service

ESRD - End-Stage Renal Disease

FA - Flip Angle

FDA - Food and Drug Administration

FMD - Flow Mediated Dilation

FoV - Field of View

GLM - General Linear Model

HD - Haemodialysis

HIC - Health Informatics Centre

HV - Healthy Volunteer

IMT - Intima Medial Thickness

KDOQI - Kidney Disease Outcomes Quality Initiative

KNN - K-Nearest Neighbours

MEDIC - Multi Echo Data Image Combination

MRI - Magnetic Resonance Imaging

NCE- Non-Contrast Enhanced

NiH - Noeintimal Hyperplasia

NO - Nitrous Oxide

OLS - Ordinary Least Squares

OSI - Oscillatory Shear Index

PAT - Peripheral Arterial Tonometry

PC - Phase Contrast

PD - Peritoneal Dialysis

PRF - Patient with Renal Failure

PSV - Peak Systolic Velocity

PTA - Percutaneous Transluminal Angioplasty

PWV - Pulse Wave Velocity

RC - Radio-Cephalic

RCT - Randomised Controlled Trial

RMS - Root Mean Squared

ROI - Region of Interest

RRT - Renal Replacement Therapy

SRR - Scottish Renal Registry

ST - Slice Thickness

SWE - Shear Wave Elastography

SWV - Shear Wave Velocity

Tx - Transducer

TE - Echo Time

ToF - Time of Flight

TR - Repetition Time

Tx - Transducer

US - Ultrasound

VA - Vascular Access

VENC - Velocity Encoding

VVI - Velocity Vector Imaging

WSS - Wall Shear Stress

Abstract

The arteriovenous fistula (AVF) is a lifeline for patients requiring renal replacement therapy, allowing repeated access to the high blood flow needed for haemodialysis. However, failure rates for AVFs remain high, at around 30-40 % after one-year, typically occluding secondary to stenosis. Many risk-factors for AVF failure have been identified, such as diabetes, age, gender and pre-operative vessel diameters. In this work, existing and potential risk-factors are investigated in a local cohort, with the ultimate aim of identifying new risk-factors for AVF failure, and opening new pathways for risk-factor identification in the future.

Three main avenues were followed: The first approach involved using health informatics, electronic records and data linkage to create an accurate picture of a patients AVF timeline. This retrospective single centre study assessed known risk-factors such as age and diabetes, and various serological markers such as albumin, c-reactive protein, ferritin and phosphate in 137 patients. AVF patency rates were also examined in this cohort. Decreased pre-operative levels of ferritin and increased phosphate were markers of interest due to association with AVF failure at 1-year. Known risk-factors such as gender and age showed no effect on AVF outcome in this cohort. Primary patency was observed to be 67 % at one-year, in line with literature values, and primary assisted patency 91 %.

The second approach assessed if modern ultrasound markers of arterial elasticity (shear wave elastography) and strain (velocity vector imaging) were feasible methods of assessing arterial stiffness in the peripheral vasculature in a group of 40 volunteers and 47 patients. The methods were then assessed to determine if they could act as risk-factors for AVF failure in 33 patients who underwent AVF creation. Both methods were feasible for the assessment of the peripheral vasculature, showing good repeatability, homogeneity, and were straight-forward to implement. Using shear wave elastography an increase in brachial artery elasticity following AVF creation was observed. None of the markers studied could be proven to act as risk-factors for AVF failure.

The third approach aimed to determine if 3T MRI sequences was a feasible modality for the pre-operative workup and followup of these patients in a prospective study of 6 patients and 10 healthy volunteers, using three different sequences. 3T MRI was found to agree with measurements from ultrasound, and also provided the benefit of 3D depiction of the vessels and high resolution. Finally, using these same MRI images, it was demonstrated that computational fluid dynamics simulations do not produce equal results if one changes the MRI sequence used for geometry acquisition.

The difficulty in identifying reliable risk-factors suggests that a multi-factorial approach may be beneficial. Studies with larger cohorts, and longer followup which combine serological markers, comorbidities, and results from imaging may be needed to identify risk-factors which finally increase patency rates.

Chapter 1

Introduction

1.1 The Kidneys and Kidney Disease

1.1.1 The Kidneys

The kidneys are vital organs, supporting life through the filtration of waste products from the blood. They are two bean-shaped major organs which lie in the posterior abdominal region (see figure 1.1), and are surrounded by a layer of perinephric fat. The main function of the kidney is to process the blood, filtering and reabsorbing different chemicals and proteins. In this process, the kidneys produce urine for excretion, which is transported to the bladder through tubes called the ureters. The functional component of the kidney is the nephron, where the exchange of filtrates occurs. Kidneys also have a role in water regulation of the body, blood pressure regulation, and hormone excretion.

Decrease in kidney function is a natural consequence of aging, and in old age reports suggest that the rate of decline is 0.75-1 ml/min/1.73m^2 per year. Other factors such as blood-pressure, injury or diabetes can cause a decline in kidney function. If kidney function declines to an unsustainable level, some form of renal replacement therapy (RRT) is required in order to sustain a patients life.

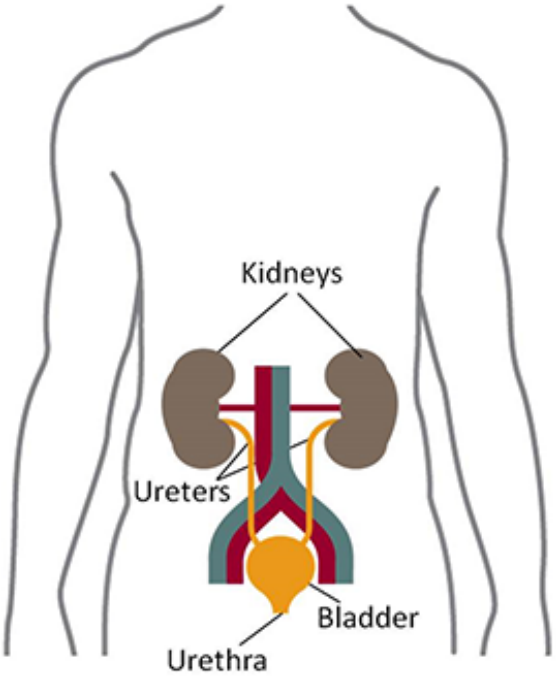

Figure 1.1: The kidneys are two bean-shaped major organs, producing urine which is then transported to the bladder for excretion. (National Institute of Diabetes and Digestives and Kidney Disease)

1.1.2 Chronic Kidney Disease and End-Stage Renal Disease

Chronic kidney disease (CKD), describes a spectrum of conditions which reduce the function of the kidneys. CKD is commonly defined by a decrease in glomerular filtration rate, increased albumin excretion, or both. Severe CKD is a significant cause of death, and a significant reduction in healthy life expectancy. Kidney function can decline to a point where recovery is unlikely, leading to end-stage renal disease (ESRD), which is the final stage of CKD when the kidney function has dropped to a level incompatible with life.

Uremic syndrome is the clinical manifestation of kidney failure, and results in an increased concentration of urea in the blood. Implications include reduced endothelial function; fluid overload and ureaemia can cause impaired maximal oxygen consumption resulting in shortness of breath. Decrease in body mass from muscle atrophy, retention of salt and phosphates, anaemia, and a reduction in the production of hormones are common, amongst other complications.

When a patient progresses to ESRD, it is necessary to have RRT available to replace or replicate the function of the kidneys. CKD can be insidious, with earlier stages having little effect on a patient's life, and can be asymptomatic.

1.1.3 Prevalence

Prevalence of CKD is estimated to be around 8-16% globally, however this is likely an underestimation due to treatment gaps in poorer countries [97]. In the US, approximately 12 % of people are estimated to have some form of CKD. Very few patients with CKD progress to the stage that they develop ESRD and require RRT.

The Scottish Public Health Observatory indicates that there are 179,850 patients with CKD stage 3-5 in Scotland, giving an estimated prevalence of 3.2 per 100 persons. A local study conducted in Grampian estimates an 4.7 times higher mortality rate in patients with CKD compared to the general population [102].

Reports from the Scottish Renal Registry (SRR) state that as of 2016, 5026 individuals were receiving RRT in Scotland [165] with 573 patients commencing RRT, at an incidence rate of 10.6 per 100000 persons. The median age of these patients was 61 years. One-year survival for patients of all age in Scotland receiving RRT was 79 %, falling to 67 % at 2-years and 43 % at 5-years.

1.1.4 Diagnosis

Diagnostic tests for CKD include blood tests, urine tests, imaging and biopsy. Blood tests assess levels of waste products in the blood, which may be indicative of inadequate filtration from the kidneys. Commonly, tests for urea or serum creatinine are performed. Creatinine tests are used to calculate a filtration rate for the kidneys, the estimated glomerular filtration rate (eGFR). An eGFR of less than 90 ml / min is indicative of CKD. Similarly, urine tests commonly assess levels of creatinine and albumin. The ratio of albumin:creatinine, the ACR ratio, can be used to further assess kidney function. Imaging such as or computational tomography (CT) can be used to assess blockages in the renal artery, which can be another cause of kidney failure, and ultrasound can be used to identify other causes of renal failure such as nephrocalcinosis [23]. Biopsies are also used for cellular examinations of kidney tissue.

CKD can be categorised into five stages, depending on the eGFR:

- stage 1 (G1) a normal eGFR (above 90ml/min), with other indications of kidney disease;
- stage 2 (G2) a slightly reduced eGFR (60-89ml/min), with other indications of kidney disease;
- stage 3a (G3a) an eGFR of 45-59ml/min;
- stage 3b (G3b) an eGFR of 30-44ml/min;
- stage 4 (G4) an eGFR of 15-29ml/min;
- stage 5 / ESRD (G5) an eGFR below 15ml/min

CKD stage 5 / ESRD indicates that the kidneys have lost almost all their function.

Similarly, staging exists for concentrations of albumin:creatinine, provided from the ACR ratio. Increasing concentrations indicate increasing severity of kidney damange:

- stage 1 (A1) Optimum and high-normal ACR <29;
- stage 2 (A2) High ACR 30 - 299;
- stage 3 (A3) Very high ACR > 300

An informative graphical interpretation of these disease stages is provided by Levey *et al* [93], see figure 1.2.

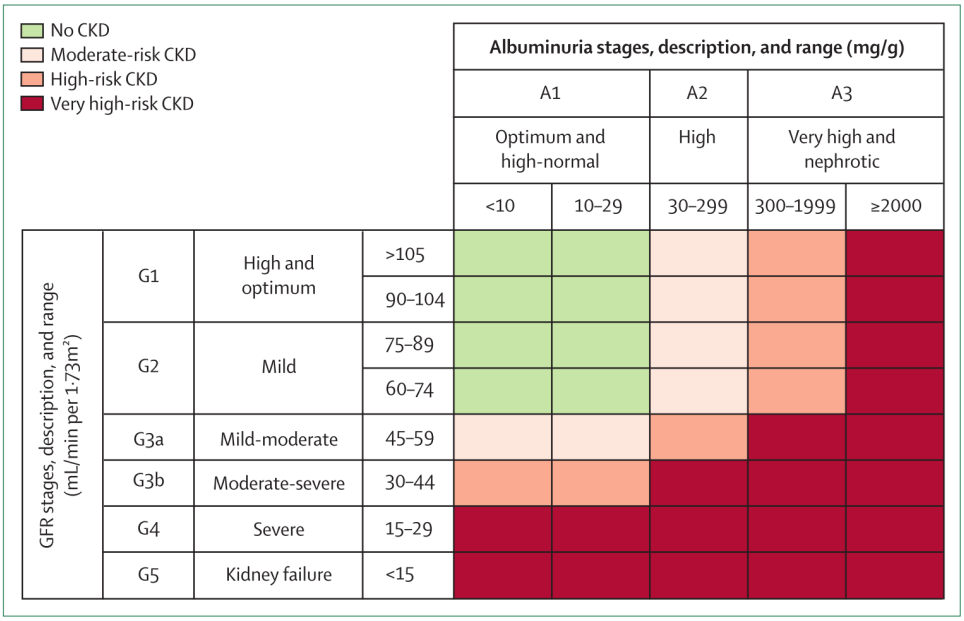

Figure 1.2: CKD stages and associated risk. Colours indicate relative-risk for the set of outcomes all-cause mortality, cardiovascular mortality, kidney failure treated by dialysis and transplantation, acute kidney injury, and progression of kidney disease, (Levey et al, [93], Elsevier)

Symptoms of CKD can include high levels of urea in the blood, high levels of phosphates in the blood, blood presenting in the urine, and fatigue, but CKD can also develop insidiously with no symptoms, and it is not uncommon for patients presenting with ill-health to be diagnosed with CKD or ESRD and require RRT immediately. However, it is difficult to predict which patients will develop ESRD, and not all patients with CKD will progress to ESRD.

1.1.5 Risk factors and causes

Risk factors for ESRD are both non-modifiable and modifiable. Age, acute kidney injury, cardiovascular disease, renal tract disease, socio-economic status and family history are non-modifiable risk factors for developing ESRD. Modifiable risk factors have been identified including smoking, alcohol and drug consumption, obesity, and chronic use of non-steroidal anti-inflammatory drugs. Diabetes and hypertension are modifiable, but not curable risk-factors for ESRD development. Appropriate management of these conditions can help minimise the impact of these conditions.

Diabetic nephropathy causing glomerulonephritis is the most common cause of ESRD world-wide and affects around 15- 40 % of patients with type-1 diabetes [66], and 5-20 % of patients with type-2 diabetes [66, 1]. Diabetic nephropathy can be characterised histologically, typically presenting nodular glomerulosclerosis, tubulointerstitial fibrosis

and atrophy. Interstitial causes refer to interstitial nephritis, which is a condition affecting the interstitium of the kidneys, manifesting as inflammation of the spaces between kidney tubules. Most commonly, interstitial nephritis is caused by a reaction to medications, in particular analgesics or antibiotics. Multi-system causes generally indicate conditions such as systemic lupus erythematosus, which may have implications on kidney function. During the period 2012-2016 in Scotland [165], the most common cause of starting RRT was due to diabetic nephropathy (28 %), followed by interstitial nephritis (22 %), and multi-system (22 %) causes.

1.1.6 Co-morbidities

ESRD increases in likelihood with age, and is therefore most likely to occur in a setting of pre existing co-morbid conditions. Hypertension, diabetes, ischemic heart disease, heart failure, peripheral vascular disease, cerebrovascular disease, chronic respiratory disorder, depression, thyroid disorder and anaemia are common co-morbidities in patients with CKD-3 [42]. These co-morbidities may impact on treatment burden, medications management, quality of life, and survival of patients [104, 69, 53].

Cardiovascular causes were the leading cause of death in patients receiving RRT in 2016 in Scotland, accounting for 30 % of deaths. A large study performed in 2006 observed high incidence of co-morbidities such as anemia, coronary artery disease, congestive heart failure, diabetes mellitus, hypertension, hyperlipidemia, and peripheral vascular disease in a group with eGFR less than 90 with a higher rate of mortality, when compared to an age and eGFR matched index group with lower mortality [58]. They found that co-morbidities most strongly associated with death were congestive heart failure, anemia, proteinuria, and peripheral vascular disease. Due to the presence of these co-morbidities, patients with CKD are more likely to die than progress to ESRD [53].

1.2 Treatment

Any treatment for ESRD is designed to reduce or reverse the uremic syndrome of patients, reduce the concentration of blood-borne toxins, and restore the fluid balance of the patient. This involves replacing the kidney function, through either transplantation, or dialysis. Transplant is the preferable option, but is limited in availability. Dialysis is more available, but requires a significant change in a patient's life style.

1.2.1 Transplant

The most successful treatment for ESRD regarding patient quality of life is transplantation of a donor kidney. In 2016 in Scotland, the most common form of RRT was transplantation, which counted for 57 % of treatment [165]. Donors were primarily cadaveric, with 82 % of transplantation coming from cadaveric donors over the 2012 - 2016 period.

Current Scottish data shows transplant / graft survival at approximately 95 % at one-year, 87 % at five-years and 74 % at ten-years in Scotland [165]. In 2015, 1-year survival for patients who had received a transplant was 97.1 %. Most recent data for 5 and 10-year survival shows rates of 90.6 % and 75.7 % respectively.

1.2.2 Dialysis

The term dialysis refers to "diffusion across a semipermeable membrane". Dialysis treatment relies on some form of membrane which allows diffusion of waste products out of the blood. Two main forms of dialysis exist, peritoneal dialysis, and haemodialysis.

Peritoneal dialysis (PD) is a corporeal dialysis, which makes use of a natural cavity in the body, the peritoneal cavity. During PD, the peritoneal cavity is used as a storage space for around 2.5 L of dialysate (see figure 1.3). The peritoneum is a semi-permieble membrane which allows diffusion of blood-borne waste products into the dialysate fluid. Due to the presence of many arteries and veins in the peritoneal cavity, diffusion occurs readily into the dialysate fluid.

Dialysate fluid is placed in this cavity through a catheter, which is then regularly used to add and remove dialysate fluid. Waste products filter into the dialysate fluid through diffusion, and excess water is removed via osmosis. The dialysate requires regular changing, and patients are commonly trained to perform this themselves. Peritonitis is a common complication from PD, with reports of a rate of one incident every two years [155].

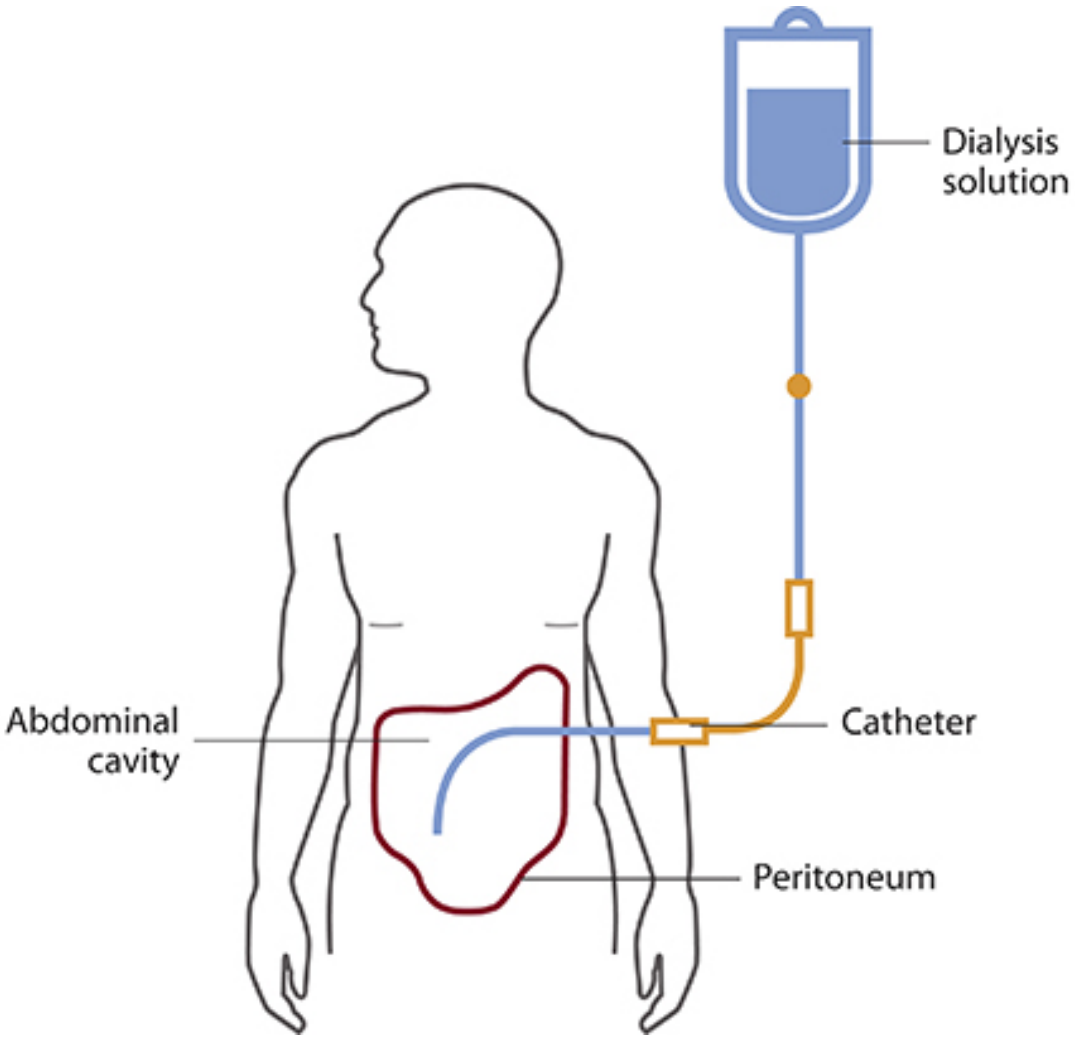

Figure 1.3: During peritoneal dialysis, the dialysate fluid is placed in the peritoneal cavity through a catheter (Circle Medical Management)

Complications arising from the catheter are a significant source of morbidity for patients undergoing PD, and can lead to a change of RRT to haemodialysis. PD is the least common form of RRT in Scotland, with only 6 % of patients treated by PD in 2016 [165]. PD is more common in the rest of the UK, accounting for 10 % of patients in northern Ireland, 9 % in wales and 7 % in England [147].

Haemodialysis (HD) refers to dialysis of the blood, and is an extra-corporeal technique. HD involves rerouting a patients blood through a machine which replicates the function of the kidney. The machine removes unwanted products and excess water from the blood. Diffusion across a concentration gradient allows a dialysis machine to remove excess solutes and fluid from the blood.

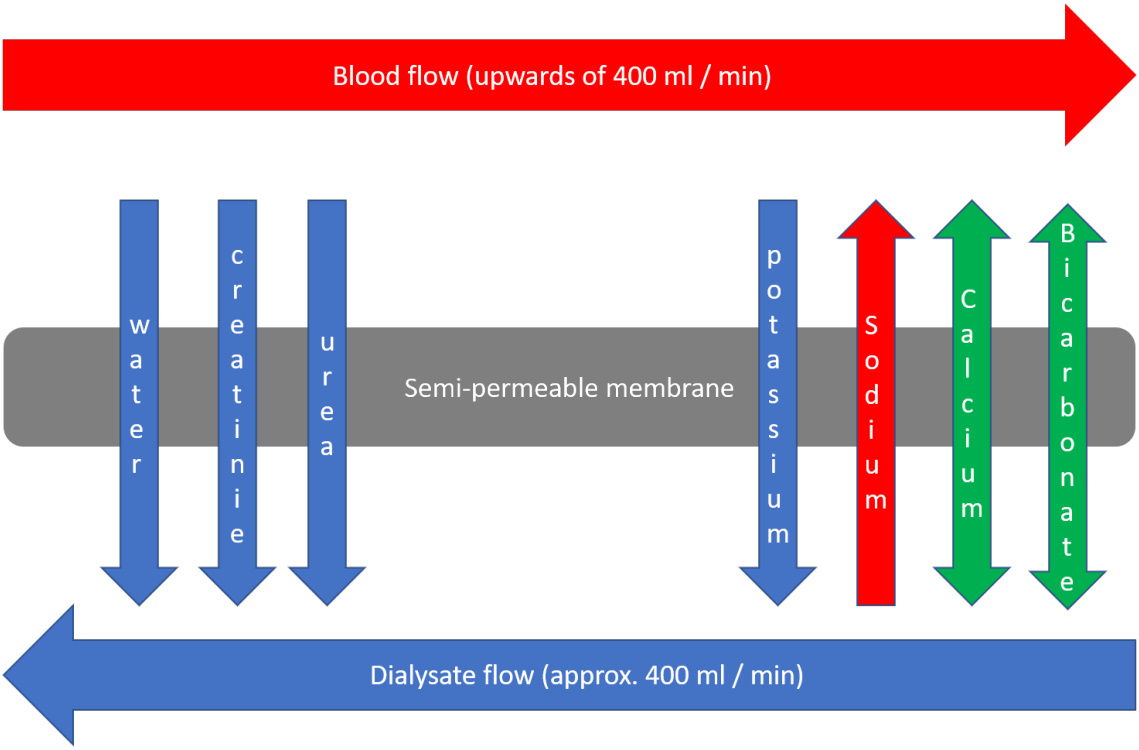

Figure 1.4: Diffusion across the semi-permeable membrane attempts to reach equilibrium between blood and dialysate. Water, and various toxins such as urea diffuse out of the blood, and essential minerals such as sodium diffuse into the blood.

A continuous stream of dialysis fluid is passed in the opposite direction of the blood flow in order to create the concentration gradient. The dialysis fluid contains a buffer and electrolytes which diffuse in the direction of the blood, as in figure 1.4. Excess water is removed through pressure filtration of the blood as it passes through the dialysis machine, this is known as ultrafiltration, although this is not always routine.

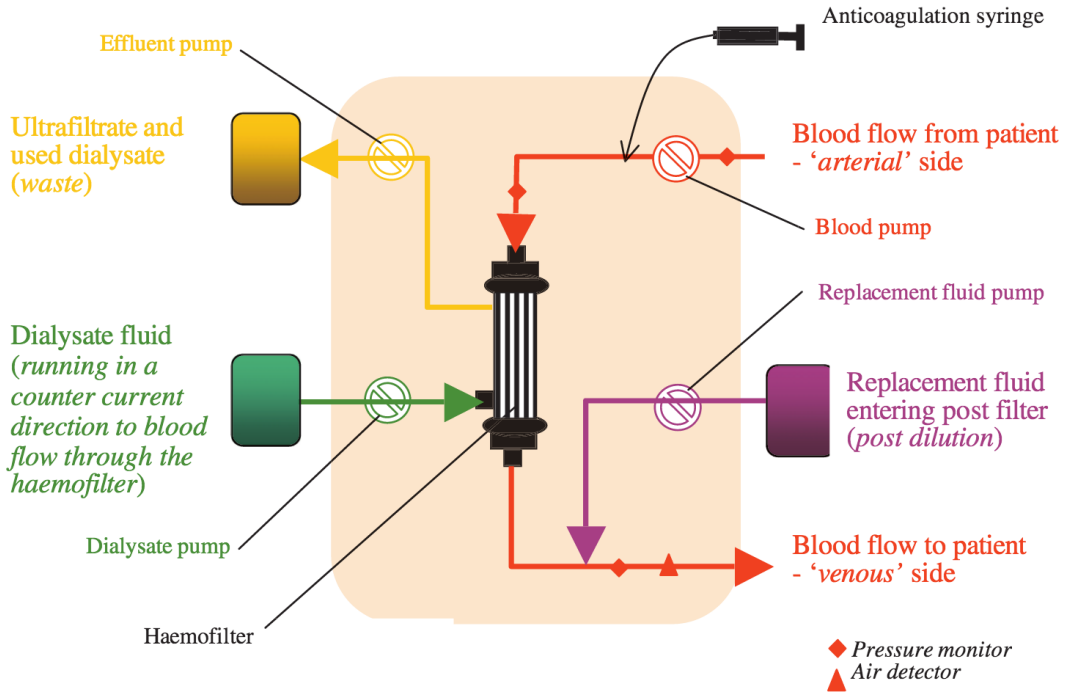

Figure 1.5: In the dialysis schematic, blood leaves the body from an arterial site in the vascular access. Anticoagulants are administered to prevent clotting in the machine. The hemofilter contains the semi-permeable membrane where diffusion occurs to rectify the uremic state of the blood. If needed, fluid content is replaced in the blood. Air monitors are used to remove bubbles in the blood, and pressure monitors used to screen for stenosis. Filtered blood is then returned to the body at the venous site.

Typically patients receive treatment 3-4 times a week, for 3 hours a session. The adequacy of HD is typically measured using a ratio, Kt/V. K represents the clearance, t the time spent dialysing, and V the volume of water a patient's body contains. The urea reduction ratio (URR) is another test used to determine the adequacy of dialysis:

$$URR = \frac{Urea_{Pre} - Urea_{Post}}{Urea_{Post}} \times 100 \tag{1.1}$$

Ideally, the URR should be 70% or over.

HD is the second most common form of RRT in Scotland, with 37 % of patients in 2016 receiving hospital HD, and 1 % of patients receiving home HD. HD prevalence is similar in the rest of the UK, accounting for 20 % of patients in northern Ireland, 26 % in wales and 30 % in England [147]. HD will typically last until transplant or death, as

kidney function is unlikely to recover. Median survival times for patients on HD have been reported as 4.4 - 4.8 years [127], and five-year survival of around 50 % [181].

It is desirable to have a high blood flow pass through the machine, as this reduces the time patients need to receive treatment. Typically blood flows used are around 400 ml/min, and are taken and returned via a vascular access (VA). Blood is taken from an arterial site, and returned to a venous site. The VA must be able to provide the flow needed, as well as be able to support the large needles used - typically 15-17 gauge. VA problems are the main source of morbidity in patients undergoing RRT, but different forms of VA are associated with different rates of morbidity. Three main forms of VA exists, with their respective benefits and problems: the central venous catheter, the arterio-venous graft and the arterio-venous fistula.

1.3 Vascular access

1.3.1 The Arterio-Venous Fistula

The Arterio-Venous Fistula (AVF) revolutionised vascular access by allowing repeated access to an autologous high flow vessel. Pioneered by Brescia and Cimino, the AVF is a surgical anastomosis between an artery and a vein [24]. In the original paper, a side to side anastomosis of the vessels in which the sides of an artery and a vein are stitched together using arterial silk is described. Other geometries of the anastomosis can be seen in figure 1.6.

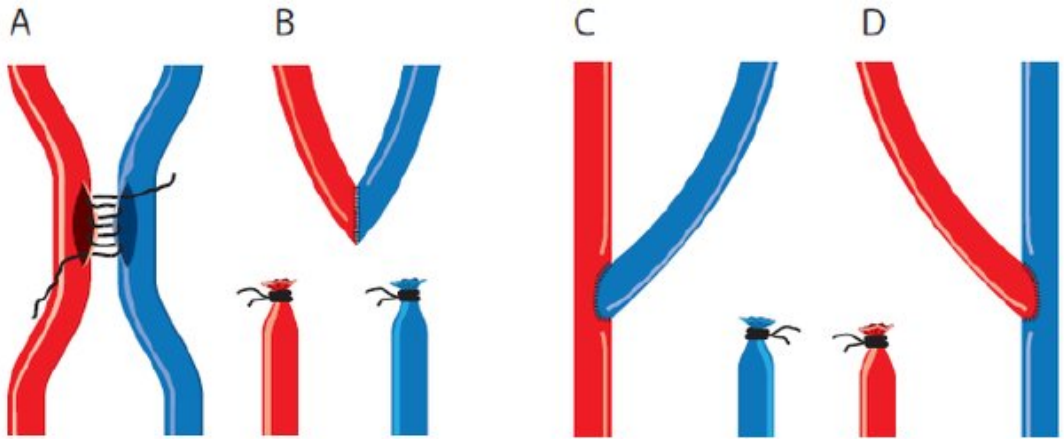

Figure 1.6: Four different types anastomotic configurations: A) Side-to-side anastomosis, B) End-to-end anastomosis, C) End-to-side anastomosis, and D) Side-to-end anastomosis [20]

AVFs vary by placement site, with potential sites located in the wrist (radio-cephalic (RC)) on the non-dominant arm, by the elbow (brachio-cephalic (BC)) or in the upper arm (brachio-basilic transposition (BB)) - see figure 1.7. AVFs created in other limbs are possible, such as in the legs. Distal AVF locations (such as the wrist) are commonly chosen as the first access, as failure in these still leaves the possibility of more proximal locations such as the BC-AVF [85]. Venous valves are not commonly considered, as blood-flow continues in the natural direction, thus valves are typically left alone.

The best outcomes have been observed when patients initiate HD with an arteriovenous access [135], and this is reflected in guidelines stating patients should ideally start HD with an AVF [85, 166]. UK Renal Association standards indicate that 60 % of patients should commence HD with an AV access, and 80 % of patients should dialyse with an AV access [85]. Over the period 2012 - 2017 in Scotland, approximately 45 % of patients started HD with an AV access [165]. However, as of 2017, 72.9 % of patients were receiving HD via an AV access, primarily a fistula. This indicates that a large number of

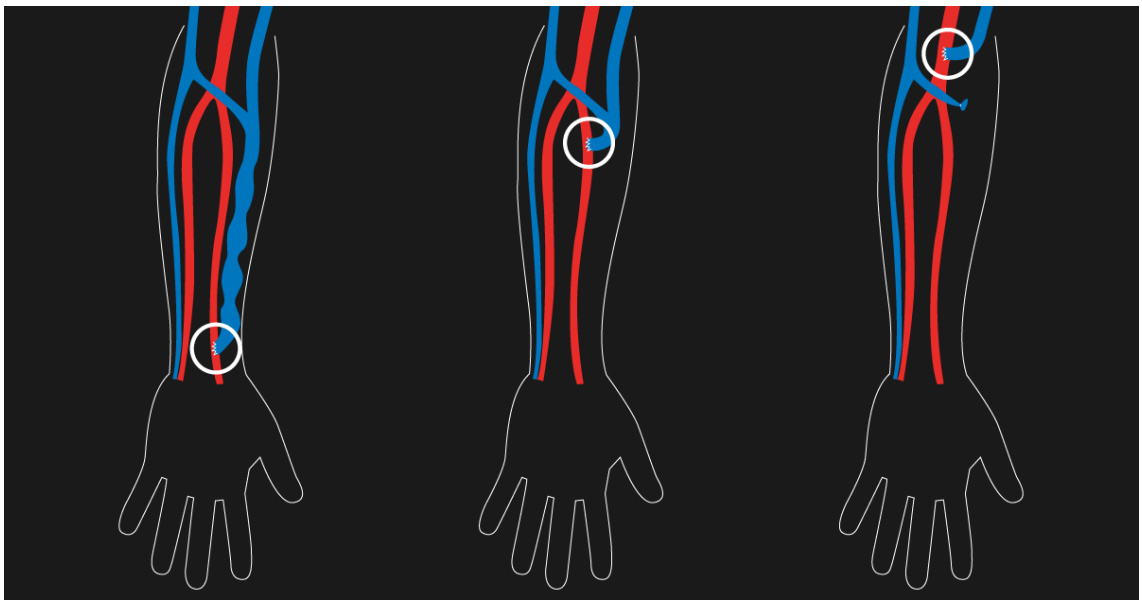

Figure 1.7: Multiple types of AVF are possible in the fore-arm. The radio-cephalic is typically the first choice, as failure leaves the brachio-cephalic and brachio-basillic viable for further attempts (Laminate medical technologies)

patients are having an AV access created after initialising HD. It is possible that poorer access outcomes for other modalities are due to the slightly different demographic of patients requiring immediate access typically through a catheter: they may be crash-landers presenting to clinic with low renal function requiring immediate HD, or they may have required catheter usage due to failed AV access or poor vessel quality.

1.3.2 Central venous catheters

A central venous catheter (CVC) is an access which uses the large veins as a blood source for HD. A CVC is inserted through the skin, before being placed inside the internal jugular vein (see figure 1.8). Subclavian access is also possible, but is less common. The external limbs of the CVC are then connected to the dialysis machine.

CVCs fulfill basic emergency requirements, and no is surgery required to place the CVC. No waiting post dialysis for bleeding to stop is required, and access to blood is instant. Placement in the large veins removes the requirement of functional peripheral venous vessels (as is required for other forms of VA), which certain patients may lack. There are many vessels which can support a CVC, and it is also generally the most comfortable access for a patient due to relatively painless and easy use [59]. CVCs are generally used as a shorter term option before placement of an arteriovenous graft (AVG) or AVF, but initial HD with a CVC has been linked to future problems with VA - likely caused by central venous stenosis[151].

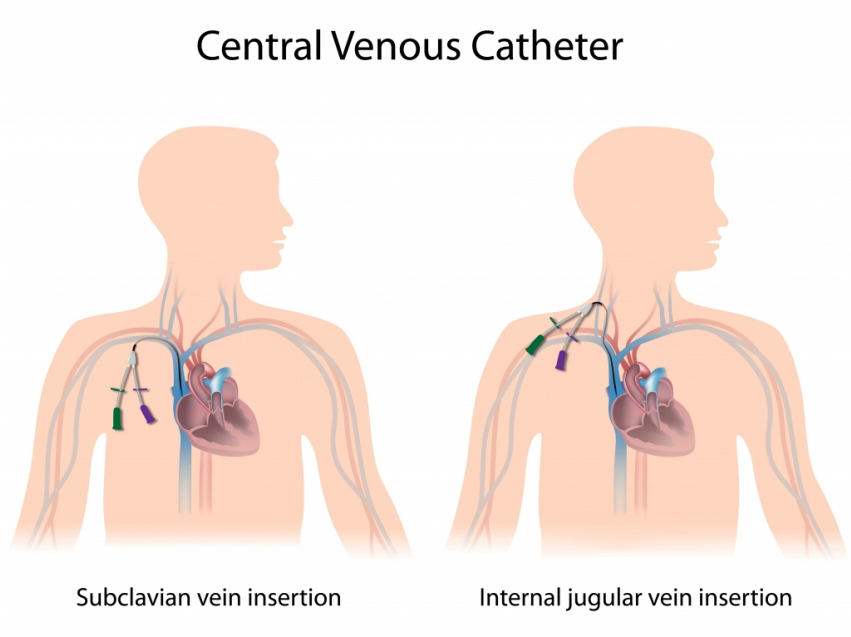

Figure 1.8: CVC placement is possible in the subclavian or the internal jugular. Internal jugular is preferred as complications with stenosis are less severe on fistula function (Michigan Institute)

However, due to higher overall mortality [46], CVCs are the least preferred VA for HD. In particular, long-term CVC use is associated with a myriad of problems including thrombosis, central vein stenosis and and serious catheter related infections [59]. Again, the higher mortality is likely explained by the differing patient demographic. Patients requiring immediate HD will likely have poorer outcomes than patients with time to prepare for RRT.

1.3.3 Arteriovenous grafts

An AVG is an artificial tube (polytetrafluoroethylene) connecting an artery and a vein. Blood is taken from, and returned to the tube during dialysis. AGVs are associated with a ten times higher rate of infection than arteriovenous fistulas, due to the introduction of foreign material in the body [156]. AVGs are beneficial when a patient has poor peripheral vessels, and can be unsuitable for fistula creation [151]. AVGs are typically ready for use within one-month of placement [14], but early cannulation grafts can be ready for use within as little as 72 hours [158].

AVGs are more likely to occlude than the arteriovenous fistula, and offer lower long-term patency. The most common causes of failure for AVGs is intimal hyperplasia and stenosis on the venous anastomosis [14]. A systematic review of AVG patency rates found 72 % primary patency at 6 months and 51 % at 18 months [68].

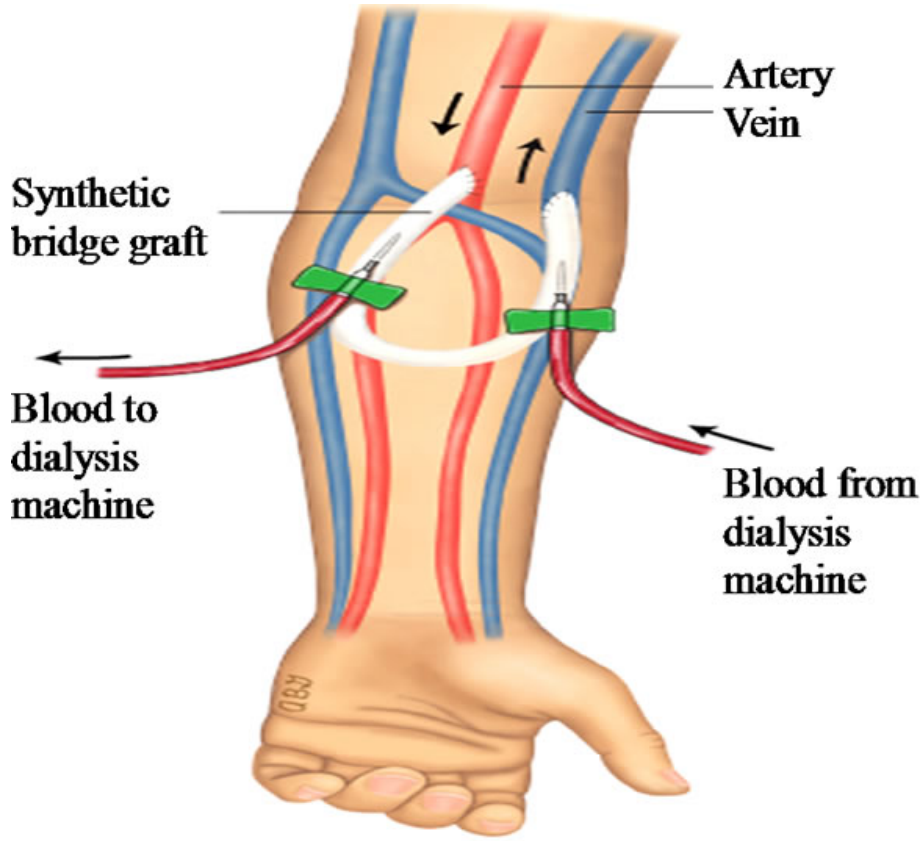

Figure 1.9: An AVG is an artificial tube connecting an artery and a vein, used to provide blood for HD (Kim et al [75], Scientific Research Publishing)

1.4 AVF Maturation and Failure

1.4.1 Physiological changes after AVF creation

In the landmark paper by Brescia and Cimino the arterio-venous fistula was first described [24]. They described an immediate palpable thrill at the site of the fistula, and attempted dialysis the day after surgery (which is no longer the common case). The vein is describe in this case as undergoing 'arterialisation', due to medial thickening. The main physiological changes which occur after AVF creation are vessel dilation, and flow increases. Interestingly, with 13 patients and over 800 total dialysis sessions, Brescia and Cimino reported extremely good outcomes, with only one fistula failing to function. Modern AVF usage does not reflect these results.

At rest, mean normal blood flow in the brachial and radial arteries are 50 and 25ml/min, increasing around 3-5 times with exercise. Healthy brachial arteries have been shown to be around 4mm [173], and the radial artery lower at around 2mm [180]. Arterial flow is characterised by its triphasic waveform when imaged with doppler ultrasound (see figure 1.10). Venous flow is typically much lower in the peripheral vessels, and is steady-state.

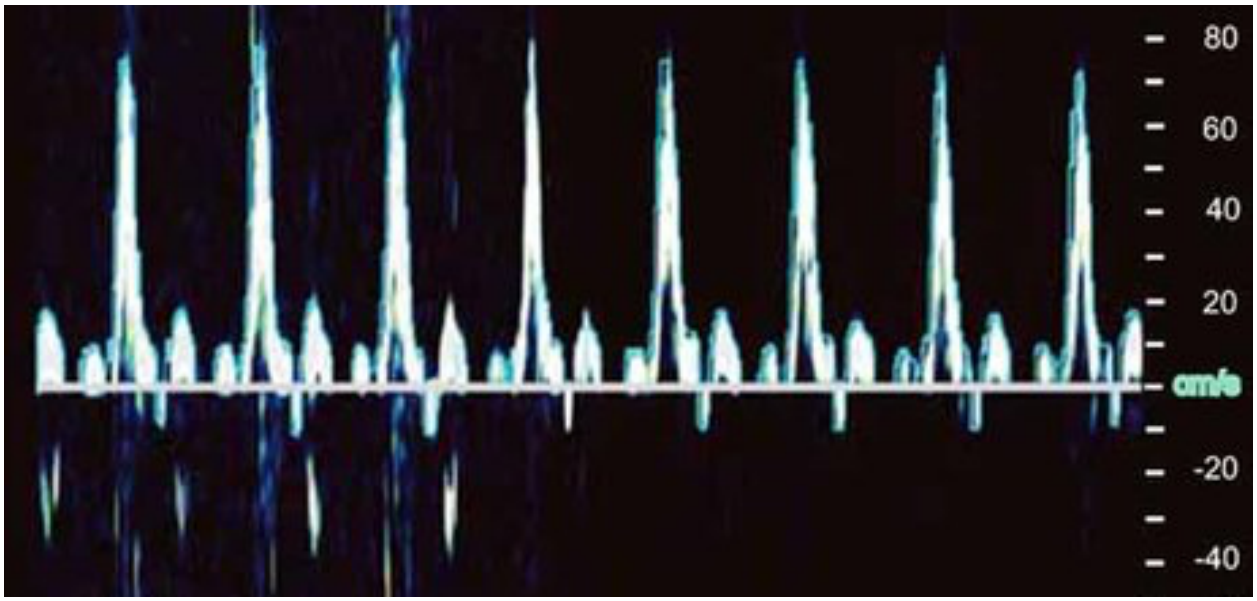

Figure 1.10: Doppler US image of a healthy brachial artery showing typical tri-phasic arterial flow

Creation of the AVF causes arterial blood to by-pass the higher resistance arterioles and venules. This creates a lower resistance pathway for arterial blood to return back to the heart through the arteriovenous anastomosis. As a result of the increased forward flow and decreased resistance, the artery loses its typical tri-phasic flow pattern. AVFs exhibit continuous forward flow, with a higher peak-systolic velocity and end-diastole

than is normally exhibited in the arteries. This results in a larger share of total blood passing through this newly created circuit. The larger blood volume results in a higher radial pressure exerted on the vessels. Clinically successful fistulas have arterial flows of at least 600ml/min, and in order to accommodate this flow, the artery should ideally dilate. Previous studies have described arterial dilation of 40-50% [44, 98].

Pouseuille's law demonstrates that blood flow (Q) with a viscocity n is proportional to the pressure gradient (ΔP) and vessel radius (r):

$$Q = \frac{r^4}{n} \times \Delta P \tag{1.2}$$

Pouseuille's law would predict an 80 % dilation to achieve a 10 times higher blood flow, as is required in the arteries and veins of AVFs. Previous studies have described arterial diameter increases of 40-50%[44, 98] following AVF creation. Lomonte *et al* [98] observed that arterial diameters increased by 41.9 % and blood flow rate by 1182 % at 28 days compared to the baseline values taken pre-surgery. Demmers *et al* [44] also demonstrated an increase in radial wall thickness over a year following RC-AVF placement. Lower than expected dilation can be explained by a larger than expected pressure gradient caused by pulsatile flow, and a lowering of blood viscosity at higher flow velocities.

Venous diameter and flow has been shown to steadily increase after AVF creation. Robbin *et al* [150] found venous flow in both lower and upper arm AVFs to reach 50% of its 6-week flow value one-day post AVF creation, and most AVF veins to reach 4 mm in size after 2 weeks, increasing from an average of 2 mm for lower-arm AVFs. Contrary to Brescia and Cimino, Corpataux *et al* [39] found that the vein wall thickness remained constant, indicating an increase in the tissue mass of the vein. This process of dilation and increasing flow is termed maturation of the AVF, and ultimately is the process by which the AVF becomes suitable for dialysis.

1.4.2 Effect of wall shear stress

A major stimulus in AVF remodelling is the increase in shear stress at the vessel wall, known as wall shear stress (WSS) [129]. Wall shear stress is a frictional force applied tangentially to a vessel wall, due to some flow (see figure 1.11). Wall shear stress (τ) is described by the Haagen-Poisseuille equation:

$$\tau = 32n\frac{Q}{\Pi d^3} \tag{1.3}$$

where Q is the mean flow rate, n is the viscosity and d is the diameter of the vessel. The increased flow from AVF creation results in an increased WSS in both vessels, and has been verified in vivo [146].

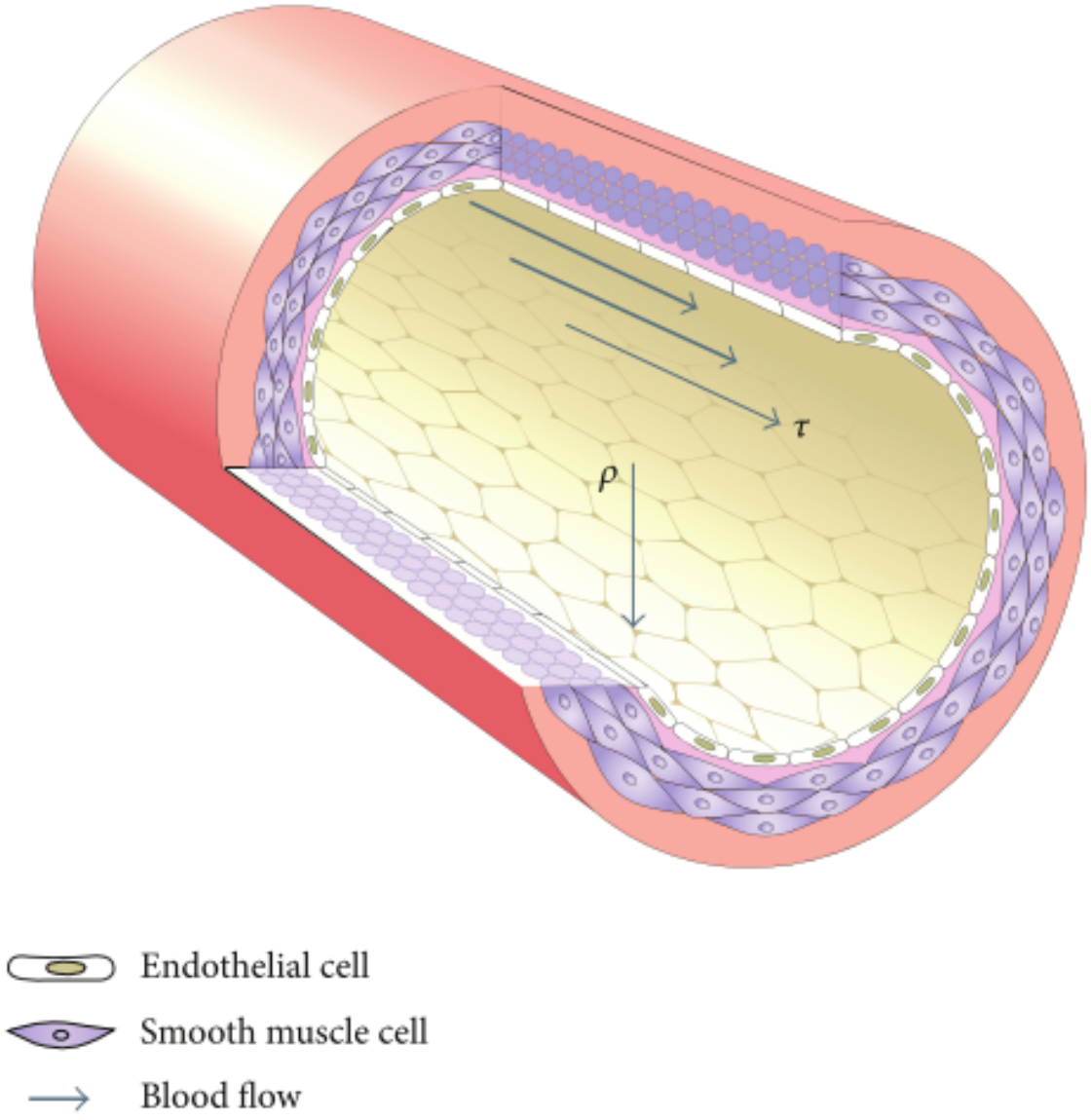

Figure 1.11: WSS (τ) located at the endothelial layer, and pressure (ρ) directed perpendicularly to the vessel wall. WSS is confined to the endothelial layer and follows the direction of flow (Macmillan Publishers Ltd)

WSS is confined to the endothelial layer in blood vessels, and enodthelial cells can respond to changes in WSS levels. The increase in WSS causes endothelium cells to release vasodilating mediators such as nitrous oxide (NO) [46]. These agents act to increase the diameter of the vessel, in an attempt to reduce WSS values to their baseline value. Dammers *et al* [44] observed that WSS values in AVFs are never truly normalised to baseline in both radial and brachial arteries, despite the vessels increasing in diameter.

There is strong evidence suggesting that AVF maturation is dependant on a healthy

endothelium [128]. It is well established that arterial dilation as a response to an increased flow is due to the endothelial response [40, 171, 4]. Owens *et al* [128] linked endothelial function to the percentage of arterial and venous remodelling experienced after fistula creation, by measuring flow mediated dilation (FMD). Brachial artery dilation post-AVF creation was positively correlated with endothelial function as measured by FMD. Impaired endothelial function is associated with a decreased vasodilation effect, from lower production of NO [60]. Endothelial function is widely variable in patients with CKD [5], so the extent of its influence requires further study and in more controlled circumstances[96].

Computational fluid dynamics (CFD) simulations of AVFs using patients' medical images have been used to assess blood-flow patterns and WSS in AVFs. These studies have attempted to draw conclusions between these metrics and the clinical outcome of an AVF. Typically, a patient's medical images are used to create stylised 3D geometries of the patient's AVF. Computational solver packages are then used to solve the Navier-Stokes equation, which describe the flow-distributions inside containers. He *et al* [63] studied one fistula at multiple time-points in order to create a pipeline for using computational simulations. They were able to locate an area of stenosis, and observed that it correlated to an area of high wall shear stress in their model. It was also demonstrated that WSS continued to decrease throughout the length of the study - up to 7 months after creation. A study by Sigovan *et al* [161] tracked vessel cross sectional area over a number of months for 3 patients, showing increases in the venous and arterial segments over three months (see figure 1.12). They observed that flow patterns in the curved regions of the AVF were associated with higher values of WSS on the outer curve wall, and lower WSS values on the inner curve wall, and that low WSS areas were commonly sites of recirculation.

WSS is the parameter that has received the most attention in these simulations. A meta-analysis by Browne *et al* [26] identified 15 studies which investigated the role of WSS in fistula maturation using CFD. They conclude that the studies show that configuration of the AVF, vessel wall thickness, and the reduction of shear stress all contribute to maturation.

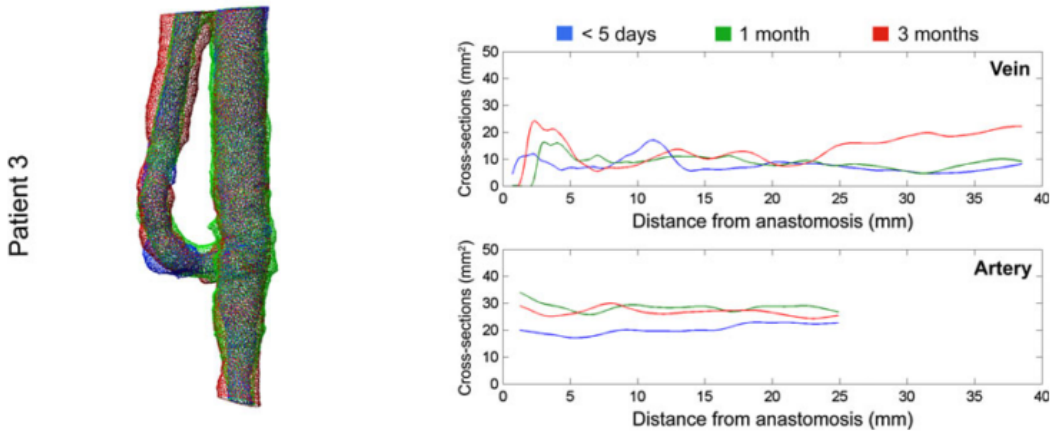

FIGURE 3. Center-line based co-registration of luminal geometries for Patient 1, Patient 2, and Patient 3 (left). Venous and arterial cross-sectional area change over time (right). Note the strong increase in cross-sectional area in several regions of the vein at 1 month post surgery for Patient 2 followed by a decrease at 3 months.

Figure 1.12: Measurement of vessel area over a 3-month time period, using 3D models of the AVF derived from MRI images (Sigovan [161], Biomedical Engineering Society)

1.4.3 The AVF for haemodialysis

A fistula is deemed ready for dialysis when it produces an appropriate flow to support dialysis and the venous segment is an appropriate diameter for cannulation. The rule of sixes [159] is commonly cited as a general set of criteria for a mature fistula, and is presented in table 1.1. The rule of sixes gives the criteria that flow should be at least 600 ml / min, the vessel diameter should be at least 6mm, and the depth of the fistula should be less than 6mm.

Fistula Flow	600 ml / min
Cannulation segment diameter	>6mm
Cannulation segment length	10cm long or 2 segments of 4cm
Depth of fistula	<6mm from skin surface

Table 1.1: Rule of sixes, giving properties of a "mature" AVF [159]

Kidney Disease Outcomes Quality Initiative (K-DOQI) guidelines recommend that AVFs are planned 6 months prior to the start of dialysis [85]. The clinical success of an AVF depends on its ability to be cannulated and support dialysis. This depends on the dilatory ability of the vessels, as well as the development of a high-flow. A good fistula will provide a high flow, be easily cannulated, and cause minimal problems for patients. As long as none of these criteria are broken, an AVF will not require an intervention. Even if a stenosis develops in the fistula, if it does not affect the flow, there is no need for an intervention. Due to the time period required before an AVF is suitable for HD, forward planning is essential if patients are to commence HD with an AVF.

AVFs are the preferred method of vascular access due to lower occlusion and infection rates. Long-term patency from AVFs is shown to be higher than for both AVGs and CVCs [135]. A meta-analysis by Almasri *et al* observed higher mortality in patients dialysing with a CVC when compared to AVFs and AVGs [7], and also demonstrated that highest long-term patency is achieved when using an AVF.

AVFs still suffer from relatively high failure rates. Meta-analyses have found average 1-year patency rates of around 60%, meaning around 40% of AVFs are inadequate to sustain dialysis for a year without intervention [7, 152, 3]. Multiple studies have been conducted comparing patency rates of the different forms of AVF. In 2004, Rooijens *et al* highlighted high failure of RC-AVFs using meta-analysis of 38 studies. They 1-year primary (time from creation until intervention) and secondary (time from creation until abandonment) patency rates of 62.5% and 66% respectively. In 2014, another review

found that the picture was much the same [3]. Primary patency at 1-year was found to be 60%, dropping to 51% at 2-years. Secondary patency increased slightly to 71% at 1-year and 64% at 2-years.

Failure of an AVF can cause additional catheter insertion or missed dialysis sessions for patients. AVF failure can broadly be categorised into 'failure to mature' 'late AVF failure' and 'primary failure'. Certain AVFs will never reach a point where they can be used for HD (failure to mature), and others will be useable for HD, but later occlude secondary to stenosis (late failure). Primary failure describes a fistula that is unsuccessful at creation due to surgical implications or disease. Typically, failure to mature will arise due to poor flow development in the fistula as a result of sub-optimal arterial or, more commonly, venous dilation. The most common cause for late AVF failure is due to neo-intimal hyperplasia (NiH) leading to stenosis or thrombosis. Dixon *et al* [46] provide a graphical interpretation of the possible processes leading to failure to mature or late AVF failure, see figure 1.13.

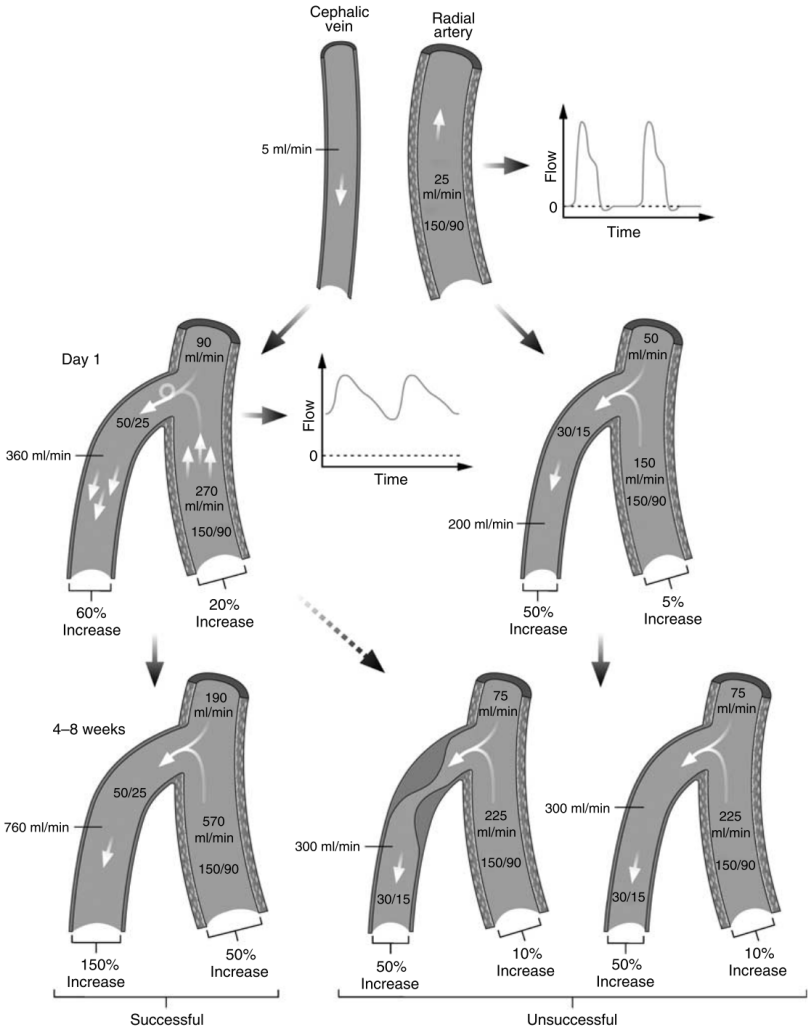

Figure 1.13: “The figure depicts the temporal pattern [...] of [...] fistula maturation in a radiocephalic fistula. The top of the figure shows the preoperative flow and pressure in the radial artery and cephalic vein... The middle two figures depict the situation 1 day after fistula creation for a fistula that has dilated rapidly and is likely to mature (left) or one that has not dilated sufficiently and is likely to fail (right). The middle graph inset shows that after creation of the low-resistance circuit, volume flow rate remains high and significantly above zero throughout both systole and diastole. Thus, the mean volume flow rate is much greater than predicted for the extent of arterial dilation by Pouseuilles law[...] The three figures at the bottom depict the situation at 48 weeks after fistula creation for a successful fistula (left) or two possible modes of early fistula failure the development of a juxta-anastomotic stenosis (middle) or impaired dilation (right). Between 20 and 50% of radiocephalic fistulas will fail to mature and between 65 and 100% will have evidence of a stenosis.” (Dixon [46], International Society of Nephrology)

1.4.4 Failure to Mature

Failure to mature typically means that the AVF cannot produce a flow which is suitable for HD. Inadequate venous dilation can restrict the flow passing through the venous segment, commonly manifesting in failure to mature. Accessory veins can also contribute to poor venous flow in the venous AVF segment due to the sharing of the total blood flow, but can be easily ligated during AVF creation. Calcification has been seen in the veins of patients with CKD, which may reduce the ability of the vein to dilate, similar to a calcified artery [139]. However, the exact mechanisms which may impair venous dilation are not currently understood.

Another possible mechanism for AVF failure to mature is poor arterial dilation. If the artery cannot dilate adequately, a high flow-rate may be hard to achieve. When assessed by FMD, patients with CKD are shown to have reduced endothelial function [186], which limits the dilatory ability of the artery. Similarly, the presence of arterial calcification [139], which increase vessel stiffness, has been shown to reduce the vessels dilatory ability [18]. Low arterial elasticity has been linked to reduced maturation, in a small cohort study by Kheda *et al* [74], however the mechanisms were not determined. This study also observed that small arteries dilate less (% diameter increase) than larger arteries, regardless of AVF type. A study in 2016 by Masengu *et al* [103] observed no relation between arterial elasticity as measured by pulse wave velocity and AVF outcome.

1.4.5 The Effect of Stenosis and Occlusion

The main antagonist to outward remodeling is NiH - the thickening of the vessel walls, resulting in decreased lumen diameter [140] (see figure 1.14). NiH can lead to stenosis, which can lead to a reduced flow, or thrombosis [91]. It is hypothesised that upstream events such as vascular injury during AVF creation or other endovascular procedures causes the downstream biological response which allows for the development of NiH [91]. NiH is common after endovascular procedures, and in some cases is a physiological healing response to reconstructive procedures [82].

Multiple studies have assessed the relationship between WSS, flow, and NiH in an array of vessels, including the AVF. In 1983 the presence of low WSS, caused by flow separation and recirculation (see figure 1.15), was linked to increased IMT and arteriosclerosis in the carotid artery [189]. In 1985, Ku et al [83] again found positive correlation between low WSS and increased intima-medial thickness (IMT) in the carotid, but also found pos-

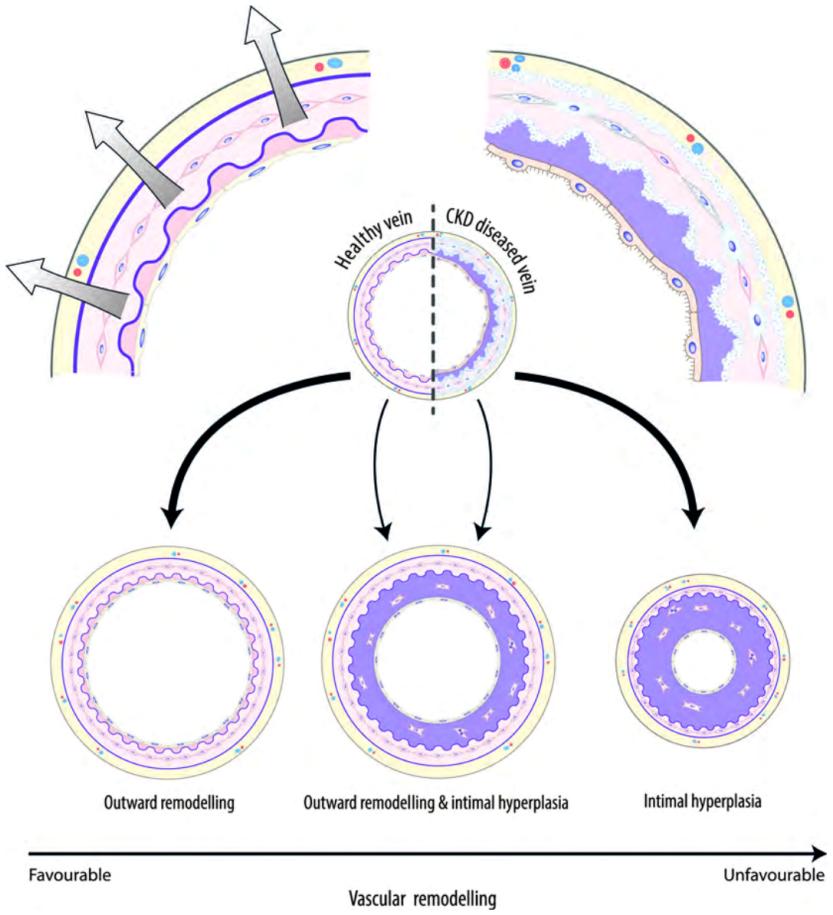

Figure 1.14: NiH can cause stenosis leading to dysfunction in a mature or developing fistula (Rothuizen [153], with permissoin from Oxford University Press)

itive correlation between oscillations in the direction of WSS and IMT. CFD studies have linked regions of abnormal WSS, such as those caused by flow separation, recirculation and vortexes, with the characteristic sites of NiH and stenosis in AVFs [50]. A review by Browne *et al* [26] suggests that outward remodelling occurs in the AVF to reduce WSS levels, and that particularly low, or oscillating levels of WSS are associated with inward remodelling.

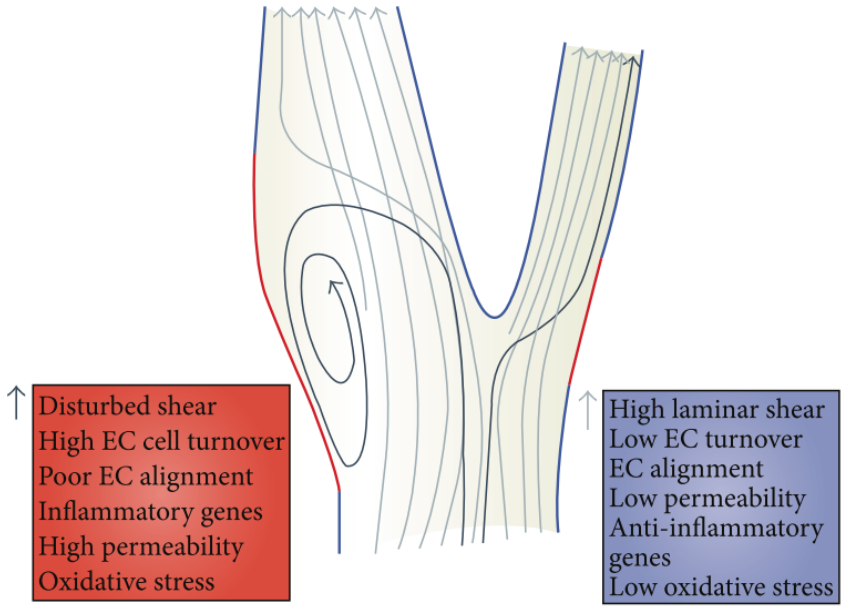

Figure 1.15: Changes in vessel geometry can affect flow-patterns in both arteries and veins. Branches such as at the carotid bulb are associated with areas of high WSS and disturbed flow. EC : endothelial cell (Macmillan Publishers Ltd)

Access type	Common sites of stenosis
radio-cephalic fistula	juxta-anastomotic segment
brachio-cephalic fistula	cephalic arch
Brachial arterytotransposed basilic fistula	transposed vein segment

Table 1.2: Common sites of AVF stenosis [141]

Most AVFs which do not function as intended for HD are found to have at least one lesion if imaged [16]. These stenotic lesions can be functionally important, reducing flow, or can be benign and have little effect on HD. If severe, stenosis can restrict flow in a young AVF causing a failure to mature, or it can occur once a fistula has matured and is being used for HD, resulting in late-AVF complications.

Most frequently, stenosis occurs around the anastomotic area. Quencer and Arici [141] described the common sites of stenosis in RC, BC and BB-AVFs, as shown in table 1.2, and figure 1.16. Inflow stenosis can have the effect of restricting flow, and subsequent maturation in a new AVF, or limiting flow and causing occlusion in a mature AVF. Outflow stenosis, such as in the cephalic arch, can cause aneurysmal dilation, a pulsatile, tense AVF, and poor flow.

In the RC-AVF the juxta-anastomotic stenosis is the most frequent observation, but this site is also common in BC-AVFs [142]. BC-AVFs are reported to suffer from an increased number of cephalic arch stenoses, with rates between 30 - 77 % reported in dysfunctioning fistulas [142, 143]. BB-AVFs are reported to have a large number of stenoses in the venous swing-site, which has commonly been transpositioned in order to create the fistula [143]. Literature reports that around 70 % of stenoses in these fistulas occur at the swing-site.

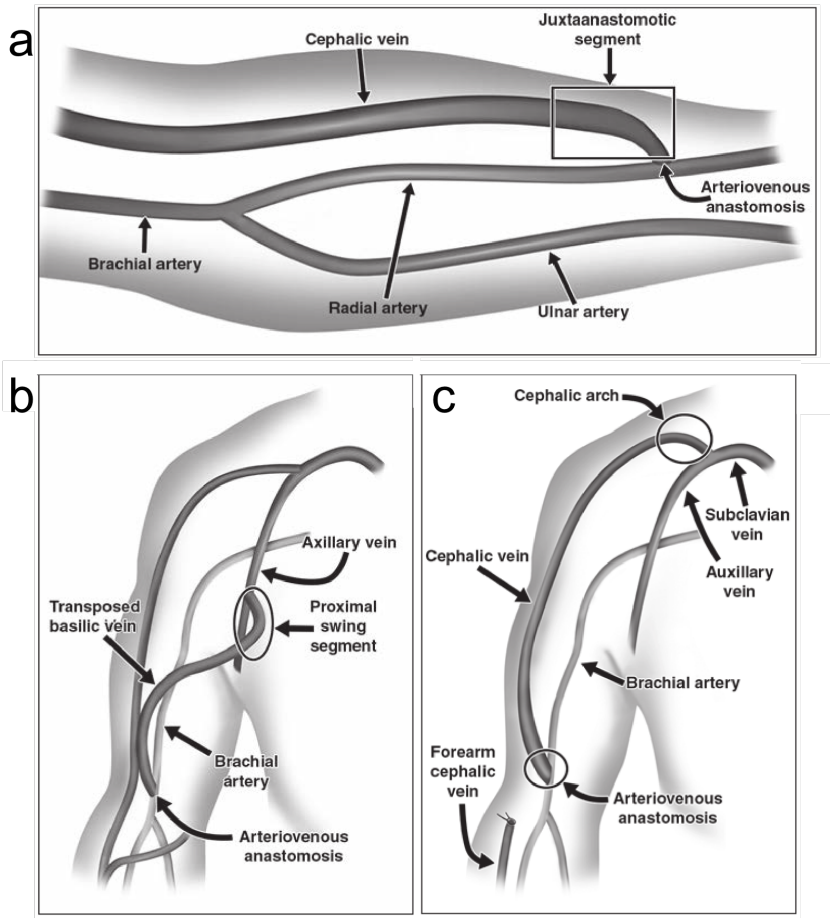

Figure 1.16: Characteristic sites of AVF stenosis (Quencer and Arici [141] American Journal of Roentgenology)

1.5 Preoperative assessment

1.5.1 Clinical Assessment

In a bid to increase AVF patency rates, pre-operative assessments of the blood vessels are performed. KDOQI guidelines recommend physical examination using assessments of the vessels such as palpitation. Allen's test is common, where the speed of blood reperfusion after occlusion is used to assess the circulation. Medical history of the patient is also assessed, recording the presence of co-morbidities and risk-factors for AVF failure such as diabetes and hypertension, and patients are screened for the use of previous CVCs and other radiological or surgical interventions.

This information alone can be enough to determine a fistula site, but subtle features can be missed, such as narrowings or calcification of the vessels. Clinical assessment does not allow determination of the type of flow, the presence of thrombus in the veins, and does not allow verification of vessel uniformity through its length. Central vein stenosis can be missed during clinical evaluations, as well as problems downstream where the vessels become less superficial.

1.5.2 Ultrasound assessment

Pre-operative ultrasound (US) assessment examines the morphology and flow of the veins and arteries that can be used for AVF creation [6]. Pre-operatively, arteries can be assessed for patency and phasicity - with commonly only triphasic (normal) waveforms as acceptable criteria. The diameter is also recorded with adherence to minimum criteria established by the local clinic. The degree of calcium can be qualitatively assessed. Veins can be assessed for patency, diameter and uniformity, with reductions in diameter indicative of possible stenosis. Thickened venous wall in isolated segments, which can lead to stenosis, can be identified. The number of branches in relation to possible anastomotic sites, which may reduce flow through the fistula, can also be identified via US.

Multiple studies have shown US mapping to not only increase placement, but to increase patency rates. Allon *et al* [6] cited increased placement and increased patency rates for fore-arm AVFs after introducing US screening, and Robbin *et al* [149] reported similarly, and included a reduction in unsuccessful surgical explorations. However, not all studies show positive results. A study by Patel *et al* [131] found a reduced maturation rate after introducing mapping, but they note that this may be due to secondary access

sites being used as a result of mapping. A meta-analysis by Georgiadis [55] found that mapping reduces immediate failure, and a non-significant trend pointed towards reduced long-term failure.

Ultrasound measurements of vessel diameter are perhaps the most widely-known risk-factor for AVF failure. Techniques vary, but for example, the measurement can be made of the narrowest region of a certain length of vessel, or at a certain point such as a bifurcation point. Numerous studies have addressed the question of what is the minimum diameter of a vessel acceptable for AVF creation, and can not agree on the lower limit (see table 1.3). For RC-AVFs, minimum cephalic vein diameter for creation has been reported in the range of 1.5 mm to 2.5 mm, with meta-review [79] suggesting the best outcomes are observed when the diameter is over 2 mm. This meta-review does not recommend creating an RC-AVF with a cephalic vein below 1.5 mm [79]. Radial artery diameters are reported in the range of 1.5 mm to 2.4 mm, with the most common being at least 2 mm. Similarly, meta-review reports the best outcomes when the radial artery is over 2 mm, and that they should not be created with arteries below 1.5 mm in diameter [79]. In upper arm AVFs, recommended criteria for BC or BB-AVF creation have been recorded as arterial diameter over 2 mm, and vein diameter of over 2.5 mm [105, 43].

Study	Diameter lower limit
Dageford [43]	vein <2.7 mm in BB and BC-AVF
Nakata [122]	radial artery <2 mm
Bashar [15]	vein <2.5 mm for all AVF
Sahasrabudhe [154]	vein <2 mm in BB and BC-AVF
Parmar J. [130]	radial artery <1.5 mm

Table 1.3: Variance in vessel lower limit for AVF creation from literature

Vessels which appear large enough on US and show no obvious problems (such as in figure 1.17) can still fail to mature. The continued failing of AVFs with ‘good’ vessels indicate that there are additional factors influencing the outcome, but there is limited knowledge as to what these factors are, or if pre-operative tests can identify them. Ultrasound still presents itself as a good modality to conduct the pre-operative assessment due to its relative ease of use, availability, and accuracy. Ideally, a preoperative test should be able to quickly assess important markers of AVF failure, with minimal disruption to the patient’s life.

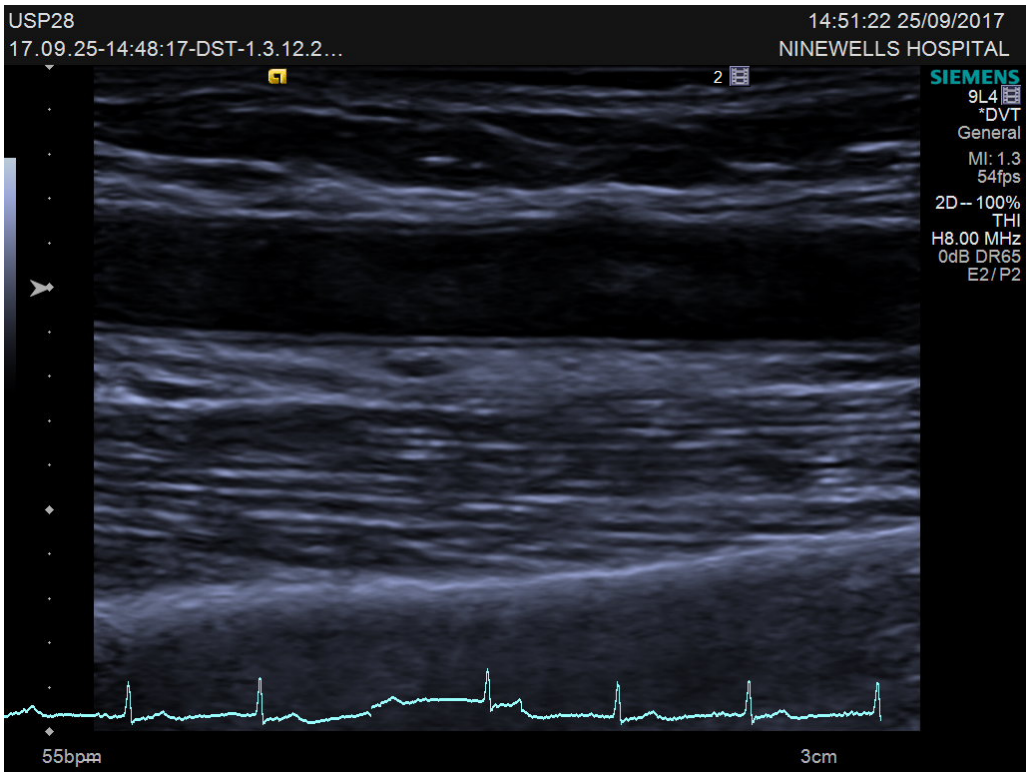

Figure 1.17: B-mode ultrasound image of a healthy patent brachial artery

1.6 Post-Operative Surveillance and Interventions

1.6.1 Post-operative Ultrasound

Surveillance describes a qualified individual performing a regular examination on a patient's vascular access. The goal of surveillance is to identify sites of potentially clinically relevant stenosis, allowing pre-emptive treatment. Treating these sites early may prevent the failure of the access, and requirement of an alternative access site or modality. Post-operative surveillance can be used to detect subclinical stenosis in all accesses, not just AVFs.

Multiple trials have found that US based surveillance reduces the incidence of thrombosis, improving patency rates. Aragoncillo *et al* [12] reported improvement in thrombosis free patency in a surveillance group ($p = 0.03$), and an increased patency rate ($p = 0.01$), compared to a control group during a 3-year multicenter randomised controlled trial (RCT). A 5-year RCT by Tessitore *et al* [170] reported that surveillance, along with pre-emptive interventions could reduce thrombosis rates ($p = 0.03$) and prolong functional patency rates ($p = 0.001$). In a single centre RCT, Han *et al* [61] reported a decrease in failure to mature rates in a group undergoing US surveillance compared to a control group through the use of early/pre-emptive interventions (non-significant, $p = 0.1$). A meta-review of post-operative surveillance practice found strong evidence that surveillance can decrease the risk of thrombosis in a patient's AVF [174], however no evidence was found for predicting thrombosis in patients with an AVG.

Typically, an US post-operative procedure (see figure 1.18) consists of assessing the arterial inflow, the anastomotic region, and the venous outflow tract of the AVF. Vessel diameters will be assessed using B-mode US in both longitudinal and radial views of the vessel. Blood-flow measurements are also taken in these areas. Aliasing on a colour doppler image can indicate stenosis, due to the presence of high-veloicty jets [133].

A major benefit of US in the post-operative surveillance of an AVF is the increased knowledge of the underlying issue causing AVF dysfunction, which reduces need for invasive assessments to determine the cause. This can result in a reduction of emergency care including CVC placement, or invasive thrombectomy procedures.

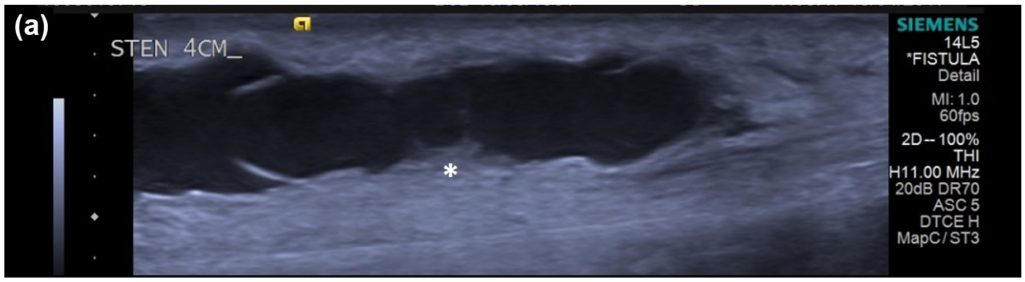

(a) Stenosis detection on B-mode US showing an area of stenosis as indicated by the * symbol

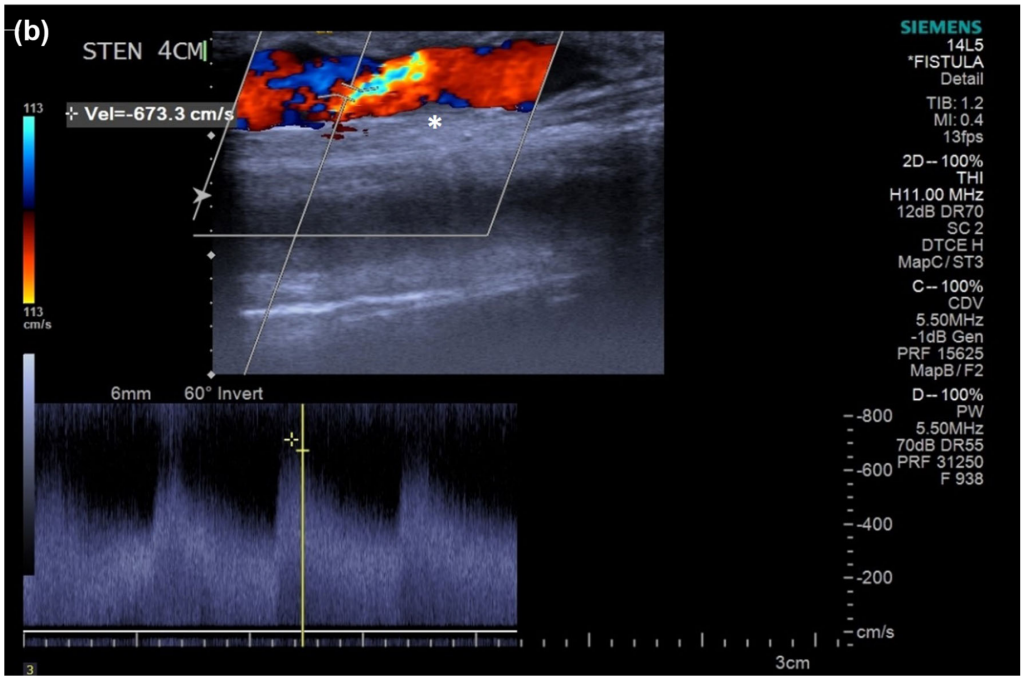

(b) Stenosis detection on colour doppler US showing aliasing from the high flow jet

Figure 1.18: Stenosis detection on US from both (a) B-mode and (b) doppler imaging. Stenosis are commonly defined by their percentage reduction in diameter, i.e. a 50 % stenosis would indicate a diameter reduction of 50 % at the site of stenosis.

1.6.2 Interventions on a failing access

The goal of any intervention on a VA is to maintain, or re-establish patency so the VA can be continued to be used for HD. Best practice guidelines recommend treating a stenosis if the diameter is reduced by over 50 %, and the access flow is reduced. Percutaneous transluminal angioplasty (PTA) (see figure 1.19), is the typical treatment for VA stenosis. Access to the vascular system is achieved percutaneously, and imaging is used as guidance to control the catheter placement, and ensure it reaches the treatment area. The first step in the technique is to use a guidewire to deliver the catheter to the location of the stenosis, through cannulation of a vessel. The delivery method will differ for different stenosis morphology, and surgical experience [176]. Once the catheter has reached the desired location, the balloon is inflated, which is potentially painful, and patients can be administered an analgesia. Balloon profile chosen depends on the non-stenotic diameter of the vessel [124]. Depending on the stenosis, and the dilation required, different balloons can be employed, with higher pressures, or balloons which contain small metal blades, known as cutting balloons. Cutting balloons possess atherotome blades which produce "controlled incisions" into the venous wall during inflation [124].

Digital subtraction angiography (DSA) is performed concurrently with balloon insertion, in order to visualise the stenosis, and assess if the intervention was successful [121]. If inadequate dilation has been achieved, the PTA can be repeated with another balloon. The interventional radiology technique has a high learning curve, and not all centres can provide this treatment 24 hours a day, and sometimes patients must be transported for treatment.

If VA thrombosis occurs, it should be treated as soon as possible to avoid the need for access via a CVC. Thrombolysis is typically performed mechanically, with a thrombectomy catheter. The device is used to remove the blood-clot, restoring patency in the vessel. The area can also be treated with balloon angioplasty after thrombectomy.

Stent usage is a further option, and can be used in cases of stenosis, aneurysm, pseudoaneurysm, and in cases of angioplasty induced vascular rupture [56].

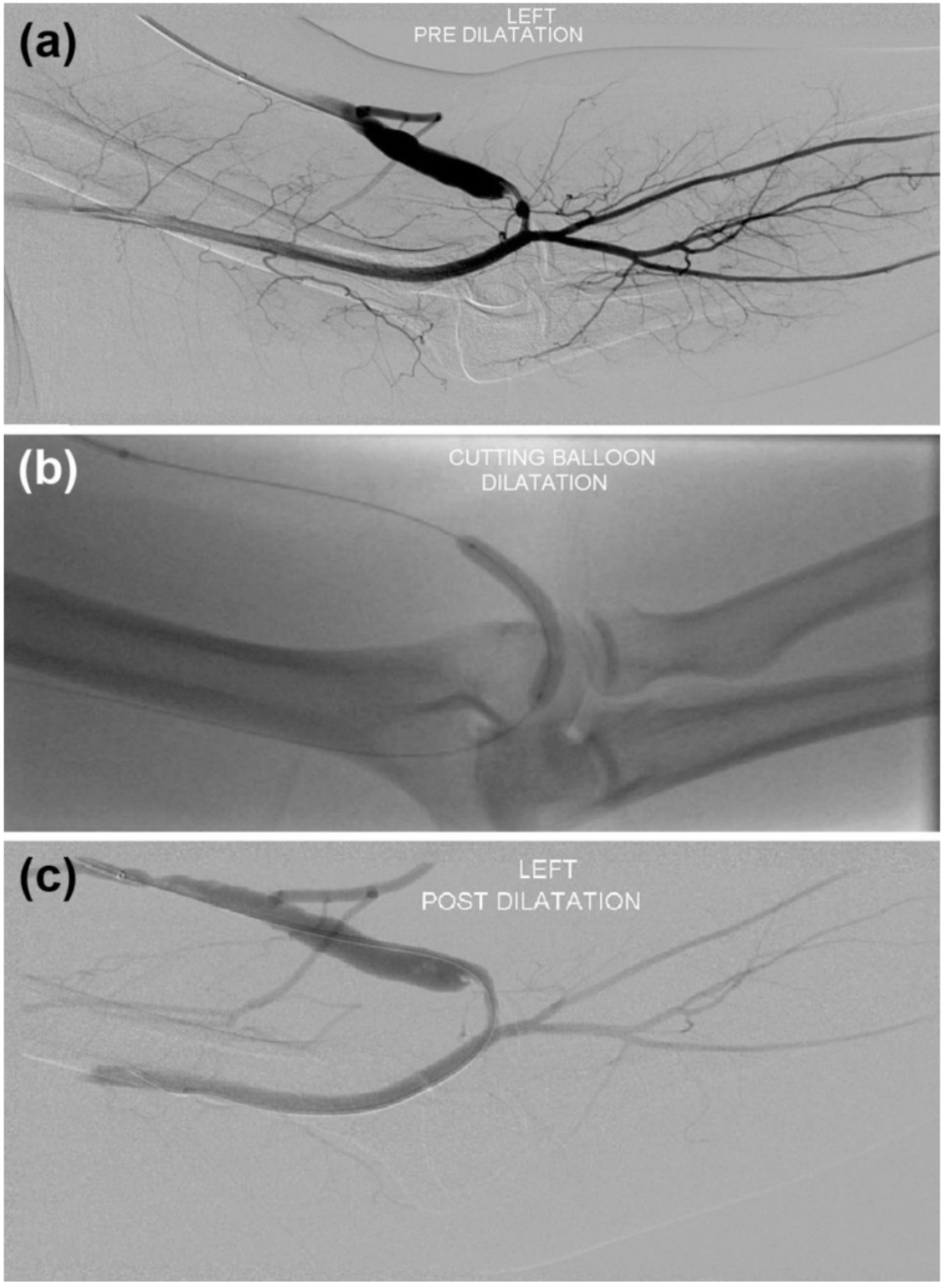

Figure 1.19: DSA image showing balloon catheter insertion and inflation at a stenosis site. Some residual stenosis is still evident post-dilation at the venous anastomosis.

1.7 Risk Factors for AVF Failure

1.7.1 Known Risk Factors

As discussed, vessel diameters from US are commonly the deciding criteria on AVF creation. Many studies have observed that AVF failure rates are increased when using lower diameter vessels (see table 1.3). However, these studies cannot agree on a lower limit for vessel sizes, and vessels used above these limits can still fail to mature.

Besides vessel diameters, numerous demographic factors have been identified in the literature as risk-factors for AVF failure. Most commonly, old age, race, gender and diabetes have been found to have a negative impact on AVF patency rates.

A landmark study by Hod *et al* [64] included over 20000 patients and found a number of risk-factors for AVF failure, including older age, female gender, black race, diabetes, cardiac failure, and duration of pre-ESRD nephrology care. They suggest that in at risk patients, for example elderly African-American women, that perhaps more aggressive early intervention should be undertaken in order to ensure an AVF remains patent, and to limit CVC placement.

Farber *et al* [51] assessed early thrombosis in AVFs in over 600 patients. They found female gender, smaller arterial diameter, draining vein diameter of 2 to 3 mm, and use of the medicine protamine to be risk-factors for early thrombosis. Forearm AVF placement was shown to increase the risk of early thrombosis when compared to upper arm AVF placement, possibly due to the smaller size of the radial artery in these AVFs. Diabetes was found to be inversely associated with early thrombosis, perhaps due to selection biases for AVF creation in diabetic patients.

Weale *et al* [182] studied BC and RC-AVFs in over 700 patients, splitting them into age groups of < 65, 65 - 79, and ≥ 80. They found no difference in the patency of either type of AVF between the age groups, but note female gender as a risk-factor for non-maturation of RC-AVFs. Miller *et al* (2003) [112] found female gender to be a risk-factor for AVF failure, despite the use of US mapping to identify suitably sized vessels. Vessel diameters were not found to be the reason for AVF failure in this group, as the diameters of successful and unsuccessful AVFs did not significantly differ.

Two meta-analysis have confirmed the negative effect of old-age on AVF patency. In 2007, Lazarides *et al* found a 50% increased risk of RC-AVF failure in elderly patients (most commonly > 65 years old). BC-AVFs were found to have a 12% higher patency

in this group, suggesting this may be a more appropriate choice in elderly patients, when salvaging of access sites is less important due to lower life expectancy. Almasri *et al*, in 2016, conducted another meta-review including all VA types. Again, they found that female gender, old-age (> 65) and diabetes were related to decreased AVF patency at 2 years.

If patients are screened for risk-factors prior to AVF creation, clinicians can make an informed decision as to the best option for vascular access, and patient's can become more aware to the risks of AVF creation, and the likelihood of failure.

1.7.2 Novel pre-operative markers for AVF failure

Despite pre-operative US assessment, and the detection of risk-factors, AVF failure is still high. This has led to researchers attempting to identify additional risk-factors for AVF failure [106]. Suggested markers are typically physiological assessments of the vasculature, or biomarkers indicative of reduced endothelial function.

Arterial Stiffness

Arterial stiffness (AS) is an age related structural change that occurs in the cardiovascular system, leading to the stiffening and thickening of major arteries [11]. AS increases with age, and in the aorta stiffening is associated with fracture of elastin and an increase in collagen, increased arterial wall thickness, and calcium deposits [30]. Other vessels change differently with age and peripheral vessels have been observed to stiffen less than the aorta [114, 13]. Increased arterial stiffness limits the ability of the arteries to accommodate blood ejected from the heart. Due to the physics of waves, stiffer materials propagate waves with a higher velocity. This is the most recognisable feature of AS, and forms the basis for its measurements with techniques such as pulse wave velocity. A secondary consideration of AS is the resulting impedance matching between different arterial segments [35]. This can result in increased propagation of pulse energy throughout the entire arterial tree.

Increased AS has two important implications, caused by the increased pulse wave velocity, and impedance matching. The increased velocity of the reflected waves causes their earlier return to the heart. Earlier arrival of these reflected waves can interfere with and increase the workload of the heart, particularly if they arrive during ejection release [35]. Conversely, impedance matching can reduce the amplitude of pulse reflections,

meaning that more pulse energy can be delivered to more distal points in the arterial tree. Waves can then propagate into the smaller vascular beds of the organs, and the increased energy transfer here can result in targeted organ damage [113].

AS increases with age, and is increased in diseases such as hypertension, diabetes mellitus, hypercholesterolemia [139], and is an independent predictor of cardiovascular mortality in patients with ESRD [33]. Patients with ESRD are observed to have increased AS, when compared to hypertensive patients with identical arterial pressures and controls, suggesting kidney failure can have a significant effect on the composition of the arteries [119]. Pulse-wave velocity (PWV) is the gold-standard method for assessing arterial stiffness, and involves tracking the pressure pulse through at least two points in the cardiovascular system. Using pressure sensors, the speed of the pulse is indexed by measuring the time taken for the pulse to propagate between two points in the cardiovascular tree. Stiffer arteries will permit faster propagation of the pressure pulse, which is detected as an increased pulse wave velocity.

AS has been identified as a possible biomarker of AVF failure [106]. A study by Korsheed *et al* [80] revealed that AVF creation had the effect of reducing global values of AS, diastolic and systolic blood pressure, and that patients with a successful AVF showed a decrease in PWV after two weeks. In 2010 a study by Kheda *et al* [74] linked high arterial stiffness to AVF stenosis, but noted that adequate blood flow was still seen regularly in their group of 32 patients despite high stiffness. A 2016 study of 59 patients concluded that AS (measured by PWV) was not predicative of failure to mature [103], but recommended further research.

Endothelial Function

Markers of endothelial function have potential use in predicting AVF outcomes. The common US based examination of endothelial function, FMD, has been assessed prior to AVF creation [45, 128], with mixed outcomes. Owens *et al* [128] found endothelial function to correlate well with the degree of arterial remodelling observed in a small cohort study, demonstrating that arterial remodeling in AVFs is an endothelial process. However, this study did not assess links to the clinical outcome of the AVF, so its predictive value is unknown. Dember *et al* [45] assessed endothelial function using FMD in 602 patients awaiting AVF creation, and found that it varies to a large extent in this group of patients. However, the AVF outcome of these patients was not reported. Using a different tech-

nique, peripheral artery tonometry (PAT), MacRae *et al* [101] assessed the endothelial function of patients awaiting AVF creation. Patients with higher PAT values had a higher chance of reaching AVF maturation than those with lower values in a small cohort of 28 patients. Larger studies of suitable design are needed to assess if endothelial function testing can be used as a marker for AVF outcomes.

Inflammatory Markers

Patients receiving RRT routinely have bloods taken for analysis to track progression of the disease, and this opens an accessible pathway for longitudinal studies of chemicals and proteins in the blood. Certain markers such as C-reactive protein (CRP) and albumin have been well-studied in realtion to AVFs, likely due to the abundance and ease of measurement in many institutions. CRP is known to correlate with endothelial dysfunction [187], so an increased baseline value, as experienced by ESRD patients, could hinder arterial dilation. Correlations between CRP and AVF failure have been observed in a number of studies [188, 111, 38].

Other blood-borne markers are of interest: Anti-symmetric dimethyrarginie (ADMA) has a known negative effect on endothelial function through the impairment of nitric oxide production [160]. Meng *et al* [109] demonstrated elevated ADMA in patients on HD. A study by Wu *et al* [184] demonstrated a relationship between increased ADMA and AVF re-stesnosis after intervention. In 2012 a small study of 68 patients [22] identified that the red blood cell distribution width was predicative of reduced patency after 2 years, whilst finding that CRP levels were not. However, a 2016 meta-analysis [118] determined that zero blood-borne markers were significantly related to AVF outcome. The authors state that this is primarily due to hetrogeneity in the assessed studies; different outcomes were analysed, blood measurements were taken at different time-points, and different statistical analyses were used.

1.7.3 Alternatives for pre-operative assessment

New methods of assessing arterial stiffness or compliance via US have recently emerged, including shear wave elastography (SWE), and strain imaging.

Shear Wave Elastography

Shear wave elastography uses shear waves generated from focussed US to map tissue stiffness. A shear wave causes particles in a medium to oscillate in a transverse direction to the wave motion. The shear wave propagation velocity (SWV), in tissue of density ρ, is related to Young's Modulus (Y):

$$Y = 3 \times \rho \times SWV^2 \tag{1.4}$$

This equation relies on various mechanical assumptions, such as elastically homogeneous materials, finite in space, which are biologically unrealistic [110]. By tracking the motion of these waves through a tissue sample using high frame-rate techniques it is possible to estimate the velocity, and obtain an indirect measurement of tissue stiffness (see figure 1.20). Commercially available US SWE packages typically measure the mean value of the shear wave velocity inside a user defined ROI.

Shear wave elastography has found widespread clinical application in breast, liver, thyroid and lymph node imaging [162, 120, 52, 92]. Recently, a number of groups have used shear wave elastography to investigate the cardiovascular system. Couade *et al* [41] were the first to assess local arterial stiffness using shear wave elastography, in one healthy volunteer. They observed that the stiffness of the carotid artery varied throughout the cardiac cycle, increasing in late systole. Li *et al* [95] used shear wave elastography to assess the carotid artery in patients with ischemic stroke. The group assessed the longitudinal stiffness of the carotid, and found that this measurement correlated well with PWV (r = 0.7). They also identified increased arterial stiffness in the group with ischemic stroke using both techniques, when compared to age and sex-matched controls. Ramnarine *et al* [144] used the technique to identify increased Young's modulus in carotid plaques associated with neurological symptoms. It is possible that differences in the shear wave velocity could identify patients at increased-risk of AVF failure.

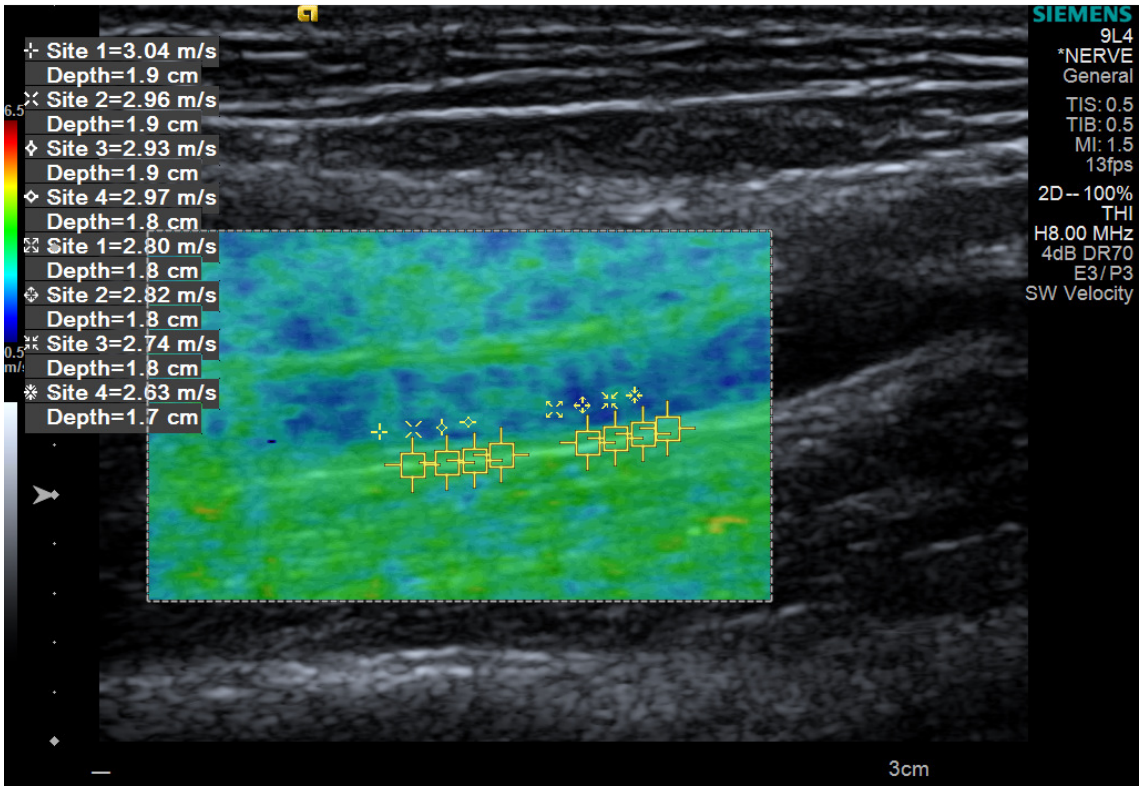

Figure 1.20: Shear wave velocity map of a brachial artery

Strain Imaging

Strain imaging is a technique primarily used to in the assessment of myocardial damage after infarction, and involves quantifying tissue deformities, typically via US. Strain (ϵ) can be described as a deformation, and expressed as a relative change in length (L) or volume due to some force :

$$\epsilon = \frac{\Delta L}{L_0} \tag{1.5}$$

Strain is expressed as a percentage, with positive values describing thickening and negative values describing stretching.

The rate at which strain occurs, the strain rate, can be calculated according to:.

$$\frac{\Delta \epsilon}{\Delta t} = \frac{\Delta V}{L_0} \tag{1.6}$$

Where ΔV is the velocity gradient in the sample studied.

Strain imaging is possible in 2D due to the advent of speckle tracking. The speckle on an US B-mode image is the result of scattered waves from rough structures smaller than the US wavelength. These scattered waves can then interfere, causing constructive peaks (bright dots) and destructive troughs (dark dots) in the resultant signal, known as speckle. The speckle remains stable spatially throughout frames during an US scan [89]. Complex algorithms allow tracking of the speckle from frame to frame. Geometric differences in the speckle between frames allows for measurement of displacement, and knowledge of the frame rate allows calculation of the velocity. In this way, the motion of the speckle represents the motion of the tissue. Typically, a contour is placed on a tissue of interest on a B-mode ultrasound image, and this contour tracks tissue movement through the speckle tracking technique. The strain and strain rate are calculated through the measured displacement and velocity of the contour.

Multiple groups have adapted the speckle-tracking packages to analyse other parts of the cardiovascular system such as the aorta and carotid [168, 77, 100, 8], finding good correlations (r = -0.7) with markers of arterial stiffness [138, 77]. Healthy subjects have been shown to produce regular and periodic profiles of wall motion when assessed with strain imaging [185, 77]. Ma et al [100] observed that the carotid of patients with pre-eclampsia produce non-uniform velocity profiles and Cho et al [36] had similar findings in patients with Takayasu's arteritis. This suggests that in certain groups of patients, the vessel movement is not synchronised.

Multiple strain imaging platforms exist, developed by various manufacturers. The Velocity Vector Imaging (VVI) package by Siemens, is "an advanced 2D quantitative tool for assessment of global and regional myocardial muscle and motion mechanics". VVI can analyse the strain, strain rate, velocity and displacement of imaged tissue, and can graphically display tissue movement patterns. It is possible that differences in VVI measurements of strain or strain rate could identify patients at increased-risk of AVF failure.

Other US-based Methods

Other US-based assessments may have potential uses in predicting AVF outcomes. A study by Ku *et al* [84] used US to assess the intima medial thickness (IMT) of the radial artery prior to AVF creation. They found increased IMT to have a negative effect on maturation, but did not elude to reasons this could cause failure, other than poor vasculature. IMT could benefit from further study, and perhaps increased IMT could act as a risk-factor for AVF failure.

Magnetic Resonance Imaging

Magnetic resonance imaging (MRI) has been previously explored as a potential modality for the pre-operative assessment of patient's vessels prior to AVF creation. MRI is an attractive diagnostic tool as it can provide excellent angiographic images, with or without contrast agent [47, 57]. Specifically, Planken *et al* [136] have shown contrast-enhanced (CE) MRI as an accurate modality for providing pre-operative measures of forearm vessel and upper arm venous diameters in patients indicated for AVF creation. In this study, agreement was seen between diameter measurements obtained from US and CE-MRI. Results taken intra-operatively showed a deviation from those obtained by US, but in agreement with CE-MRI. The results on US showed a larger standard deviation, suggesting that the US method used was less precise. A further study by Planken *et al* [137] found CE-MRI to be superior to US in detecting venous pathologies in 73 patients prior to AVF creation, with the most frequent being upper arm cephalic vein occlusion. CE-MRI was able to identify pathologies missed by US responsible for future AVF dysfunction and for AVF 'failure to mature' in 33% of the study population with AVF dysfucntion, however clarification is not given as to where these mismatches occurred. The authors remark that in the remaining 67% of failures, venous stenosis was the main cause, and these stenosis

developed rapidly after AVF creation.

However, commonly used contrast in MR imaging is currently contraindicated for patients with renal failure, due to associations with a disease called nephrogenic systemic fibrosis [88]. Non-contrast enhanced (NCE) or alternate contrast MRI methods are emerging as a research tool for patient's undergoing AVF creation. Pre-operatively, few studies have used NCE-MRI to image the vessels of patients indicated for AVF creation. Menegazzo *et al* (1998) [108] compared Time of Flight (ToF) imaging with venography to assess the depiction of veinous diameters prior to AVF creation. The found a greater correlation between the ToF measurements and surgical findings than venography, but venography is less commonly used compared to US. In 2012, a study by Bode *et al* [21] used CE-MRI and a NCE balanced turbo field echo sequence to detect stenosis prior to AVF creation. The NCE-MRI detected 66% of (non-significant) stenosis found on CE-MRI, but importantly these were not seen on previous US imaging. More recently, NCE-MRI sequences, such as the Multi Echo Data Image Combination (MEDIC) [78], along with increases in magnetic field strength, have shown promising results when used to image the lower limbs, suggesting that non-contrast MRI may once again be considered a suitable choice for pre-surgical mapping and surveillance of AVFs.

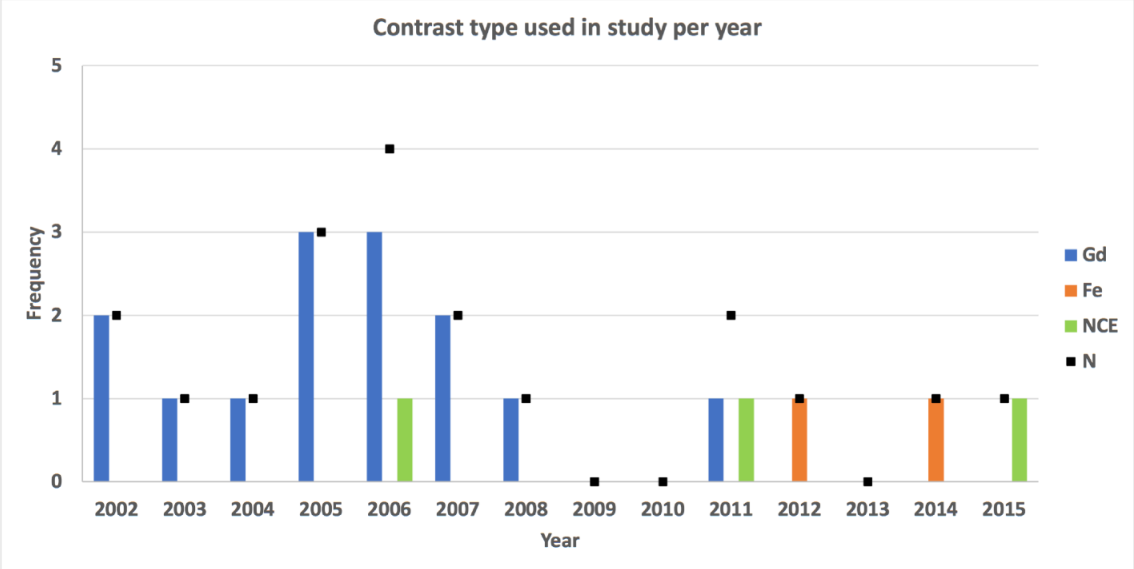

Figure 1.21: In recent years a growing trend of NCE and alternate contrast material being used in studies of VA is observed, proceeded by the growth and fall of Gd based contrast pre-NSF. From work presented at UKRC, 2017. NCE: non-contrast enhanced, Gd: Gadolinium, Fe: Iron

1.8 Aims

The main aim of this thesis is to assess whether existing and potential risk-factors for AVF failure are related to the AVF outcome in a local cohort. A secondary aim is to address a gap in the CFD literature regarding reproducibility of CFD simulations from different MRI sequences.

As such, this thesis can be separated into the introduction, and three main research questions.

- Chapter 1 introduces the AVF, discusses attempts to identify risk-factors for AVF failure, and includes computational efforts to understand the effect of wall-shear stress on AVF stenosis. Multiple known risk factors such as diabetes, age and vessel diameters are discussed, and potential markers of failure introduced.

- Chapter 2 aims to answer the question *are known risk-factors and serological markers predicative of AVF outcome?* Previous research involving identification of risk-factors for AVF failure have been conducted in different settings, with differing patient demographics. It is possible that risk-factors identified in studies conducted in the USA for example may not be applicable to UK, or more specifically Scottish populations. Knowledge of which patients are likely to have an unsuccessful fistula can lead to choices of an alternative vascular access, such as an AVG placement, identification of patients who may benefit the most from US-based surveillance, or to better patient counseling towards the risks of AVF creation and subsequent failure. This section uses health informatics and machine learning methods to determine if a link exists between known risk-factors such as diabetes, age and gender, and pre-operative blood measurements, and the outcome of a patients AVF, in a single centre, retrospective study;

- Chapter 3 aims to answer the question *are US markers of arterial elasticity and strain risk-factors for AVF failure?* This uses modern ultrasound technologies (shear wave elastography and velocity vector imaging) to determine if pre-operative measurements arterial elasticity and strain are related to the outcome of a patient's AVF;

- Chapter 4 aims to answer the question *is 3T MRI useful as part of the pre and post-operative workup for patients indicated for AVF creation?* A major draw-back of

US imaging is its inability to image the central veins. MRI imaging offers superior central vein depiction, and could be used to screen for central vein pathology prior to AVF creation. This study involves piloting modern MRI sequences in a small prospective study to determine if any benefit could be gained from this underutilized imaging modality, in order to pave the way for central vein study. Using the same images, chapter 5 compares CFD simulations from the two different MRI sequences used, and in a series of phantoms in order to determine if similar CFD results are obtained regardless of imaging sequence.

Limitations of the research are described in each chapter. Chapter 6 concludes the work, provides impact and suggestions for future work following on from this research.

Chapter 2

Blood-Borne and Demographic Risk-Factors

2.1 Introduction

Biomarkers are widely studied in the field of nephrology. Certain biochemical markers are associated with increased mortality in ESRD patients, such as CRP, albumin and interleukin-6 [126]. These markers are also associated with adverse cardiovascular outcomes [148, 34]. A small number of studies have examined the association between blood-serum markers and AVF failure. Low serum albumin has been observed in patients with primary AVF-failure [2], and in patients with a high-risk (three or more dysfunction events) of VA failure when compared to patients with a lower-risk [32]. Further studies have observed a combined increase in CRP and decrease in serum albumin in patients with AVF failure [22, 72], however, a number of studies have found CRP and albumin to be unrelated to AVF outcome [17, 28, 76].

Additional markers have been studied, and have been found to have an effect on AVF patency. Increased levels of ADMA taken at the time of angioplasty, have been correlated with re-stenosis of AVFs after intervention [184] (see section 1.7). High levels of free P-cresol A, which is possibly associated with increased oxidative stress and inflammation, measured after AVF creation and during HD treatment have been linked to lower levels of AVF patency [32]. A separate study observed that high levels of fibrinogen, a blood clotting protein, at the time of AVF creation were linked with increased failure rates [164].

A meta-analysis of blood markers including albumin and CRP, found that none were associated with all-cause AVF failure [118]. The authors of this review suggest that this is due to heterogeneity of failure definitions and the time-point of blood measurements. Of the 12 studies they assessed, most included under 100 patients, and only three assessed marker values prior to AVF creation, making conclusions about the predictive power of markers difficult. Currently, there exists no pre-operative blood-borne risk-factor for AVF failure, perhaps due to heterogeneity in study populations. A local study allows determination if risk-factors which have commonly been identified in large american studies can also be applied to local UK cohorts, which can vary demographically between cities. If a marker of AVF failure can be identified, patients could be better counselled to the risks of AVF failure, or ultimately an alternative choice of vascular access with reduced risk of failure could be recommended for the patient.

This chapter aims to answer the question: *Are known risk-factors and serological markers related to AVF failure in a single centre retrospective study?*. This chapter also provides the population overview of the ESRD cohort in Ninewells hospital, the main

study cohort of this thesis, and describes their AVF patency outcomes. This institution performs US based surveillance, with patients scheduled for follow up at six weeks, three months, six months and one-year post AVF creation, allowing detailed tracking of a patients AVF. Data was linked from multiple sources to create accurate timelines of each AVF, including analysis of dysfunction events. Health informatics was used to create a detailed picture of each individual patient, and logistic regression to identify factors associated with AVF failure. Finally, an algorithmic approach is used to demonstrate the classification potential of markers identified in this cohort.

2.2 Methods

2.2.1 Patients

A retrospective review was performed on all patients undergoing RRT via HD with a primary AVF at our institution. Patients were identified by their presence on the Scottish SRR. Data analysis was performed on demographic factors, and on routine blood biochemistry measurements taken during the work-up six-months prior to RRT, and follow-up to RRT for each patient.

2.2.2 Inclusion and Exclusion Criteria

All patients who were placed on the SRR between October 2012 and January 2017, and were known to have a primary autologous AVF created at this institution were included. This date range was chosen as confidence on data accuracy prior to 2012 was limited. All patients were on a routine US-based surveillance program. Only the first AVF was considered, patients subsequent AVFs were not included in the analysis. Patients who were on peritoneal-dialysis at the time of AVF creation were excluded from the study.

2.2.3 Data Collection

Caldicott approval from the local Ethics Service was obtained, anonymised patient data (including biochemistry, demographic, surgery, diabetes) was supplied by the universities Health Informatics Centre (HIC, Farr Institute) in .csv format. AVF creation data was manually collected from vascular laboratory databases. Data on AVF surgical interventions was manually collected from radiological records, and vascular laboratory databases. All manually collected datasets were then passed to, and anonymised by HIC. For each patient, a timeline was created including date and type of AVF creation, date of starting HD or RRT, and the date of any surgical interventions, AVF related events or death. Timeline creation was performed using Python 2.7. Biochemistry measurements were linked to the patient's timeline, and recorded as a 6-month mean prior to AVF creation. Biochemistry results were available for % saturation of transferrin, HbA1C, albumin, aldosterone, alkaline phosphatase, alanine transferrase, aluminium, amylase, Beta-microglobulin, bence jones protein, bicarbonate, bilirubins, c-peptide, c-reactive protein, caeruloplasmin, calcium, chloride, cortisol, creatinine, digoxin, ferritin, glucose, haptoglobin, hdl-cholesterol, iron, lactate, ldl-cholesterol, magnesium, parathyroid hormone,

phosphate, potassium, procalcitonon, prolactin, total cholesterol, transferrin and urea. If 25 % of the cases lacked a certain blood measurement for analysis it was excluded from analysis.

2.2.4 Study Outcomes and Definitions

The aim of this study was to determine if routine blood measurements taken as part of a patients work-up to RRT could predict the outcome of AVF creation at 1-year. The "high-risk" group was defined as including those who had at least 1 intervention event or AVF abandonment within 1-year of creation, with 1 year chosen to match the commonly reported 1 year patency rates. Dysfunction events were identified retrospectively from vascular laboratory and radiological intervention databases. Those without an event or failure at 1-year were included in the "low-risk" group.

The predictive power of various blood markers, and various categorical variables such as sex, diabetes status, and AVF site were analysed. The type of vascular access used prior to AVF creation, and the time from commencing RRT to AVF creation was recorded.

For patency analysis, primary patency was defined as the "intervention free access survival" or the interval from time of access placement to any intervention designed to maintain or reestablish patency. Assisted primary patency was defined as "thrombosis-free access survival" or the interval from time of access placement, including intervening manipulations, to access thrombosis or abandonment (patients whose loss of primary patency resulted in AVF abandonment were censored from primary assisted patency analysis).

2.2.5 Ultrasound Assessment

All patients within this study had a pre-operative ultrasound assessment prior to fistula creation and then were subsequently placed on a routine surveillance programme. Using a high frequency 14MHz transducer (Tx) the veins and arteries of the arms were assessed both in longitudinal and transverse plane.

Pre-operatively, the arteries were assessed for patency and phasicity, with only triphasic or biphasic (normal) waveforms as acceptable criteria. The diameter was also recorded with a minimum acceptable diameter of 2mm. The veins were assessed for patency, diameter, and uniformity, with a reduction in diameter to less than 3mm indicative of possible stenosis.

Post operatively patients were placed on a routine surveillance programme. When a significant stenosis was identified the cases were discussed within a multi-disciplinary meeting and patients were referred for intervention.

2.2.6 Statistical Analysis

All analysis was performed using Python 2.7 and R. Biochemistry data was recorded as mean $\pm$ standard deviation. Continuous data was graphically assessed for normality. Differences between categorical and continuous variables in the high and low-risk groups were assessed using chi-squared, Student's t, and Mann-Whitney U tests, and are presented in section 2.3.1. Sub-group analysis was performed on patients with and without dialysis history prior to AVF creation.

General Linear Models (GLM) of the binomial family (i.e. logistic regression) were created in RStudio (RStudio Inc, USA) to assess the predictive power of variables, with inclusion in the high-risk group as the dependent variable. Variables were placed in the model owing to identification in the literature, or if a statistically significant difference ($p < 0.10$) was identified between the high and low-risk group according to statistical tests (chi-squared, Student's t, Mann-Whitney U).

As per SAMPL guidelines [87], model accuracy, and variable correlations were assessed. Predictive accuracy of the models was assessed using McFadden's Pseudo R-squared [67]. Goodness-of-fit of the predicted distributions was assessed using Pearson's Chi-squared statistic [65].

As a form of verification, a K-Nearest Neighbors (KNN) classification machine learning algorithm was used to assess the predictive power of any markers identified. This model was chosen under the hypothesis that patients with similar blood values would have similar outcomes. Data was scaled and then split into training and test-data, using Python and scikit-learn [132], using the same outcome as the GLM. The RF model was trained on the training set and used to predict the outcome of patients in the test set. Gridding methods were used to hyper-tune the RF model. Results were interpreted using a confusion matrix to show true/false positives and negatives of the model.

2.3 Results

920 patients were initially identified by HIC, but 720 were excluded as their entry on the SRR did not fall within the study period (2012 - 2017). 210 patients were identified, all on RRT at our institution, and having been placed on the SRR during the study period. 72 patients were excluded, due to lacking AVF creation data (n = 59), or first modality of RRT was not HD (n = 13). One patient was removed as AVF was created as part of a work-up for a Whipples procedure. 137 patients remained, all having a primary AVF created within the study period. The exclusions process is visualised in figure 2.1.

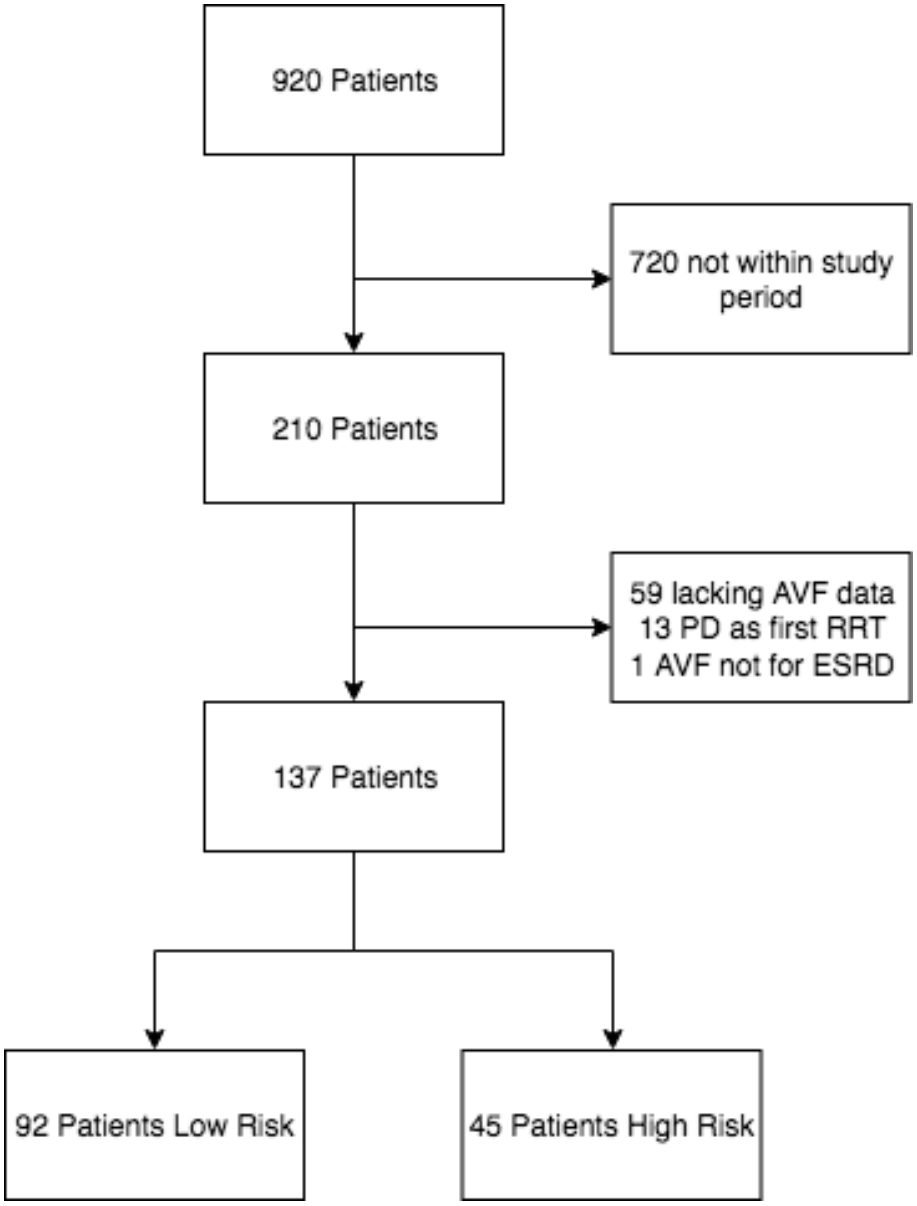

Figure 2.1: Flow chart showing patient inclusion and exclusion

The mean age of the patients was 66.7 $\pm$ 13 years, and 58 % were male. The most common cause of ESRD was diabetes (27%), followed by vascular disease and hyper-

tension (13%). Other causes of ESRD included kidney tumours, traumatic injury and polycystic kidney disease. All patients had at least one AVF created for HD. Full demographic and blood measurement data can be seen in table 2.1.

	Total (n = 137)	High risk (n = 45)	Low risk (n = 92)	p-value
Age (years)	66.7 ± 14.0	66.3 ± 12.2	66.9 ± 14.8	0.32
Sex male (count)	80	26	54	0.9
Prev. HD (count)	49	21	28	*0.06*
Diabetes (type 1/2) (count)	19 / 44	4 / 18	15 / 26	0.33
% Satn. Transferrin	21.0 ± 6.9	20.0 ± 6.9	21.5 ± 6.8	0.12
Albumin (g / L)	32.9 ± 6.7	31.0 ± 6.5	33.7 ± 6.7	**0.007**
ALT (U / L)	21.6 ± 10.7	21.1 ± 9.9	21.8 ± 11.1	0.26
Bicarbonate (mmol / L)	23.8 ± 3.3	24.5 ± 3.3	23.2 ± 3.2	**0.027**
Bilirubins (umol / L)	5.7 ± 2.2	5.8 ± 2.3	5.6 ± 2.2	0.29
C-reactive protein (mg / L)	31.7 ± 35.5	40.7 ± 36.4	27.2 ± 34.4	**0.016**
Creatinine (umol / L)	388.6 ± 106.2	397.3 ± 118.1	384.3 ± 100.2	0.31
Ferritin (ug / L)	312.0 ± 246.3	257.6 ± 185.5	340.5 ± 269.6	**0.036**
Iron (umol / L)	10.5 ± 3.6	10.2 ± 4.3	10.7 ± 3.3	0.1
Phosphate (mmol / L)	1.5 ± 0.3	1.6 ± 0.3	1.5 ± 0.3	*0.08*
Potassium (mmol / L)	4.8 ± 0.5	4.7 ± 0.5	4.8 ± 0.5	0.23
Sodium (mmol / L)	139.7 ± 2.7	139.4 ± 2.8	139.8 ± 2.7	0.26
Transferrin (g / L)	2.0 ± 0.4	2.0 ± 0.4	2.0 ± 0.3	0.43
Urea (mmol / L)	20.0 ± 5.1	20.3 ± 4.9	19.8 ± 5.3	0.17

Table 2.1: Demographic and biochemical results from the study population

Over the full study period, a total of 57 patients underwent at least one AVF intervention or failure event. 45 patients had an intervention to maintain patency, primarily due to stenosis (42 cases), and three cases of stenting a pseudo-aneurysm. 12 patients had their AVF abandoned without a prior intervention, primarily due to occlusion/thrombosis (nine cases), one failure to mature, one ligation of an aneurysmal fistula, and one unknown cause. A further 13 patients who underwent at least one intervention to maintain patency, ultimately underwent AVF abandonment. This was primarily due to thrombosis/occlusion (nine cases, five of which caused by a failed angioplasty), followed by stenosis leading to reduced flow (three cases) and one unknown cause. 11 patients died within one-year of AVF creation, with a patent AVF.

For blood marker analysis, the high risk group included 45 patients who underwent intervention or AVF abandonment within one year. The remaining patients were placed in the low-risk group. Following earlier definitions, primary patency at one year was approximately 67%. At one year, primary assisted patency was approximately 91%. Figure 2.2 demonstrates primary patency and primary assisted patency in this cohort.

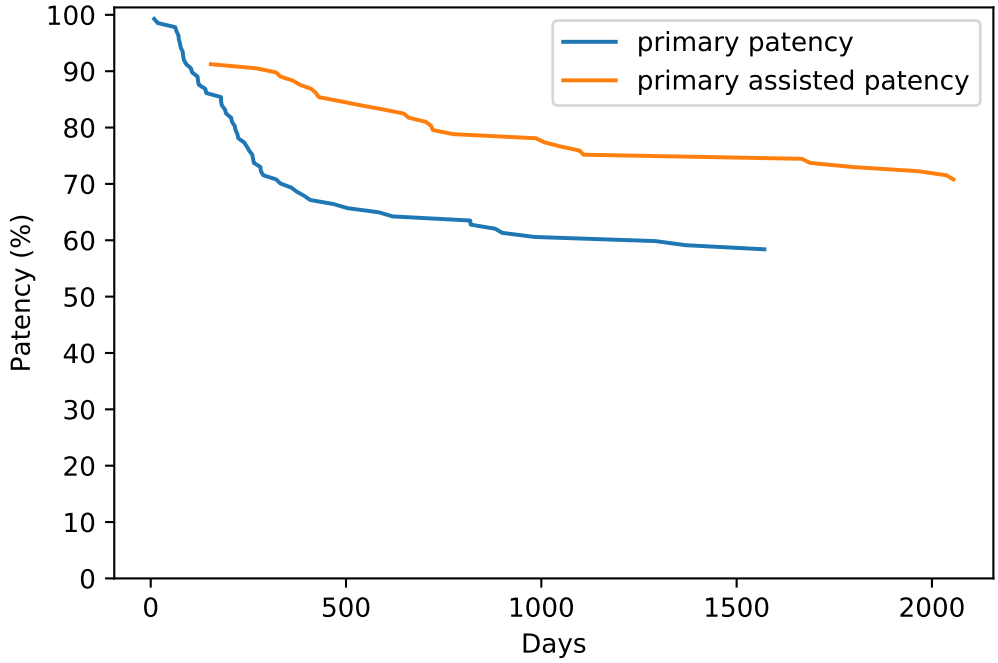

Figure 2.2: Primary and primary assisted AVF patency of the whole study cohort. Each step down represents one loss of primary or primary assisted patency in the whole group.

2.3.1 Group Analysis

Full biochemistry results for the high and low-risk groups can be seen in table 2.1. When comparing the pre-operative biochemistry results, values for albumin, bicarbonate, CRP, and ferritin were found to differ at a statistically significant level between the high and low-risk groups (all $p < 0.05$). Differences in phosphate levels were approaching significance ($p = 0.08$). Differences between the high and low-risk groups for these markers can be seen in figure 2.3. History of previous haemodialysis was more common in the high-risk group ($p = 0.06$). Percentage saturation of transferrin (SATN), and iron showed the highest correlation of 0.7 (see figure 2.4). Percentage saturation of transferrin was removed from further analysis at random as neither removal had a large effect on the final model.

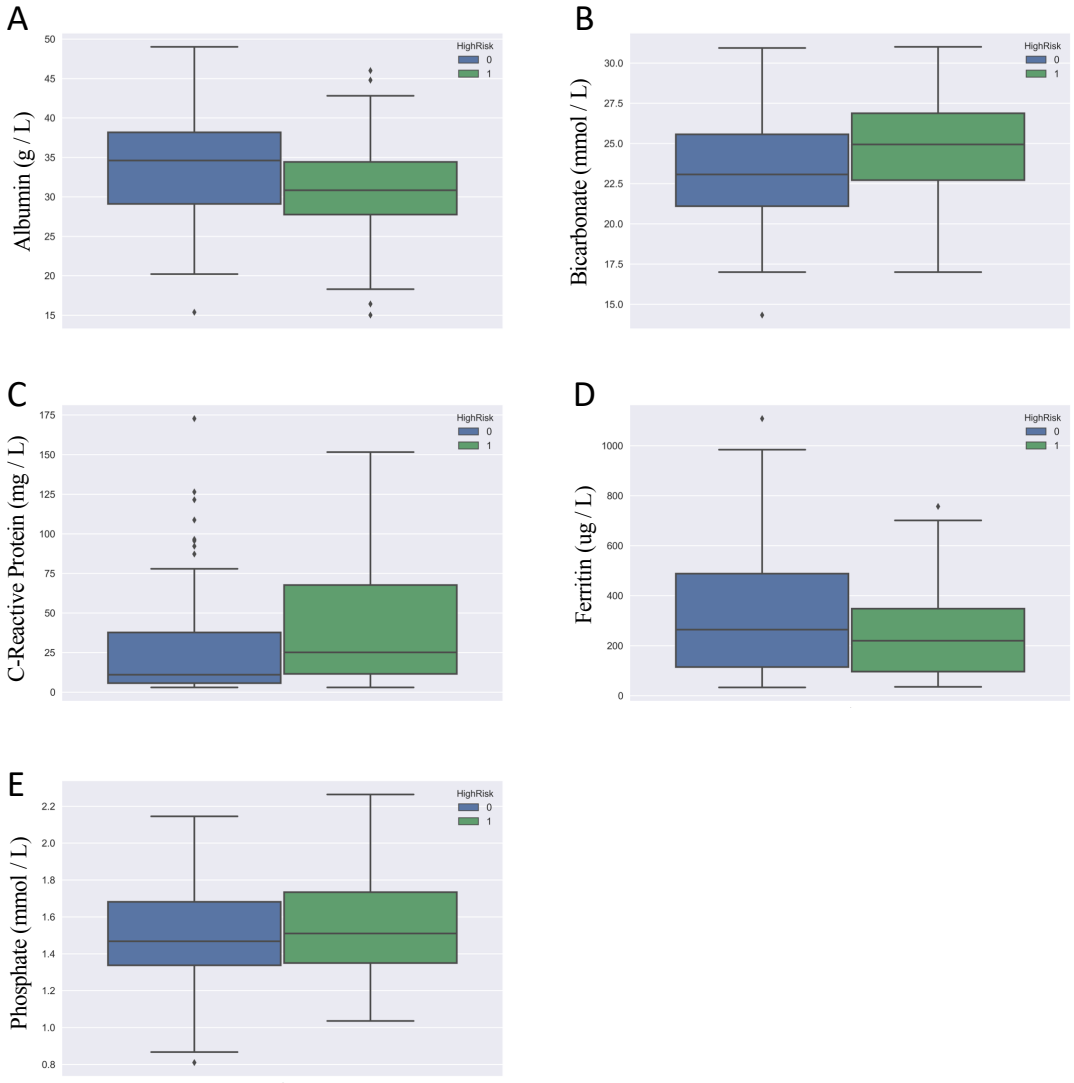

Figure 2.3: Boxplots of statistically different blood measurements between the high and low-risk groups. A : Albumin, B : Bicarbonate, C : C-Reactive Protein, D : Ferritin, E : Phosphate

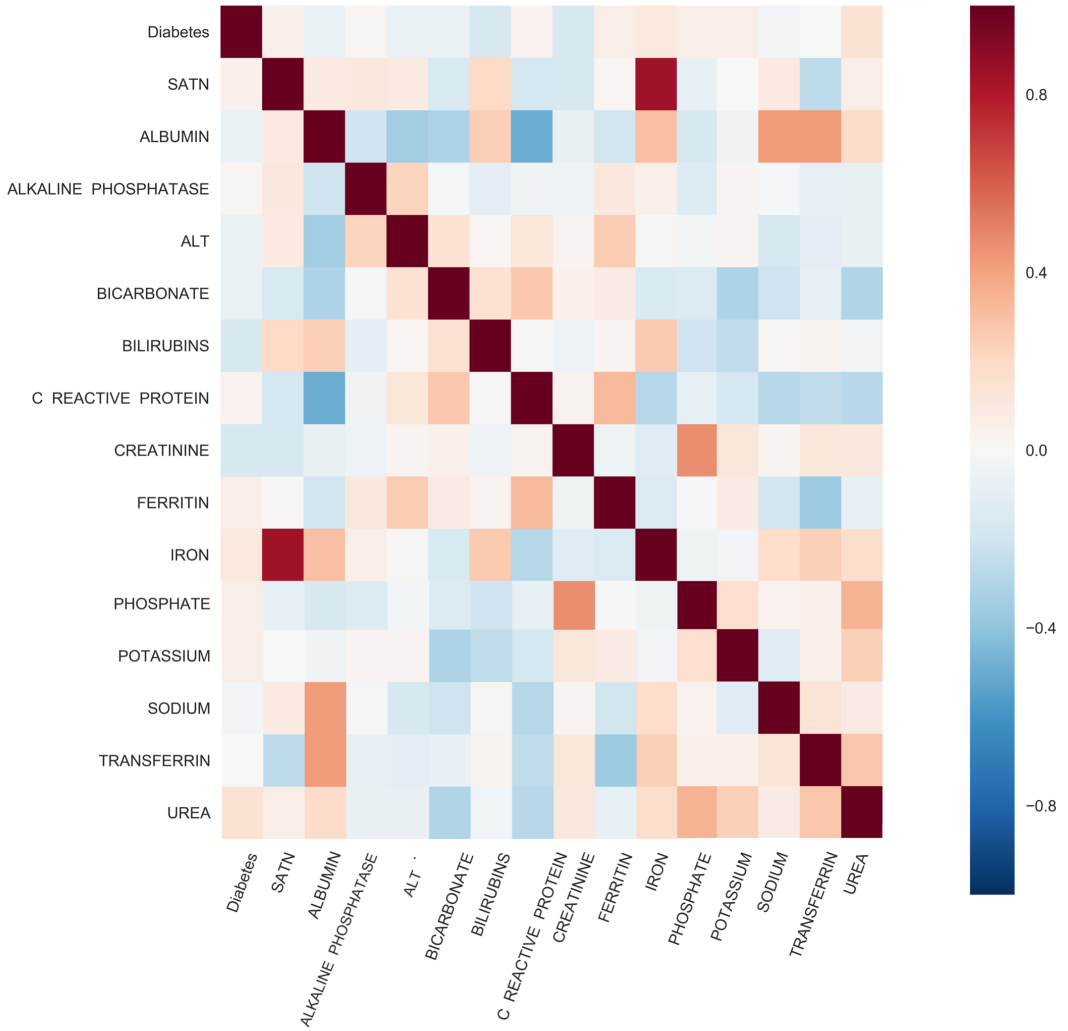

Figure 2.4: Heatmap of correlations between variables, with bolder colour indicating a higher value of Pearson's R statistic between pairs of variables as indicated on the x and y axes. A high correlation was observed between iron and % saturation of transferrin, as indicated by the bold colouring.

Sub-group analysis revealed differences in biochemistry measurements between patients with and without previous HD. These differences can be seen in table 2.2 and figure 2.5. These differences are likely caused by the different uremic state of these patients, and certain treatments in HD patients such as iron infusions, and the presence of bicarbonate products in the dialysate.

A logistic regression model was used to assess if variables were statistically associated to the classification of the patient as high or low-risk, using variables identified previously, controlled for known risk-factors. The model suggests that decreased pre-operative ferritin, and increased phosphate increases the risk of a negative AVF outcome at a statistically significant level. Full results from the binomial GLM can be seen in table 2.3. Pearson's Chi-square statistic was large for this model ($p << 0.05$).

	Prev. HD	No prev. HD
Albumin (g / L)	30.5 ± 6.2	34.5 ± 6.5
Bicarbonate (umol L)	24.7 ± 3.5	23.2 ± 3.0
C-reactive protein(mg / L)	42.1 ± 40.3	23.2 ± 28.5
Iron (umol L)	9.4 ± 2.9	11.4 ± 3.7
Transferrin (g / L)	1.9 ± 0.3	2.1 ± 0.3
Urea (mmol / L)	18.8 ± 5.4	20.9 ± 4.7

Table 2.2: Variables which showed significant differences between the group with previous dialysis history, and no previous dialysis history. All $p < 0.05$. Variables not included in this table, but present in table 2.1 were not statistically significant between the groups

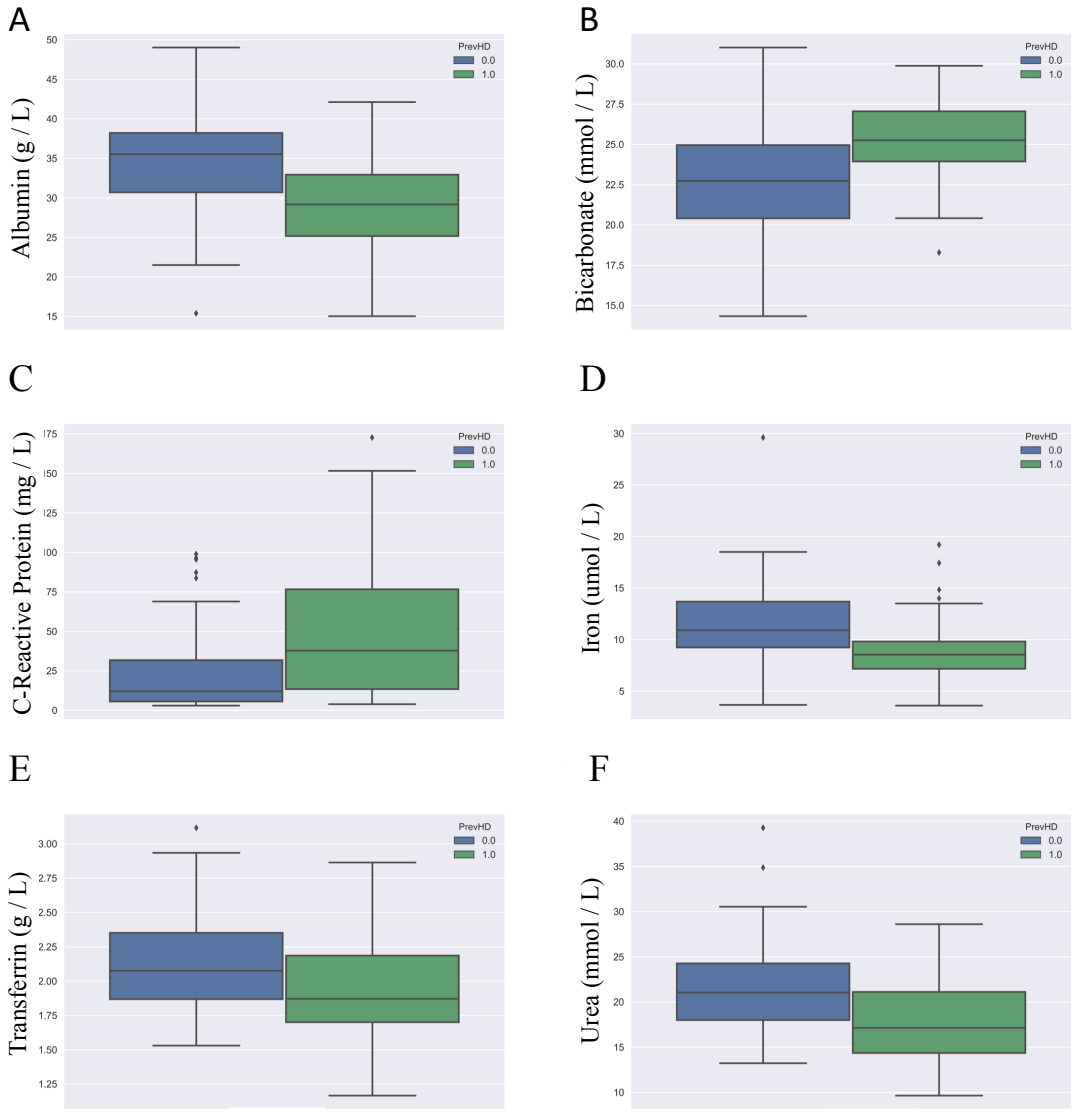

Figure 2.5: Boxplots of statistically different blood measurements between the prev. HD and no prev. HD groups. A : Albumin, B : Bicarbonate, C : C-Reactive Protein, D : Iron, E : Transferrin, F : Urea

A KNN algorithm was used to predict the outcome of 35 patients in a random test set taken from the full cohort of 137 patients, after training on a dataset including AVF outcome, ferritin, phosphate and diabetes. Optimised model parameters were: neighbors = 4, weighting = distance, train-test split = 0.25 stratified to the outcome. The accuracy

	Coefficient	p-value
Age	-0.009	0.66
Sex male	-0.6	0.22
Upper-arm AVF	0.11	0.84
Prev. HD	0.35	0.52
Diabetes (type 1 / 2)	-1.99 / 0.8	0.07 / 0.12
Albumin	-0.08	0.09
Bicarbonate	0.15	0.08
Bilirubins	0.2	0.06
C-reactive protein	0.009	0.21
Ferritin	-0.004	**0.003**
Phosphate	1.88	**0.03**
Pseudo R2	0.33	
Chi-squared	105.6	

Table 2.3: Output from logistic regression model, modeling patient outcome as high or low-risk

of predictions was 77 %. The model correctly predicted the outcome of 27 patients, including 20 true negatives and 7 true positives, 4 false positives and 4 false negatives.

2.4 Discussion

A retrospective study of primary-AVF outcome at one-year, in a cohort of patients at this institution was performed. Analysis of blood-serum markers and demographic factors, and their relations to the outcome of AVF creation was undertaken. Health informatics methods allowed creation of a detailed timeline for each patients AVF. This included detailed US-based surveillance data, allowing identification of the specific causes of AVF-failure. Retrospective studies often suffer from limitations such as incomplete data, and inaccuracies.

AVF failure is the Achilles heel of successful HD treatment. Once matured, AVFs offer increased long-term patency, reduced infection rates and likelihood of thrombosis or stenosis. However, AVF failure is a significant source of morbidity in the dialysis population, with associated costs and disruption to a patient's life. In our institution, we have observed a loss of primary patency in 33% of patients within one year. If biomarkers can be identified that can independently or cumulatively predict risk for AVF failure prior to creation, a patient could be selected for more rigorous surveillance, an alternate VA, or counseling towards the risk of AVF failure.

During statistical analysis, adherence was payed to reporting guidelines defined by SAMPL [87]. This included assessing model fits and attempting to validate the model. Logistic regression analysis suggested lower pre-surgical ferritin and increased phosphate levels can increase the risk of all-cause AVF-failure within one year. A large chi-square statistic suggested that the predicted distribution of high-risk patients in the logistic regression models did not fit the expected distribution, indicating poor model fit. Along with the small sample size, this causes us to question the power of the markers (phosphate and ferritin) as independent risk-factors of AVF failure. Although only consisting of 137 patients, this is an improvement over previous attempts, which have primarily been in cohorts smaller than 100 [118]. Bivariate analysis showed a difference in albumin measurements between the two groups, however this was likely explained by the previous dialysis history of the patients. In agreement with multiple previous studies [17, 28, 76, 118], logistic regression analsysis demonstrated no relation between AVF outcome and the inflammatory markers CRP and albumin.

As a form of model verification, a KNN algorithm was used to classify patients as high or low risk, based on their ferritin, phosphate and diabetes values prior to AVF creation. This model performed relatively well, successfully classifying correctly 77% of

patients in the test-set. Verification of this algorithm would be required in other cohorts before being fully accepted, however this represents a step towards the health-informatics approach desired in many institutions. Further prospective studies of these markers are required to determine the power of these predictions, and to determine if cut-off levels exist which can predict the outcome of the AVF.

This study includes some limitations, primarily a small sample size. Measurements of vessel diameter were not included in this analysis. If one takes the view that AVF failure is a multi-factorial problem, known risk-factors such as vessel diameter and presence of calcium in the vessels should be included in modeling. This study was not designed to assess the multi-factorial view and would have lacked statistical power for such an analysis. It is noted that none of the markers identified during the exploratory ANOVA testing would have been recorded as significant if multiple-hypothesis correcting had been applied. However, as the goal of the study was not to compare means between the groups, their inclusion in the model is justified.

Patients with ESRD can have fluctuating concentrations of proteins in the blood, due to the nature of the disease (see figure 2.6). This adds a source of noise into the measurements assessed in this study. In attempt to filter this noise, averaging over a 6-month timeframe prior to AVF creation was performed, with six-months chosen as this is within the planning period recommended by K-DOQI guidelines.

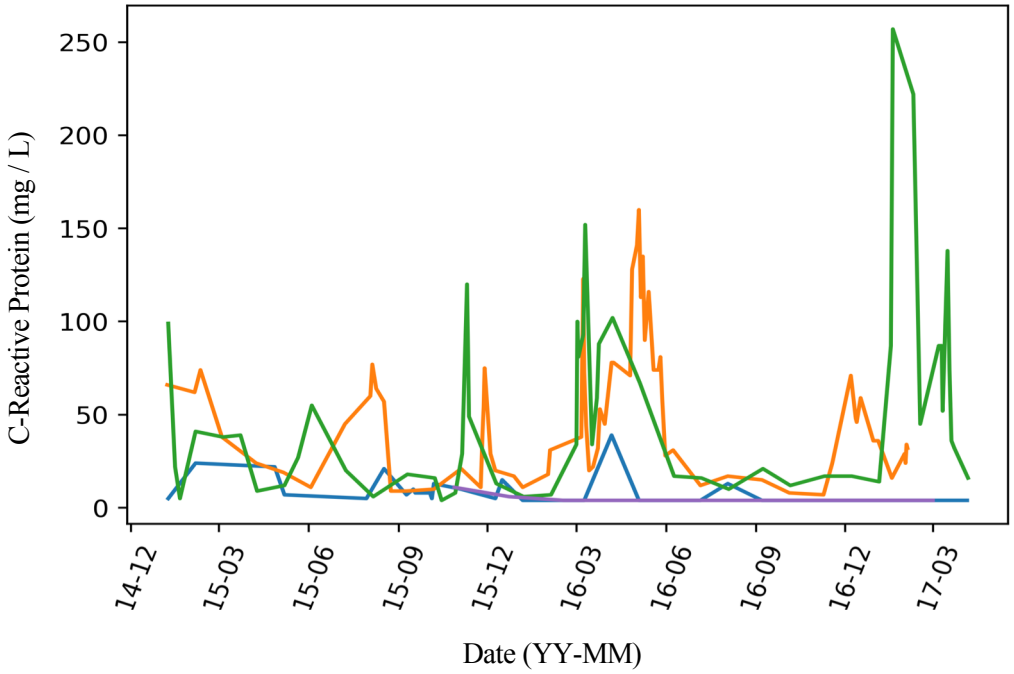

Figure 2.6: CRP measurements over time for four randomly selected patients in the study cohort, showing the varying nature of concentration in the blood. Due to this, an average was taken over the six months prior to AVF creation to reduce the apparent noise in the measurement.

Primary patency at one-year was approximately 67%. This is in agreement with literature values of 1-year primary patency [3, 90], and provides the most recent record of primary AVF patency for this institution. Primary assisted patency was very high at 1-year, at approximately 91% , superior to values previously reported at 78% at 65 weeks [7]. This institution performs a rigorous US based surveillance program with patients scheduled for follow up at six weeks, three months, six months and one-year post AVF creation. AVFs are intervened on early when stenoses are identified within the AVF and compared with relative HD parameters before intervention is confirmed - typically only if the stenosis is adversly affecting HD. It is however possible that this surveillance/intervention practice reduces primary patency in exchange for increased primary assisted patency, cost analysis would be required to determine if this is a justified tradeoff. In light of this results, perhaps a more appropriate use of these serological markers may lie in the differentiation of patients who require surveillance, and those who do not. Future work could assess if ferritin and phosphate show high sensitivity towards those who do not require intervention, thus acting as a screening tool for those who require surveillance of their AVF. If successful, this would act to free up valuable time in vascular clinics.

It is possible that the observation is related to early signs of vascular calcification. Phosphate and ferritin have both been observed to act in the vascular calcification pathway, having inductive and inhibitive effects respectively [48, 99, 73, 190]. The combined observation of increased phosphate and reduced ferritin is in line with results from Zarjou *et al* [190], suggesting that ferritin inhibits calcification of smooth muscle cells, whilst phosphate inhibits calcification through the up-regulation of bone lineage genes. Calcium phosphate products have been identified in vascular samples of stenotic AVFs previously [125]. Hyperphosphatemia has previously been identified in patients with AVF failure [115, 116], suggesting a preventative treatment may be beneficial. There may be some value in phosphate binding therapies in this population if further evidence is found.

In conclusion, low pre-operative ferritin and increased phosphate were found to be related to AVF outcome, however a poor model fit and small cohort causes us to question this relationship. Additional research into pre-operative ferritin and phosphate levels may be beneficial, in particular to determine if cut-off levels exist which can aid in decision making. We have observed very low loss of primary assisted patency in this cohort, demonstrating the benefits of rigorous US-based surveillance of a patient's vascular access. However, loss of primary patency remains comparable to literature reports.

Chapter 3

Novel Pre-Operative Ultrasound Risk Factors

3.1 Introduction

Vessel diameter measurements from US remain the deciding factor for AVF creation, yet failure rates remain high. US presents as a good modality for identification of additional risk-factors due to its high specificity and sensitivity, as well as its availability, cost, and current implementation in many vascular access clinics. Modern markers of arterial strain and stiffness from US have proved useful in certain patient groups.

Using VVI, Ma *et al* [100] observed that the carotid artery of pregnant women with pre-eclampsia produce irregular velocity profiles, and had lower strain values than normotensive pregnant women. Cho *et al* [36] had similar findings regarding vessel wall movement in patients with Takayasu's arteritis. This suggests that in certain groups of patients, the vessel movement is not synchronised. Studies have also recorded that strain measurements from VVI correlate well with PWV [138, 77].

SWE has recently found use in the cardiovascular system. Li *et al* [94] imaged the carotid of patients with ischemic stroke using SWE. Longitudinal measurements of SWE correlated well with PWV ($r = 0.7$), and both modalities identified increased arterial stiffness in the patient group when compared to healthy controls. Ramnarine [144] found SWE to be a sensitive method for classifying carotid plaques that may be associated with neurological symptoms.

This chapter aims to answer the research question: *can US-based markers of strain (e.g. VVI) and elasticity (e.g. SWE) act as pre-operative risk-factors for late AVF failure or failure to mature?* As part of work-up for AVF creation, all patients awaiting HD in Ninewells undergo a pre-operative US assessment. This chapter focuses on the implementation of 2 new US methods, VVI and SWE. as part of the US based pre-operative workup for AVF creation in a retrospective single centre study. SWE and VVI are first demonstrated in a healthy cohort, before being compared to a patient group awaiting AVF creation. The patients underwent follow-up for a period of up-to six months post-AVF creation. These measurements were then statistically analysed in order to determine if they could act as independent risk-factors for AVF-failure.

3.2 Materials and Methods

3.2.1 Study Population and Ethical Approval

Patients were included in this study if they underwent a pre-operative US assessment for AVF creation between November 1, 2016 and December 31, 2017.

From notes held in the vascular laboratory, patient age, BMI, and co-morbidities were collected. Patient US images were acquired retrospectively from databases which hold all images taken during the pre-operative assessment for AVF creation. Pre and post-operative vessel diameters were obtained from routine B-mode US images. Brachial artery SWE maps were obtained from the pre and post-operative assessment images.

Caldicott Guardian approval was granted for retrospective collection and analysis of patient data, including images. A control group of healthy volunteers was recruited locally, and informed consent was granted from each individual. East of Scotland Research Ethics Committee approval was granted for this study.

3.2.2 Volunteer Recruitment

Ethical approval was granted to recruit 40 healthy volunteers (HV) to take part in this study. A4 posters (see figure 3.1) were placed around Ninewells hospital and medical school asking those interested in the study to contact the lead researcher by email. Records of contact were maintained, and an anonymised key of participants was kept. Volunteers were asked their age, BMI, current medical prescriptions, and the presence of any disease such as diabetes or hypertension. Volunteers with conditions such as these were disqualified from taking part.

3.2.3 Ultrasound Imaging

Initial set-up for US imaging was identical regardless of the assessment performed, for both HV and patients. These scans were performed on an S2000 Ultrasound machine (Siemens, Germany), with VVI and SWE software installed, by one of two operators. The SWE software is compatible with the 9L4 range of transducers, thus a 9Mhz 9L4 transducer was used for all scans.

Three ECG patches were placed on the participant and connected to the US machine. The red electrode was placed below the right clavicle, the yellow electrode below the left clavicle, and the green electrode at the lower left ribcage.

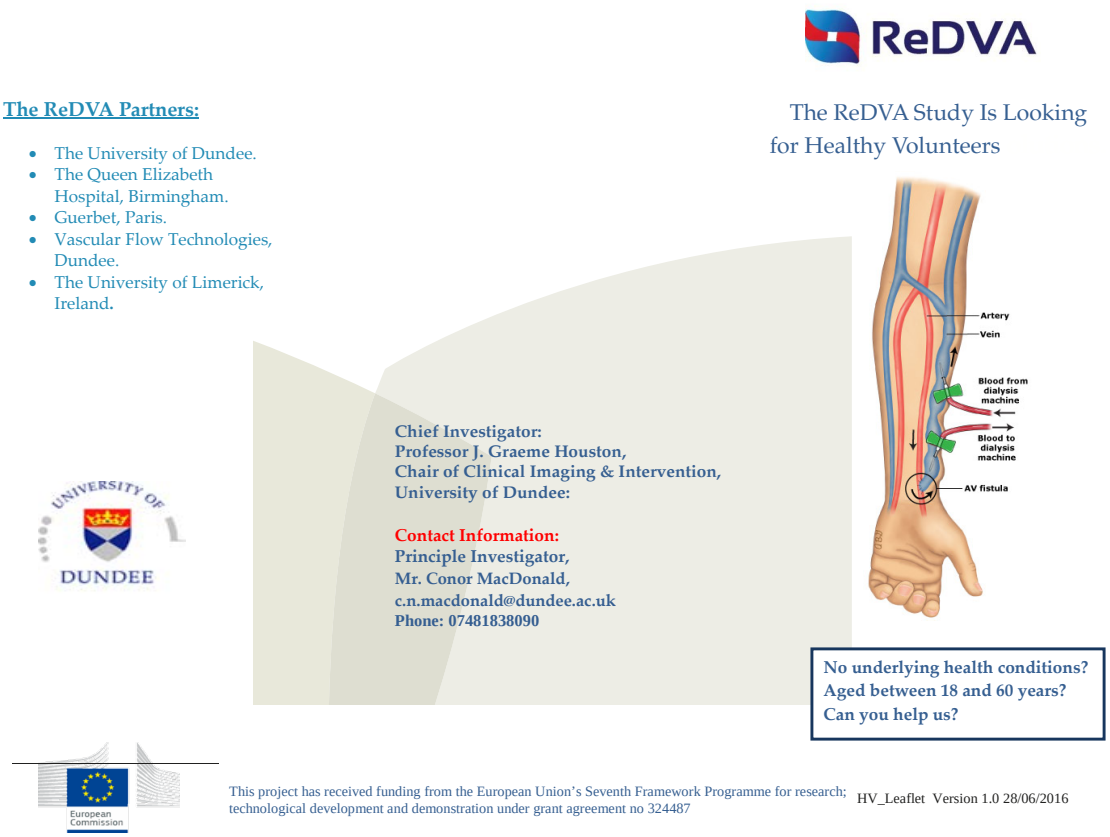

Figure 3.1: Poster advertising the study

All scans were conducted using a 9MHz linear transducer (Tx) in B-mode at a frame rate of approx. 30 Hz. Participants were seated facing the operator and the arm of interest extended over a pillow as in figure 3.2.

Figure 3.2: Participant positioning for US scanning

3.2.4 VVI Imaging and Analysis

The Tx was used to locate a straight segment of the brachial artery proximal to the cubital fossa in a cross-sectional view. Using the video capture function of the US machine, a 5 second cine loop was captured of the brachial artery in a cross-sectional view. The Tx was then rotated through 90 degrees to obtain a longitudinal view of the artery with clear intima. A 5 second cine loop was captured using the image capture button on the US machine. All images were stored on the hard-drive of the US machine for analysis.

Image analysis was performed on the Siemens syngo Velocity Vector Imaging (VVI, Siemens) package. Video series of the cross-sectional arterial view were selected and loaded into the VVI package. Selecting the "Short Curve" option allowed placement of a freehand region of interest (ROI) on the image. A freehand contour/ROI was placed within the vessel wall of the artery using 6 points as in figure 3.3, between the intima and vessel lumen.

2D velocity vectors corresponding to points on the contour are calculated via the speckle tracking algorithm, and knowledge of the frame-rate. Geometric displacement (ΔL) of the speckle between frames allows knowledge of the displacement (d) of the tissue, and the frame rate ($\frac{1}{\Delta t}$) details the time taken for this movement, allowing calculation of velocity (v) through the well known formula $v = \frac{d}{t}$. Strain (ϵ) and strain rate can then be calculated from from knowledge of the original speckle/contour geometry (L_0):

$$\epsilon = \frac{\Delta L}{L_0} \tag{3.1}$$

and

$$\frac{\Delta \epsilon}{\Delta t} = \frac{\Delta v}{L_0} \tag{3.2}$$

VVI output consists of graphs of velocity, strain, strain rate and displacement as a function of time with the vessel wall was divided into six segments (see figure 3.4). The amplitudes of peak velocity, strain, strain rate and displacement were taken for all six segments, and then averaged over three cardiac cycles.

Once analysis of the cross-sectional arterial view was completed, the longitudinal view was loaded into the VVI module. Using the "Long Curve" mode, an open rectangular ROI was placed along the wall of the artery using six points as in figure 3.5. The same measurements were taken for longitudinal motion as before.

Figure 3.3: short-axis ROI of brachial artery showing freehand ROI placement around the lumen of the artery

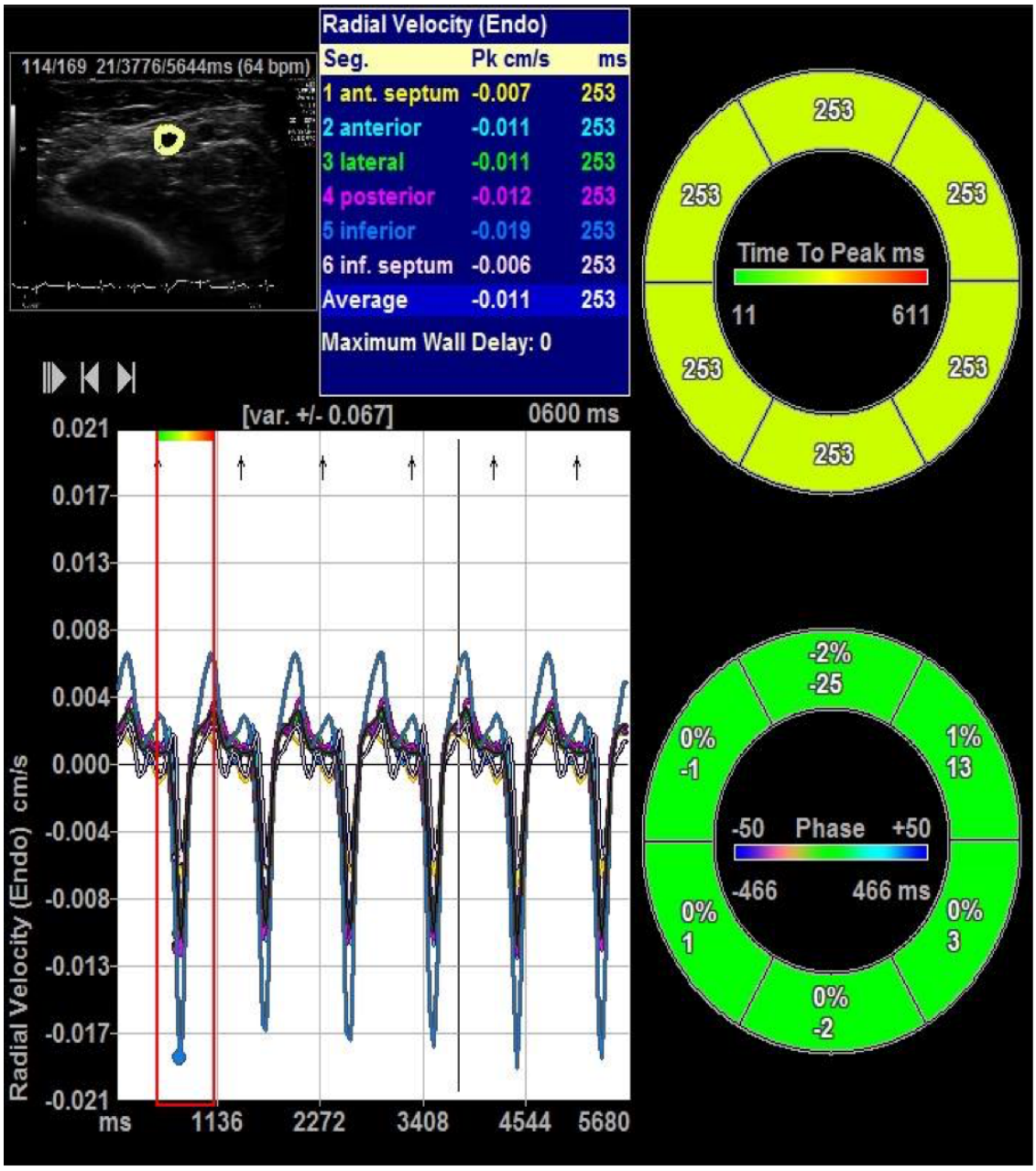

Figure 3.4: VVI output for two a healthy volunteer showing a periodic radial velocity profile

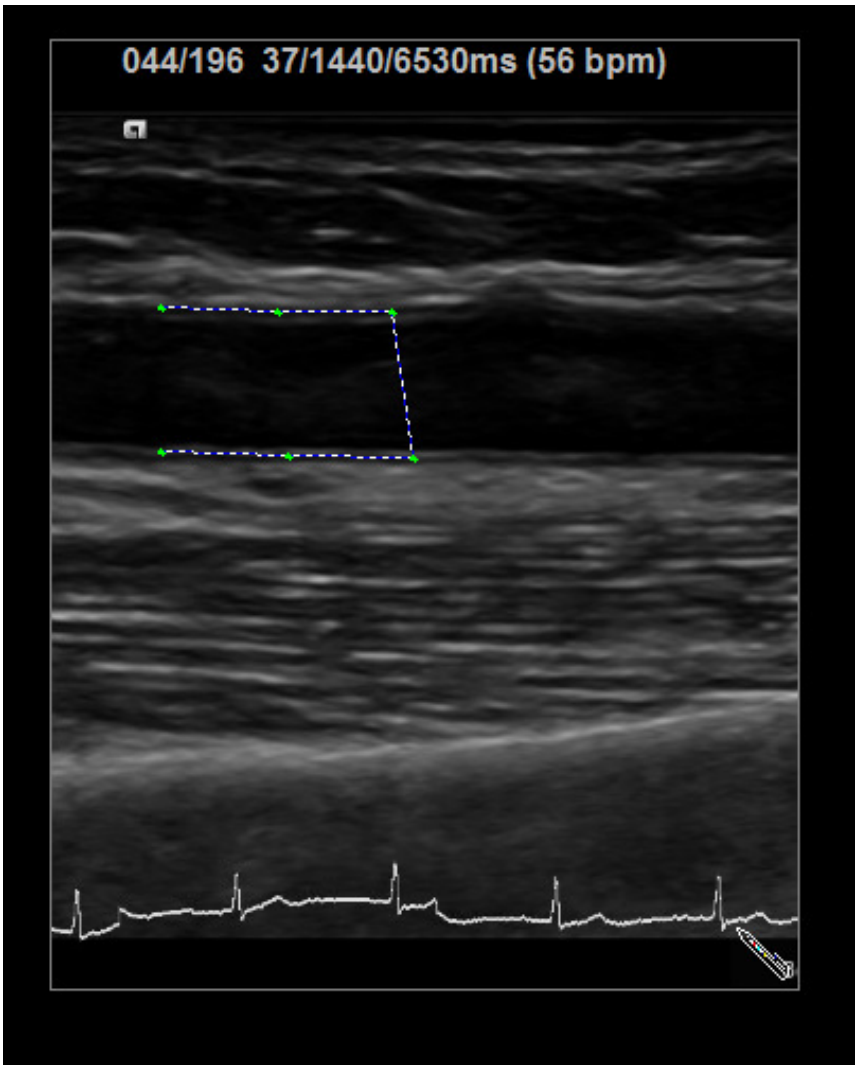

Figure 3.5: long-axis ROI of brachial artery showing open box ROI placement within the intima of the artery

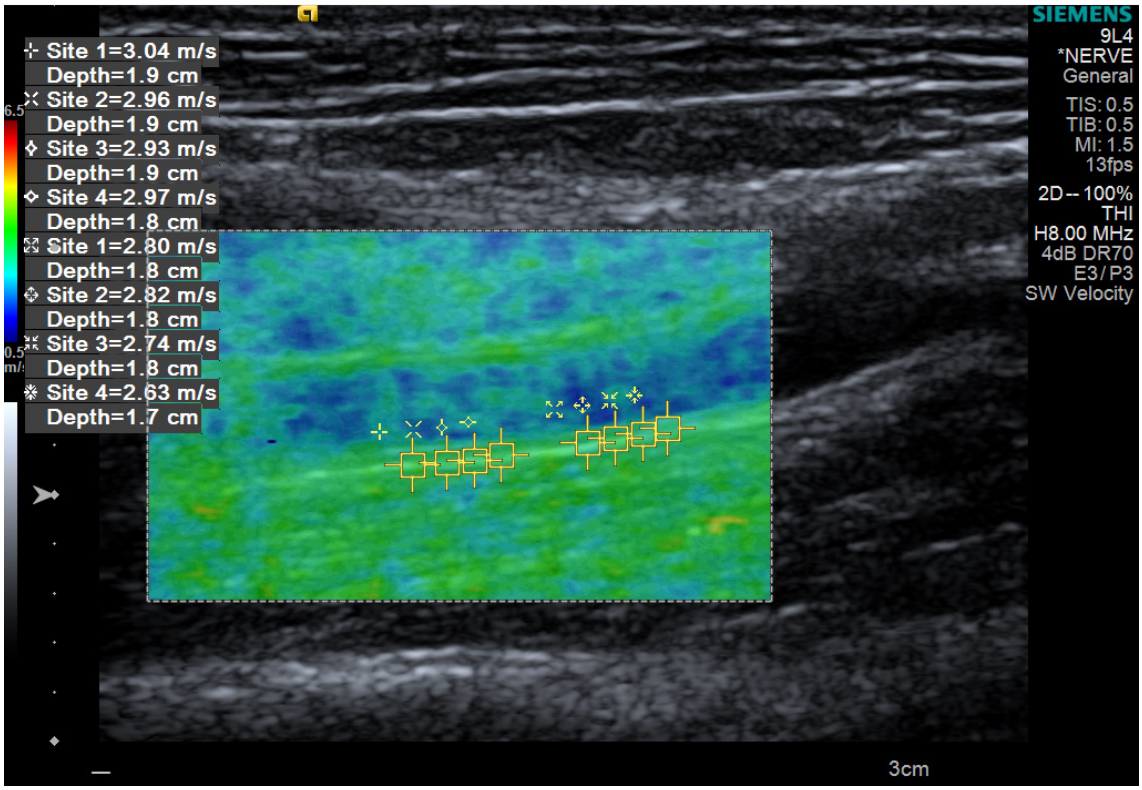

Figure 3.6: SWE map with ROI placement along the brachial artery wall, fully enclosing the intima layer. This segment was not completely parallel to the transducer surface, resulting in varying depth of measurement points.

3.2.5 SWE Imaging and Analysis

The Tx was used to locate a straight segment of the brachial artery proximal to the cubital fossa in a cross-sectional view. The Tx was then rotated through 90 degrees to obtain a longitudinal view of the brachial artery. A clear view of the intima layer of the artery was desired. Vessel walls parallel to the Tx axis were prioritised over non-parallel regions to avoid errors in shear wave velocity estimation due to varying depth.

The shear wave elastography function (Virtual Touch IQ) was selected on the machine, and a rectangular shaped ROI was placed over the vessel wall. Upon user input, the Tx produced a pulsed wave which generated a shear wave in the tissue. The shear wave velocity was then displayed as a velocity map superimposed over the B-Mode image (see figure 3.6). 8 square shaped ROIs were placed along the vessel wall enclosing the intima as in figure 3.6, avoiding any areas of noise. All images were stored on the hard-drive of the US machine for analysis.

3.2.6 Statistical Analysis

Analysis was performed in Python version 2.7, using the "seaborn", "pandas", "scipy" and "matplotlib" packages, and RStudio (RStudio inc, US). All data were collated as mean $\pm$ standard deviation. Data distributions were assessed graphically. Differences in data between volunteers and patients were assessed using the unpaired Student's T-Test and the Mann-Whitney U test. Categorical data was assessed using the chi-squared test. Correlations between variables were assessed using Pearson's r statistic.

15 HVs were selected at randomly to undergo identical tests by additional US operator. Pearson's r statistic was used to assess correlation between the users, and the intraclass correlation coefficient (ICC) to assess agreement. Agreement between the operators was assessed graphically, with an ordinary least squares (OLS) method used to fit a best-fit line, according to the code below.

```
import numpy as np
import matplotlib.pyplot as plt


def least_sq_line(x, y):
  m = np.sum((x - x.mean())*(y - y.mean()))
      /np.sum((x - x.mean())**2)
  c = y.mean() - m*x.mean()
  x1 = np.linspace(min(x), max(x), len(x))
  formula = m*x1 + c
  print("m = ", m)
  print("c = ", c)
  plt.plot(x1, formula, "--", label = "linear-fit")
  plt.scatter(x, y)
  plt.legend()
  plt.show()
```

20 HVs were selected at random to undergo assessment of both the left and right arm to determine if the measurements were homogenous between the arms. Results from the two arms were compared using a Wilcoxon signed-rank test, used to compare two related samples, allowing determination if the two samples were taken from populations having the same distribution.

Post-operatively, differences in the vasculature following AVF creation were assessed

graphically and by using the paired students T-test. OLS regression models were used to assess the influence of brachial artery elasticity or strain, pre-operative vessel diameters, and demographic factors on arterial and venous diameter 6-weeks post AVF creation. A logistic regression model was then used to assess the predictive power of US and demographic variables on the three-month outcome of the AVF. Three months was chosen due to the timeframe of the PhD, and was realistically the longest possible whilst allowing the maximum number of patients to be included. A negative outcome was defined as the presence of significant stenosis or occlusion in the AVF as indicated by vascular laboratory notes i.e. inclusion in the dysfunction group.

Model fits were assessed by analyzing the residuals, R-squared values and variance inflation factor values. Type-3 anova testing was performed to assess the effect of variable order in the models. Variables were assessed for correlation to avoid multicollinearity. Alpha values for statistical significance were taken to be 0.05.

3.3 Results

Data was available for 47 patients who underwent a pre-operative assessment between November 1, 2016 and December 31, 2017. All 47 patients underwent a pre-operative SWE assessment and 32 patients underwent a pre-operative VVI assessment. 33 patients ultimately had an AVF created in the study period, and all underwent one post-opearative SWE assessment at 6 - 12 weeks. 40 healthy volunteers were recruited to act as a comparator group and all underwent SWE and VVI assessment. Patient and HV demographics can be seen in table 3.1. Significant differences in pre-operative brachial artery diameter ($p < 0.05$), age ($p < 0.05$) and body mass index (BMI) ($p < 0.05$) were observed between the two groups. Pre-operative US measurements of SWE and VVI can be viewed in table 3.2.

	Patient Group (n = 47)	HV Group (n = 40)	p-vale
Age (years)	66 ± 13	36 ± 15	< 0.05
Male (%)	55	45	0.34
BMI (kg/m^2)	29 ± 6	23 ± 6	< 0.05
Diabetes (%)	38	0	-
Hypertension (%)	77	0	-
Pre-operative brachial artery diameter (mm)	5.0 ± 1.0	4.0 ± 0.6	**0.002**
SWE assessment (%)	100	100	-
VVI assessment (%)	100	68	-

Table 3.1: Patient and HV demographics

3.3.1 Pre-opearative US tests

Shear Wave Elastography

SWE maps were taken for all 47 patients, and all 40 volunteers. Significant differences were seen for measurements of SWV between the patient and HV groups (patient SWV 3.2 ± 0.5 m/s, HV 3.4 ± 0.4 m / s, p = 0.03) (see figure 3.7). A statistically significant negative association between age and shear wave velocity was observed (r = -0.2, p = 0.05), a scatter plot with a regression line fitted can be seen in figure 3.8. No significant difference was observed between the left and right arm in 20 patients when assessed using Wilcoxon ranked test (p = 0.70).

When considering the whole group (n = 87), no significant differences in SWV were observed between subjects with diabetes and no diabetes (no diabetes 3.2 ± 0.5 m/s, diabetes 3.1 ± 0.6 m/s, p-value=0.1). A significant difference in SWV was observed between

Measurement	Patient	Volunteer	p-value
Shear Wave Velocity (m / s)	3.2 ± 0.5	3.4 ± 0.4	**0.03**
Radial Velocity (cm / s)	0.01 ± 0.01	0.01 ± 0.01	0.23
Radial Strain (%)	2.0 ± 1.5	1.6 ± 0.9	0.11
Radial Strain Rate (/s)	0.1 ± 0.1	0.1 ± 0.1	0.15
Radial Displacement (mm)	0.03 ± 0.02	0.02 ± 0.04	0.18
Longitudinal Velocity (cm / s)	0.03 ± 0.03	0.02 ± 0.02	**0.02**
Longitudinal Strain (%)	1.6 ± 1.7	0.9 ± 0.9	0.06
Longitudinal Strain Rate (/s)	0.1 ± 0.1	0.07 ± 0.06	**0.03**
Longitudinal Displacement (mm)	0.05 ± 0.06	0.03 ± 0.04	0.06

Table 3.2: Ultrasound Measurements

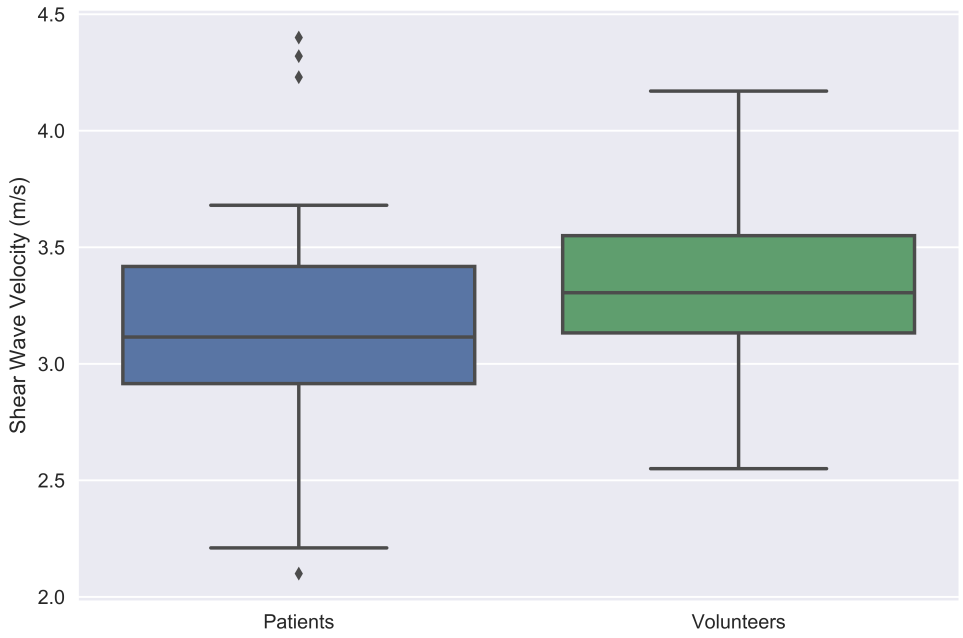

Figure 3.7: Boxplots of shear wave velocity values for patients and volunteers, horizontal lines inside the coloured boxes indicate median values

subjects with hypertension and no hypertension (no hypertension 3.4 ± 0.4 m/s, hypertension 3.1 ± 0.4 m/s, p-value=0.02) When only the patient group was considered, there was no difference between those with hypertension and no hypertension (no hypertension 3.3 ± 0.7 m/s, hypertension 3.1 ± 0.3 m/s, p-value=0.4)

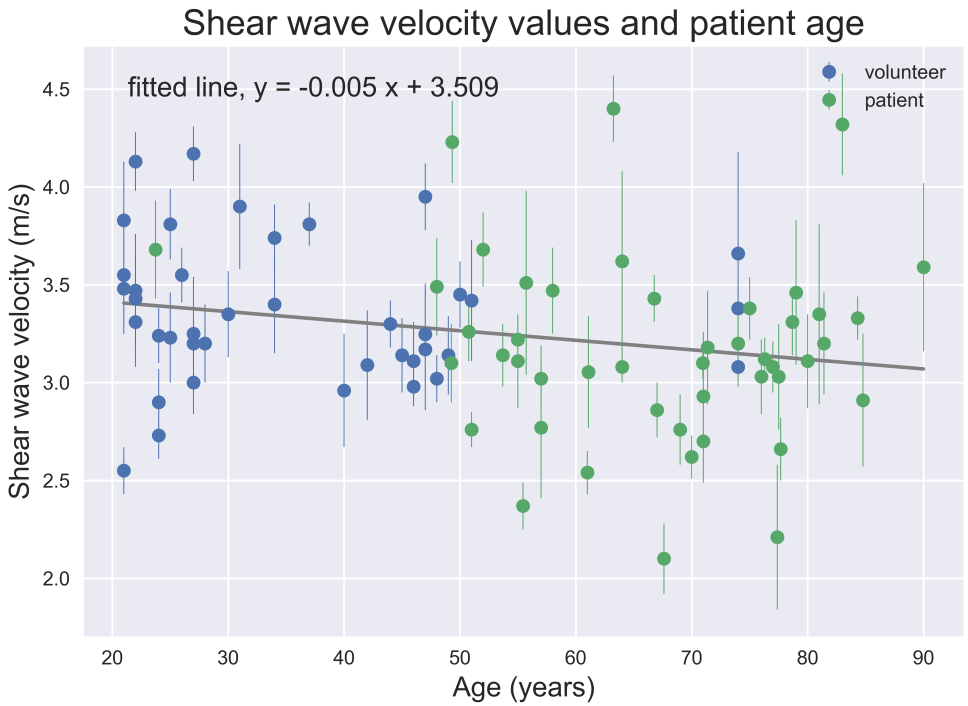

Figure 3.8: Scatter plot of age and shear wave velocity measurements for both patients and volunteers, with a regression line fitted. Vertical lines for each marker represent the standard deviation of a single measurement. A significant negative association is observed, pearson's r = -0.2, p = 0.05

Velocity Vector Imaging

VVI post-processing was attempted on images from 32 patients, and all 40 volunteers. VVI measurements were not possible, wholly or partially, in a number of patients (n = 6, 19 %). This was primarily due to problems associated with the patient's ECG readings (pacemaker n=1, 3 %, arrhythmia n=1, 3 %), and failure to obtain an ECG reading (n=1 3 %). The remaining patients (n=3, 10 %) produced vessel movement profiles that were highly out of sync and could not be interpreted. This may have been due to imaging technique, or highly dis-synchronous wall movement. Similarly, a number of HVs (n=6, 15 %) produced VVI measurements which were difficult to interpret. This was down to a poor ECG trace (n=2, 5 %) and highly dis-synchronous wall movement (n=4, 10 %). Figure 3.9 shows the radial displacement pattern for one of the 3 patients with dis-synchronous wall movement. VVI measurements were successful for the remaining cases.

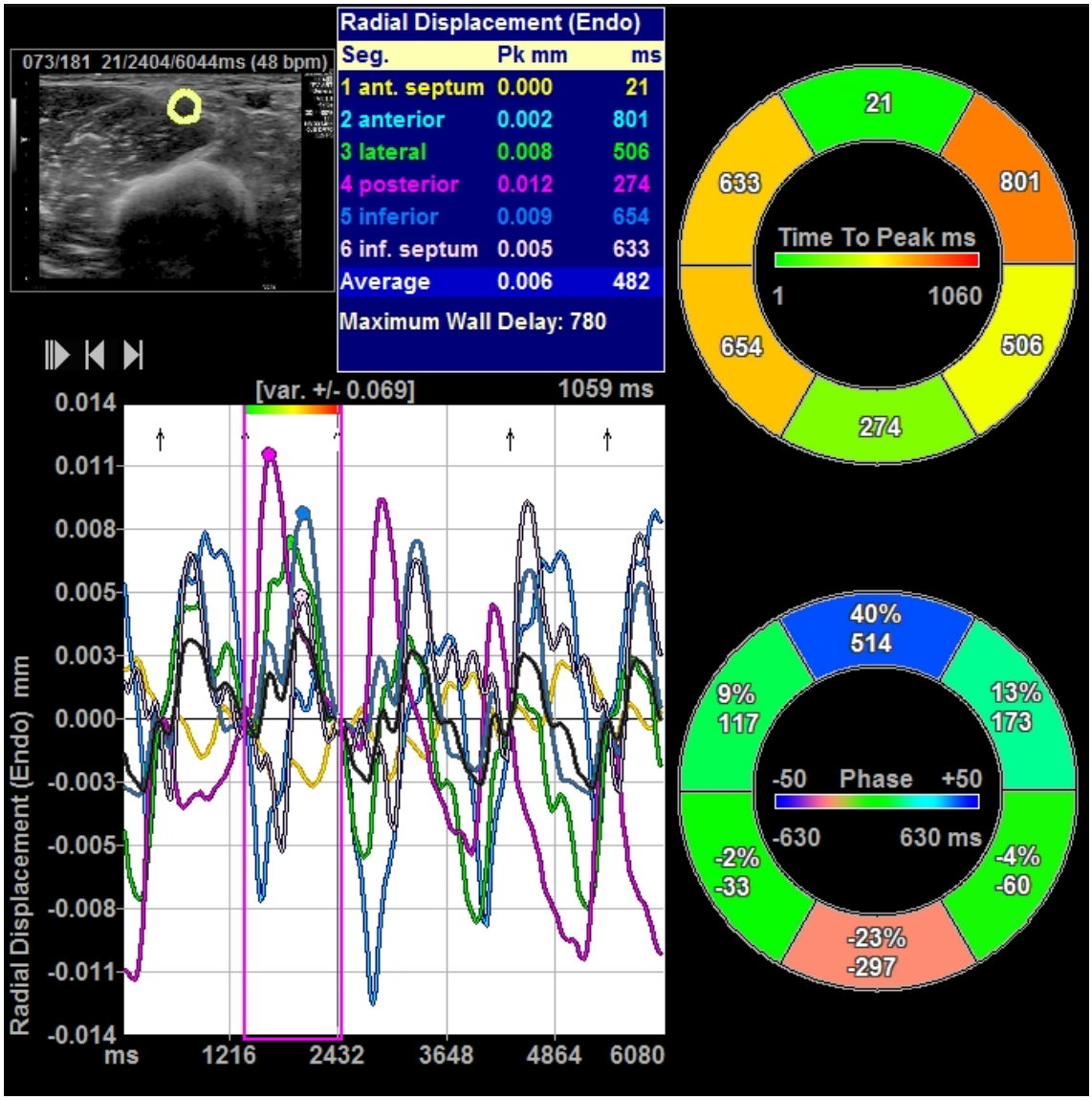

Figure 3.9: VVI output for a patient showing a highly chaotic radial displacement pattern.

Mean measurements from VVI can be viewed in table 3.2. The standard deviations were large for all measurements, indicating a large amount of noise present in the data. Significant differences were observed between the patient and HV group for measurements of longitudinal velocity (patient 0.03 $\pm$ 0.03 cm / s, HV 0.02 $\pm$ 0.02 cm / s, p = 0.02), and longitudinal strain rate (patient 0.1 $\pm$ 0.1 /s, HV 0.07 pm 0.06 /s, p = 0.03), with the HV group showing larger values for both measurements. Differences between the patient group and HV group for measurements of longitudinal strain and displacement were approaching significance (both p = 0.06).

No significant correlations with age were observed for any measurements from VVI. There were no differences in subjects with diabetes or hypertension compared to those without diabetes or hypertension for any of the VVI measurements assessed (all p $>$ 0.05 when assessed with MannWhitney U-test). In 20 patients, no significant difference was observed between the left and right arm using a Wilcoxon ranked test (p = 0.88).

3.3.2 Correlation between the measurements

The formula for the t-statistic for pearson's r given N degrees of freedom is:

$$t = \frac{r}{\sqrt{\frac{N-2}{1-r^2}}} \tag{3.3}$$

For a t-statistic of approximately 1.671 and 71 degrees of freedom we can determine that the cut-off value for a statistically significant r ($p < 0.05$) in this case is $\mid 0.16 \mid$.

A pair-plot demonstrating relationships between measurements can be seen in figure 3.10. From this plot it is evident that a number of correlations between the US measurements are present. Pearson's r statistic for these correlations can be seen in figure 3.11. A weak negative correlation between SWV and radial velocity (r = 0.2) and longitudinal velocity (r = 0.17) was observed. Significant positive correlations were observed between all radial VVI measurements, and all longitudinal VVI measurements. The strongest correlations were observed between longitudinal measurements.

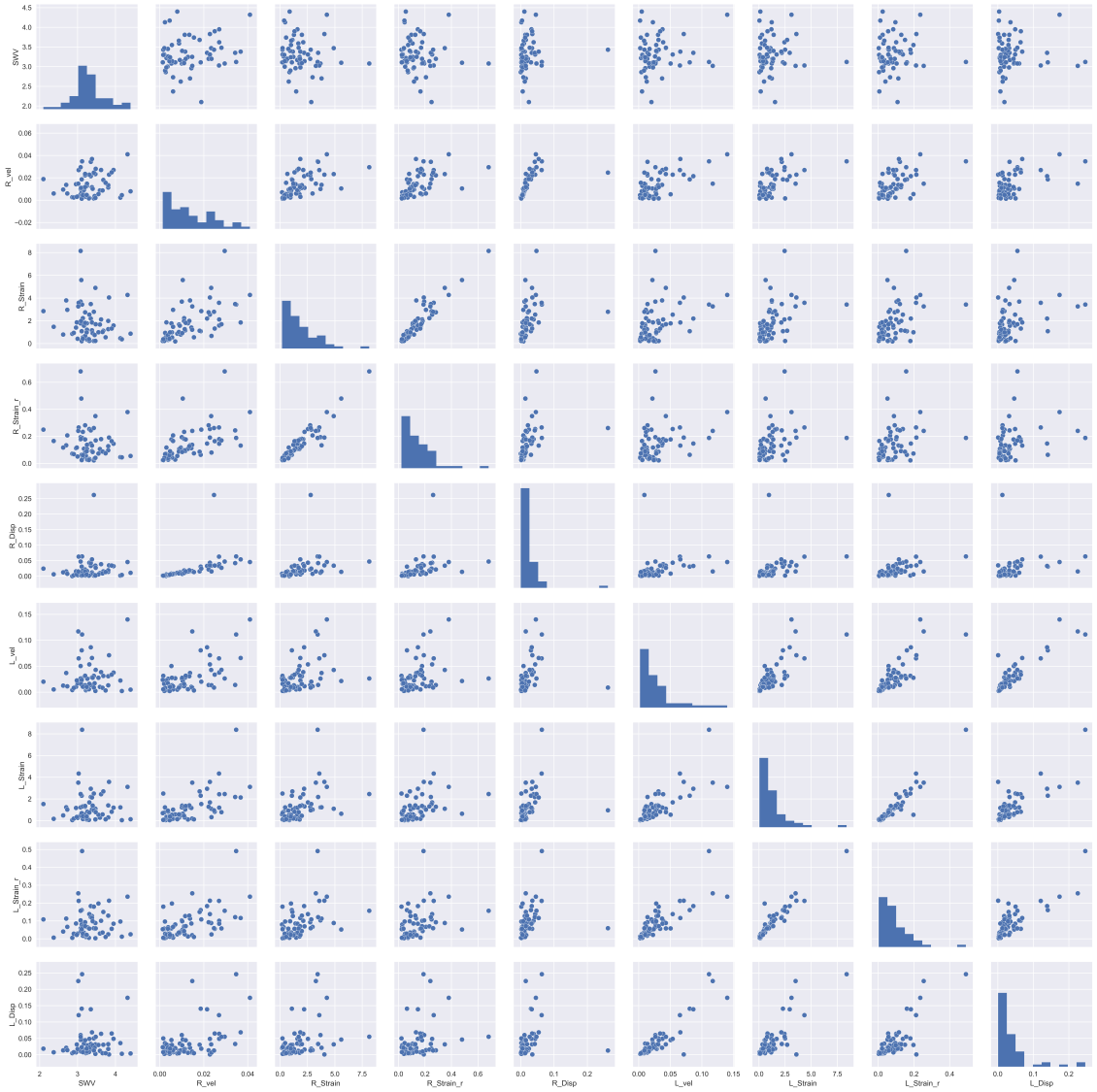

Figure 3.10: Pairwise scatterplots visualising relationships between ultrasound measurements from VVI and SWE all US variables assessed. A number of linear correlations are clear in the data, such as between radial strain, and radial strain rate. Other pairs such as shear wave velocity and radial strain rate show no association

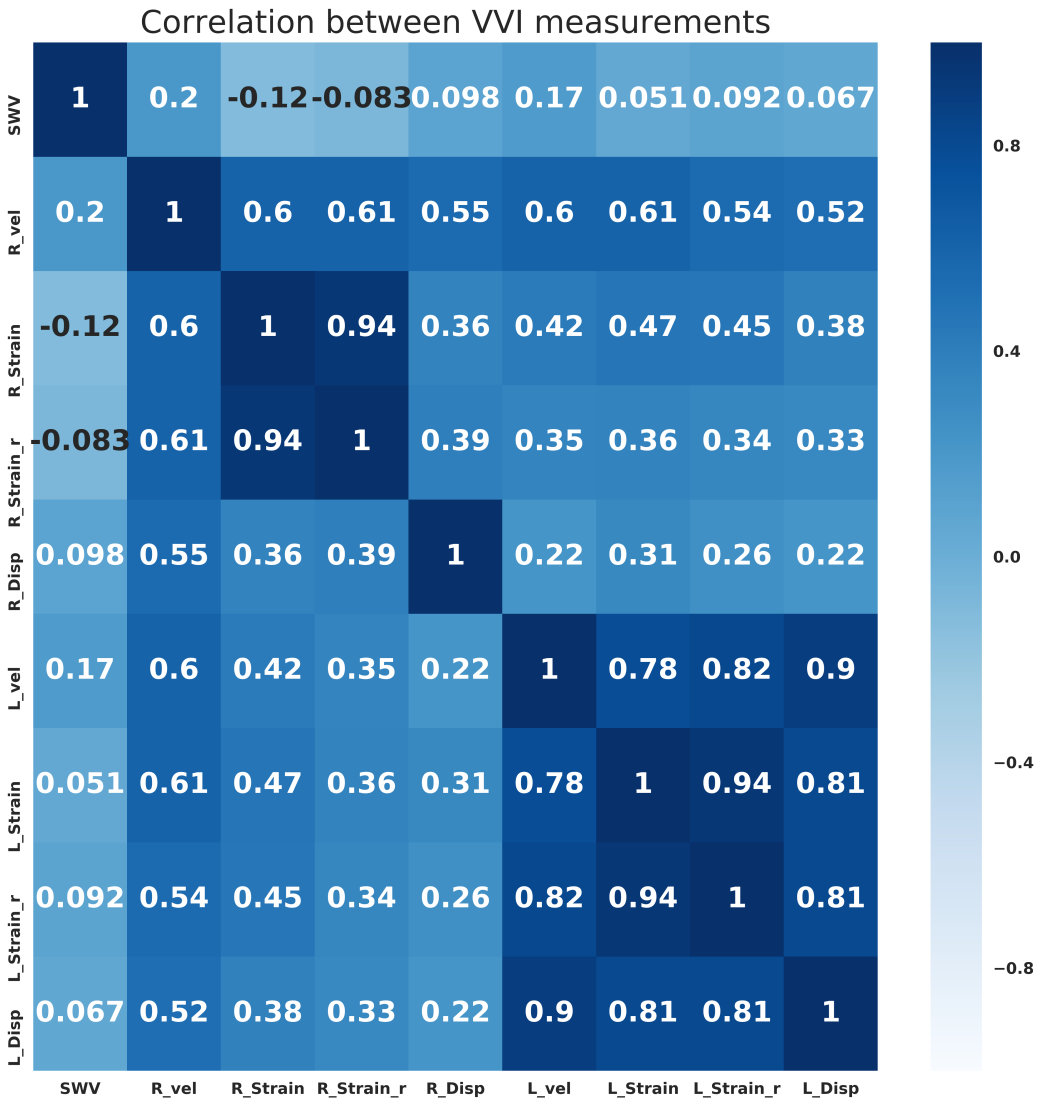

Figure 3.11: Pearson's R statistic assessing correlation between pairs of ultrasound measurements from VVI and SWE. This is essentially a statistical visualisation of the scatterplots visualised in figure 3.10

3.3.3 Reproducibility and homogeneity of measurements

A random selection of 15 volunteers underwent US (SWE and VVI) scanning by an additional operator, blinded to results of the first assessment. Strong agreement in measurements of SWV was observed between the two operators when assessed using Pearson's r statistic (r = 0.92, p = 1×10^{-6}, ICC = 0.88), a scatter plot with a regression line fitted can be seen in figure 3.12. Acceptable agreement was observed for the VVI measurement of radial displacement (r = 0.68, p = 0.005, ICC = 0.33), and can be seen in figure 3.13.

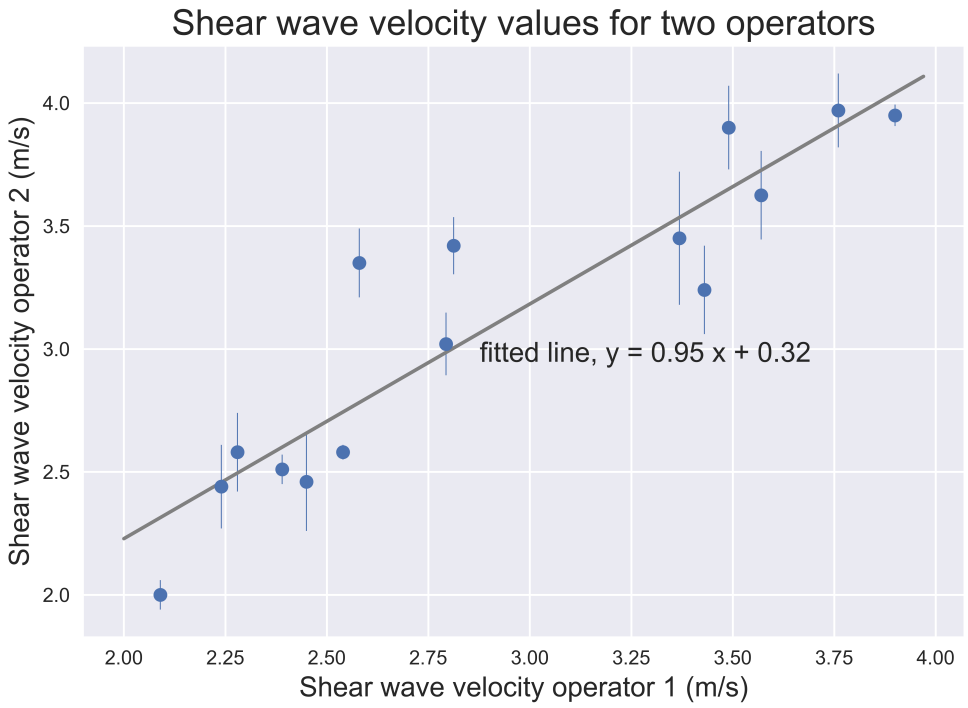

Figure 3.12: Scatter plot of shear wave velocity measurements from two operators, with a regression line fitted. Vertical lines for each marker represent the standard deviation of a single measurement. Strong significant correlation is observed, pearson's r = 0.92, p = 1×10^{-6}, ICC = 0.88, indicating good agreement.

3.3.4 Post-operative assessment and AVF outcomes

33 patients had an AVF created within the study period. Of the 15 patients with no AVF created, 4 died before the AVF could be created, one refused the operation, and the cause was unknown for the remainder.

The mean age of these patients was 65 $\pm$ 13 years, and mean BMI was 31 $\pm$ 8. 16 patients (48 %) had diabetes, and 27 (82 %) had hypertension. 7 patients had a lower arm AVF (radio-cephalic), and 26 had an upper arm AVF (22 brachio-cephalic, 4 brachio-basilic). Within the observation period, 9 AVFs were noted to have undergone some

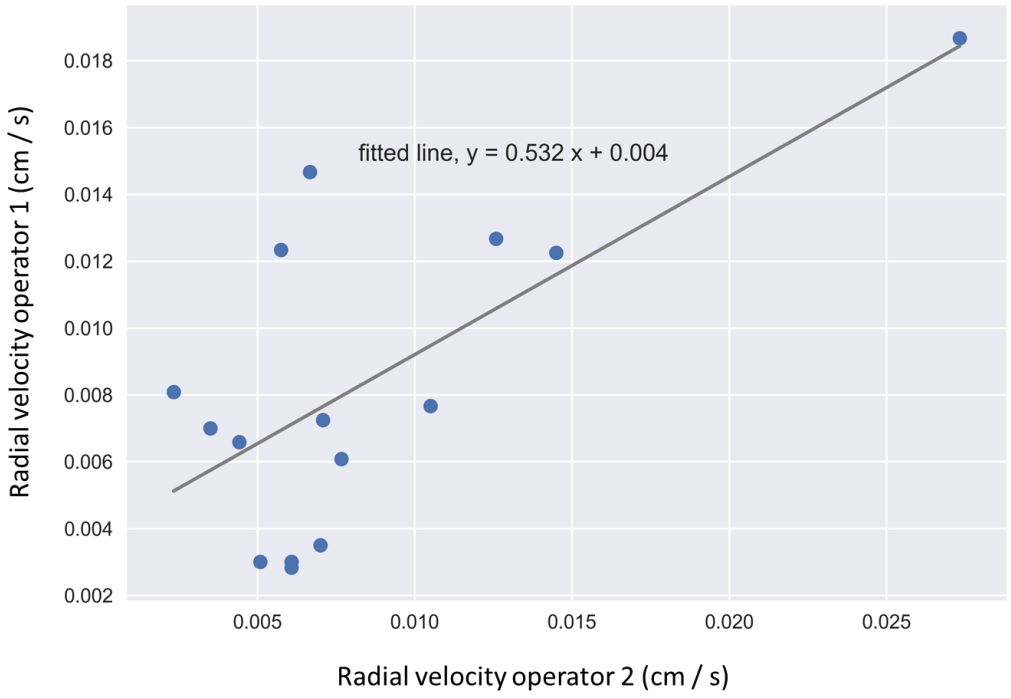

Figure 3.13: Scatter plot of VVI measurements from two operators, with a regression line fitted. Moderate positive correlation is observed, pearson's r = 0.68, p = 0.005, ICC = 0.33.

dysfunction. This was due to clinically significant stenosis (6 cases) and occlusion (3 cases).

After AVF creation the mean diameters of the arteries used increased from 3.8 $\pm$ 1.1 mm to 5.2 $\pm$ 0.7 mm (p = 2×10^{-6}). The mean increase was 1.4 $\pm$ 1.1 mm. Similarly, veins used in AVF creation increased in diameter from 4.0 $\pm$ 0.8 mm to 7.3 $\pm$ 1.6 mm (p = 5×10^{-7}). The mean increase was 3.2 $\pm$ 1.5 mm. These increases are visualised in figure 3.14. When correlations between the variables were assessed, a significant but weak positive correlation was observed between hypertension and pre-operative vein diameter (r = 0.29, $p < 0.05$, see heatmap in figure 3.15).

In the same period, the mean shear wave velocity values of the brachial artery decreased. Shear wave velocity of the brachial artery decreased from 3.2 $\pm$ 0.5 m/s to 2.4 $\pm$ 0.4 m/s after AVF creation (p = 8×10^{-6}). The mean decrease was 1.2 $\pm$ 1 m/s, and is visualised in figure 3.14.

No statistical differences were observed between the group without dysfunction (stenosis which was noted to be affecting HD treatment and requiring intervention, or occlusion), and the group with dysfunction. Pre-operative artery diameters were similar between the two groups (no dysfunction 3.7 $\pm$ 1.1 mm, dysfunction 4.0 $\pm$ 1.0 mm, p =

0.5). Vein diameters were similar between the two groups (no dysfunction 4.1 $\pm$ 0.8 mm, dysfunction 3.9 $\pm$ 0.6 mm, p = 0.4). Pre-operative shear wave velocity measurements between the two groups were also similar (no dysfunction 3.2 $\pm$ 0.4 m/s, dysfunction 3.2 $\pm$ 0.6 m/s, p = 0.8).

No difference was observed between the groups for measurements of radial velocity (no dysfunction 0.01 $\pm$ 0.01 mm / s, dysfunction 0.01 $\pm$ 0.01 cm / s, p = 0.7), or radial displacement (no dysfunction 0.01 $\pm$ 0.01 cm, dysfunction 0.02 $\pm$ 0.02 mm, p = 0.8). Similarly, no difference was observed between the groups for measurements of longitudinal velocity (no dysfunction 0.03 $\pm$ 0.03 cm / s, dysfunction 0.03 $\pm$ 0.04 cm / s, p = 0.7), or longitudinal displacement (no dysfunction 0.03 $\pm$ 0.04 mm, dysfunction 0.05 $\pm$ 0.06 mm, p = 0.8).

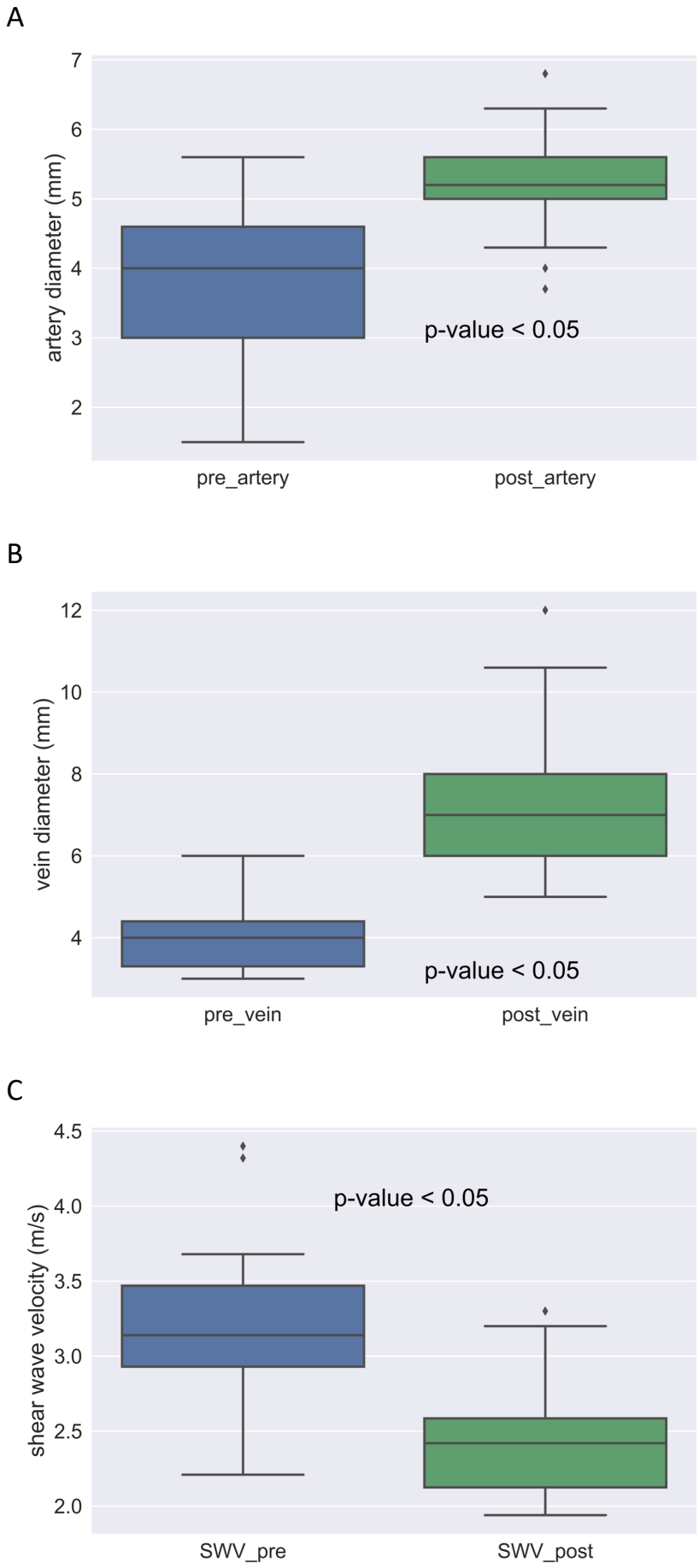

Figure 3.14: Changes in vessel morphology after AVF creation. A : arterial diameter, B : venous diameter, C : shear wave velocity of the brachial artery

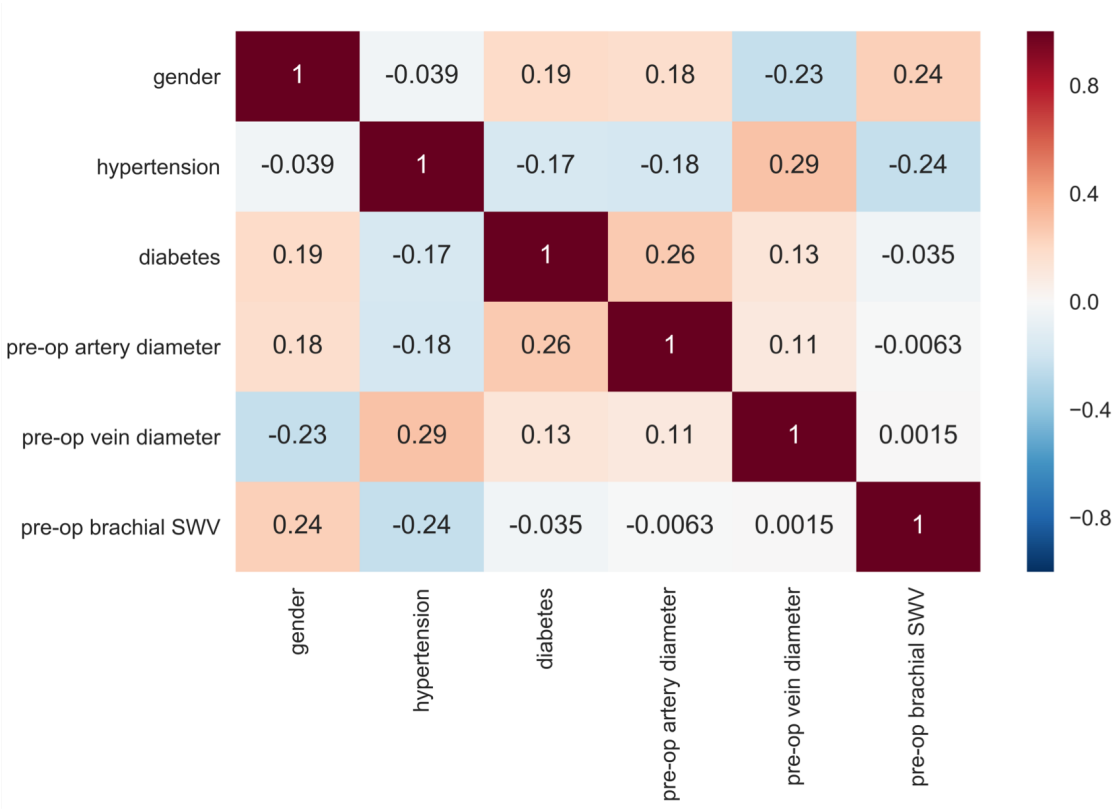

Figure 3.15: Correlations between variables used in regression modeling

OLS regression models were used to determine if pre-operative SWE measurements were predictors of the final arterial or venous diameter post-AVF creation. Known risk factors including pre-operative vessel diameter, hypertension, diabetes and gender were included in both models. VVI measurements were not included in these models, due to the lack of difference between patients and HVs, the lack of an age correlation, and the large amount of noise present in the data.

Model 1 assessed the arterial diameter achieved, and can be seen in table 3.3. Pre-operative artery diameter (p = 0.01) was the only independent determinant of arterial dilation in linear regression modeling. Model 2 assessed the venous diameter achieved and can be seen in table 3.3. No variables were significantly associated with venous dilation. Variable inflation values were low for all variables, and significant variables were found to be valid when assessed with type-3 anova. Residuals for both models can be seen in figure 3.16.

Model 1 - artery diameter achieved	B	p-value	Model 2 - vein diameter achieved	B	p-value
Hypertension 0	-0.57	0.07	Hypertension 0	-0.95	0.2
Diabetes	-0.30	0.60	Diabetes	0.25	0.60
Gender male	0.21	0.70	Gender male	-0.98	0.10
Pre artery diameter	0.26	**0.01**	Pre vein diameter	0.45	0.23
Brachial SWV	-0.17	0.55	Brachial SWV	0.05	0.94
R-squared	0.29		R-squared	0.26	

Table 3.3: OLS regressions modeling post-operative artery diameter (model 1) and post-operative vein diameter (model 2)

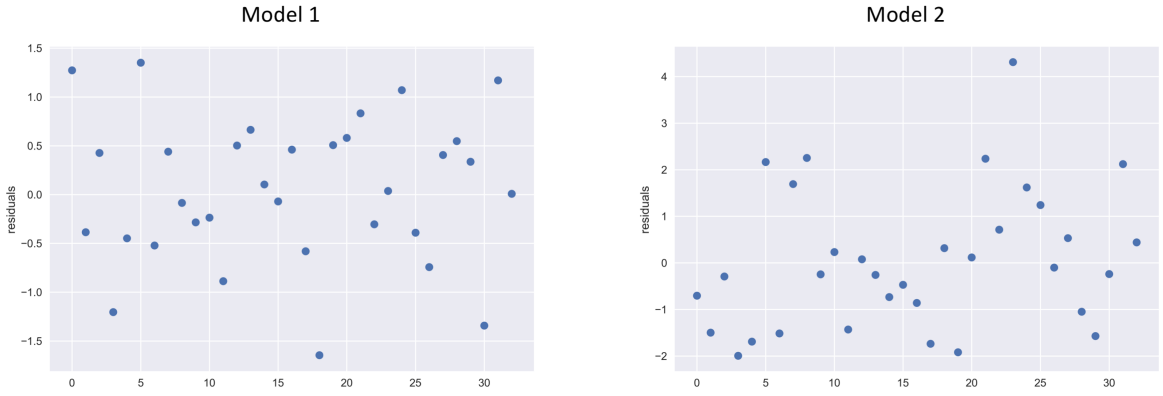

Figure 3.16: Residuals for model 1 and 2, both showing a random distribution which indicates good fit.

A logistic regression model was used to determine if any of the variables were associated to the outcome of the AVF at three months. Model 3 assessed the outcome of AVF creation at three months post-AVF creation. No markers were identified as associated to the outcome of the AVF in this model, which can be seen in table 3.4.

Model 3 - AVF outcome	B	p-value
Hypertension	1.1	0.3
Diabetes	0.15	0.9
Vein diameter	-0.32	0.6
Artery Diameter	0.20	0.6
Brachial SWV	-0.5	0.6
Pseudo R-squared	0.07	

Table 3.4: Logistic regression output modelling patient outcome as high or low-risk

3.4 Discussion

This study aimed to determine if measurements of elasticity via SWE and strain via VVI could act as risk-factors for AVF failure if used as part of the pre-operative workup for AVF creation. Initially, the feasibility of the techniques needed to be assessed in the peripheral vasculature, by comparing reproducibility and homogeneity of the measurements in the volunteer group and the patient group pre-surgery. Following this, US measurements of SWV, and strain parameters from VVI were compared between a patient and volunteer group.

Patients were then followed for up to 3-months post-AVF creation to determine if any relationship to the 3-month outcome of the AVF existed. SWE identified increased compliance in the brachial artery after AVF creation, and no post-operative relationship was observed for VVI measurements. None of the variables assess pre-operatively were statistically associated with the clinical outcome of the AVF in this small group of patients.

3.4.1 Pre-operative Assessments

Shear Wave Elastography

On initial assessment, the SWE method showed good reproducibility between operators, a significant negative correlation with age was observed and no significant difference was observed between the left and right arms of participants was seen, suggesting the measurement is homogenous. These results demonstrated the feasibility of the technique in vascular assessments. Pre-operatively, SWV of the brachial artery of the patient group was lower than the HV group. As the velocity is related to the square root of Young's Modulus, these results indicate that the brachial artery of an elderly group of patients with ESRD is more compliant than that of the healthy volunteers.

A negative correlation between SWV and age was observed, indicating that the brachial artery becomes more compliant with age, and indicates possible assessment of AS via SWE. Patients with ESRD have been shown to have increased AS, although previous studies have found that the brachial artery compliance may not decrease with age [54, 179, 27, 191]. Different trends in carotid and aortic stiffness have been observed in patients with CKD [25], and it is possible that similar phenomena are being seen in the brachial artery.

The SWE method is limited by a number of technical factors, mainly age and BMI.

It was observed that some elderly participants showed arteries that were more tortuous than younger participants. For some participants within this group, it was difficult to find a suitable region of artery close to the cubital fossa that was parallel to the transducer surface. High BMI resulted in shear wave velocity measurements taken at a greater depth than in patients within the healthy BMI range. In younger participants with a healthy BMI, a suitable patch of artery for shear wave velocity measurements was commonly found just proximal to the cubital fossa.

On our machine (Siemens S2000), it was not possible to gate the SWV measurements to the cardiac cycle. This is a limitation of the current technique, as one study in a single volunteer has shown that shear wave velocity measurements in the carotid vary throughout the cardiac cycle [41]. This limitation is noted in other vascular studies of shear wave velocity [144, 94]. However, the strong inter-operator agreement, and lack of difference between arms suggests that if there is some time dependent effect on these measurements, the effect is too small to introduce a significant error in the results.

Velocity Vector Imaging

The VVI assessment demonstrated required only a 5 second cine-loop of the brachial artery in a transverse and longitudinal view, which should present no problems for any clinically qualified sonographer. VVI demonstrated acceptable reproducibility, and measurements were homogenous between two arms. However, a large standard deviation in the results suggests that the method could be further developed.

Differences in VVI measurements of longitudinal velocity and strain rate were observed between the two groups, with higher values observed in the patient group. However, the large standard deviation in the measurement suggests that these results may be affected by a large amount of noise, potentially due to the imaging technique, or limitations in the speckle-tracking software.

No significant correlations with age were observed for any VVI measurements. Inter-operator agreement for VVI measurements was acceptable, but lower than that observed for SWE. This is potentially due to operator experience, and the requirement for high-quality US images for VVI analysis.

In this study, VVI measurements were possible from each US cine-loop. However, the VVI technique has a number of technical limitations. Some patients did not give reliable results due to underlying conditions interfering with the ECG trace. One patient

had a pacemaker, with pacemaker spikes on the ECG masking some r-wave signals which may have caused constructive or destructive interference due to pulse wave reflections. Another patient with a cardiac arrhythmia had vessel movement profiles which were extremely irregular and difficult to interpret. This seems to be an unavoidable limitation with VVI measurements, which rely on user interpretation to provide meaningful analysis of the data.

Previous studies using VVI have been conducted primarily on the carotid artery in healthy and patient groups. Ma *et al* [100] have shown that patients with pre-eclampsia produce irregular velocity profiles and Cho *et al* [36] had similar findings in patients with Takayasu's arteritis. This suggests that in certain groups of patients, the vessel movement is not synchronised. In this study, highly dis-synchronous wall movement was seen in a small number of patients and volunteers, rendering interpretation of the results highly difficult. The observation in the healthy cohort suggests that this may be to probe movement during video capture, as one would not be expect to observe these patterns in healthy individuals. The study of dis-synchronous wall movement requires more attention, in order to rule out that this observation is simply a probe movement artifact.

For all assessments, participants were imaged seated, in a position which was comfortable and bearable. US measurements were simple, and no specialist equipment was needed, as is the case for pulse wave velocity measurements, except the widely available software packages on the US machine. A number of strong correlations between the measurements themselves were observed. The heatmap in figure 3.11 demonstrates that all VVI measurements correlated positively with each other. A weak correlation ($r = 0.17$) between SWV and longitudinal velocity, and between hypertension and vein diameter ($r = 0.29$) was observed. This information is required in order to avoid multicollinearity in statistical modeling, which can cause errors in modeling coefficients.

The main limitation of the study is that the two groups were not age matched. Patients with ESRD are often aged, with other co-morbidities such as high BMI, diabetes and hypertension, making it difficult to find a healthy comparator group. It is possible that blood-pressure can affect the SWV and VVI measurements, and the effect of different blood-pressure values warrants further study. However, it was nevertheless necessary to perform the tests in a control group in order to pilot the technique in a non-clinical (controlled) setting to develop the imaging protocols, and to determine if any age or disease related differences could be observed. Another limitation is the lack of comparison with another AS marker such as PWV. This study was designed to develop and assess the

technique of obtaining VVI and SWV measurements of the brachial artery - now that this has been achieved, future work can compare this technique to PWV.

3.4.2 Post-Operative Followup

33 patients in this study progressed to AVF creation during the follow-up period. As expected, arterial and venous diameters significantly increased after AVF creation. SWV values in the brachial artery were observed to significantly decrease after AVF creation.

9 patients had some kind of AVF dysfunction within 3-months, as indicated from vascular laboratory notes. US measurements were compared between the groups with and without dysfunction, and zero statistical differences in any variables were observed between the two groups. Variables were assessed using regression analysis to determine if they affected the final venous and arterial diameter achieved, as-well as the clinical failure of the AVF. Only pre-operative arterial diameter was significantly influential on the arterial dilation achieved, which has previously been observed. Zero parameters studied were found to be related to venous dilation, or to the clinical failure of AVFs.

Following AVF creation, a decrease in SWV of the brachial artery was observed. This indicated that an increase in tissue compliance had occurred, assuming that the tissue density had not dramatically changed. This effect could be due to structural remodeling in the artery, the increased volume of blood in the artery, or both. Decreases in global arterial stiffness have been reported previously, along with decreases in systolic and diastolic blood pressure [15]. Further histological studies would be required to characterise the observed changes in brachial artery elasticity.

The poor fitting model used to assess clinical outcome of the AVF indicates that these measurements may be of limited use to predict AVF stenosis or occlusion. It is possible that pre-morbidities such as diabetes and hypertension masked any effect from brachial artery stiffness. Due to the small sample size, we did not control for AVF site. It is possible that brachial artery elasticity may have more impact on brachial AVFs, as opposed to RC-AVFs.

The main limitation of this study is a small sample size, including only 33 patients that progressed to AVF creation. To increase statistical power, we limited the variables included in statistical modeling to those suspected to have the largest impact on AVF outcomes. Whilst we controlled for the presence of hypertension, we did not assess blood pressure. As noted, the effect of hypertension and blood pressure on SWV measurements

warrants further study.

Venous measurements of SWV were not taken prior to AVF creation due to the thin, and easily compressible nature of the venous wall. SWV measurements should be possible in the venous segment following AVF creation due to the increased volume of blood which would reduce its compressibility, and the increased wall thickness. VVI measurements were not taken after AVF creation, however this was due to purely logistical reasons owing to the availability of the equipment (SWE was installed on 2 US machines available in the vascular lab, but VVI only on 1 US machine). VVI measurements would in theory be possible in the venous segment of the AVF, and should be tracked easily due to the thicker venous wall following AVF creation.

In conclusion both SWE and VVI showed good reproducibility and homogeneity. SWE presents as the more feasible of the two due to a clear correlation with age, and an observed reduction in SWV values following AVF creation. The VVI method is feasible, but let down by a large standard deviation in the measurement and requires further development. A decrease in SWV of the brachial artery was observed after AVF creation, which indicates an increase in tissue elasticity. The only additional statistically significant result was that pre-operative artery diameter was associated with arterial diameter increase post-AVF creation. No variables were associated with venous dilation or the clinical failure of the AVF. Further research is required to determine if the increased elasticity is due to structural remodeling of the artery. Larger cohort studies with longer follow-up are required to determine if there is any relationship between SWE measurements and AVF failure. [1]

Notes

[1]Work from this chapter is currently published as MacDonald, C., Ross, R., and Houston, J. (2018). Shear wave velocity measurements of the brachial artery in a population with end-stage renal disease. Biomedical Physics and Engineering Express, 4(5), 057002.

Chapter 4

MRI and Ultrasound Comparison

4.1 Introduction

MRI is an attractive diagnostic tool as it can provide excellent angiographic images, with or without the use of contrast agent [47, 57]. Planken et al [136] established that contrast enhanced (CE)-MRI was an accurate modality for providing pre-operative vessel diameters in patients requiring AVF creation. Further work by the same group [137] reported that CE-MRI was superior to US in detecting venous pathologies (most commonly upper arm cephalic vein occlusions) in 73 patients prior to AVF creation.

However since 2006 there has been a marked decline in MRI based imaging involving patients with end stage renal disease and AVFs. This is likely due to the association between certain Gd-based contrast agents and nephrogenic systemic fibrosis, a fibrotic disease of the major organs [88]. NCE-MRI methods are currently the safest option for this cohort. The Gradient Echo ToF sequence is commonly used in MR angiography, and relies on the inflow of blood to produce a hyper-intense signal. Various studies have reported that this sequence can visualise, assess failure and locate stenosis in AVFs [57, 62, 86, 70].

Pre-operatively, very few studies have described the use of NCE-MRI to image the vessels of patients indicated for AVF creation. Menegazzo et al (1998) [108] compared ToF imaging with venography to assess the depiction of vein diameters prior to AVF creation. ToF measurements were better correlated with subsequent surgical findings. In 2012, Bode et al [21] used CE-MRI and a NCE balanced turbo field echo sequence to detect stenoses prior to AVF creation. The NCE-MRI detected 66 % of (non-significant) stenosis found on CE-MRI, but importantly these were not seen on previous US imaging. More recently a T2* Gradient Echo MEDIC sequence [78] has been used to highlight lower limb vessels, indicating possible future uses for this in pre-surgical mapping or surveillance of AVFs. The MEDIC sequence is a flow compensated 3D T2* weighted gradient recall echo technique where multiple echoes are acquired during the TR period via frequency encoding gradient reversals. The images acquired from each echo are then combined to form a combination image benefitting from improved SNR. For non-contrast measurement of blood flow velocity, the widely used technique of phase contrast MRA (PC-MRA) is available [123] providing the opportunity for pre-operative MR assessment of vessel structure and blood flow velocity to be used within a single modality.

A major strength of MRI compared to US is it's ability to depict the central arterial and venous vessels. Central vein pathology can be a cause for AVF failure, and cannot

easily be detected by US imaging. In certain groups of patients, such as those with previous central line usage, screening for central vein stenosis could identify patients who should not under go AV access creation, or identify patients who can. The use of MRI in these patients would reduce the need for invasive DSA assessments, which are currently considered the gold standard, but involve the injection of contrast agents, and radiation dosing.

This chapter sought to answer the research question: *is 3T MRI useful as part of the pre and post-operative workup for a patients AVF?*. Specifically, the objective was to examine the performance of three (non contrast) MRI pulse sequences (namely MEDIC, ToF and PC-MRI) for these purposes, in order to establish whether they may prove useful the pre and post-surgical assessment of patients listed for AVF creation, before the possibility of further studies assessing the central vessels in these patients. 3T NCE-MRI methods were compared against the reference standard of US for the assessment of vessel geometry and blood flow velocity in the arms of both patients and healthy volunteers at a single time-point, and also in patient volunteers before and after AVF creation.

4.2 Materials and Methods

4.2.1 Volunteer Recruitment

Ethical approval was obtained to recruit patients and healthy volunteers (HV) into this study. Patients and volunteers were recruited to undergo at least one MRI and US scanning session. For the patients, this was once before, and up to four times after AVF creation over a period of 6 months, for HVs, this was a single scanning session.

Patient and volunteer recruitment was performed over the period covering Jan 2014 - Dec 2016, and was managed by a member of the ReDVA project. Patients were recruited from the vascular laboratory in Ninewells hospital and medical school if they were listed for AVF creation within the study period. Healthy volunteers were recruited from staff and students in Ninewells hospital and medical school, and NHS Tayside. Fully informed consent was granted from each individual.

4.2.2 Ultrasound Examinations

For the US examinations all participants were seated with a pillow resting on their lap. The arm under investigation was extended palm up on the pillow. A tourniquet was applied to the upper arm for venous measurements and released before arterial measurements. Diameter measurements of the vessels were taken using electronic callipers. Peak systolic velocity (PSV) values were measured as the highest single point on the Doppler reading with an accuracy of 0.01 m/s. The velocity values obtained were subsequently used as a guide to assist with identifying a suitable velocity encoding (VENC) value on the subsequent phase contrast MRA sequences.

Pre-Operative Assessment

Lower Arm Evaluation

The cephalic vein was identified at its most distal segment, and diameter measurements taken at this location. The diameter of the radial artery was measured at the wrist position. An assessment was made of vessel uniformity and the presence of multiple branches was noted, if present. The artery was then assessed in a longitudinal view using Spectral Doppler to record the peak systolic velocity (PSV) and phasicity (presence of reverse velocity component and a clear diastolic peak velocity component).

Upper Arm Evaluation

The cephalic vein and brachial artery were identified at the cubital fossa and their diameters were measured at this location. Vessel uniformity and branches were assessed as before. As with the radial artery, the PSV was measured using a longitudinal view.

An oil capsule was then placed on the skin surface at the proposed location of the surgical anastomosis in order to guide MRI imaging i.e. to ensure that the same anatomic areas were observed using both imaging modalities (see figure 4.1).

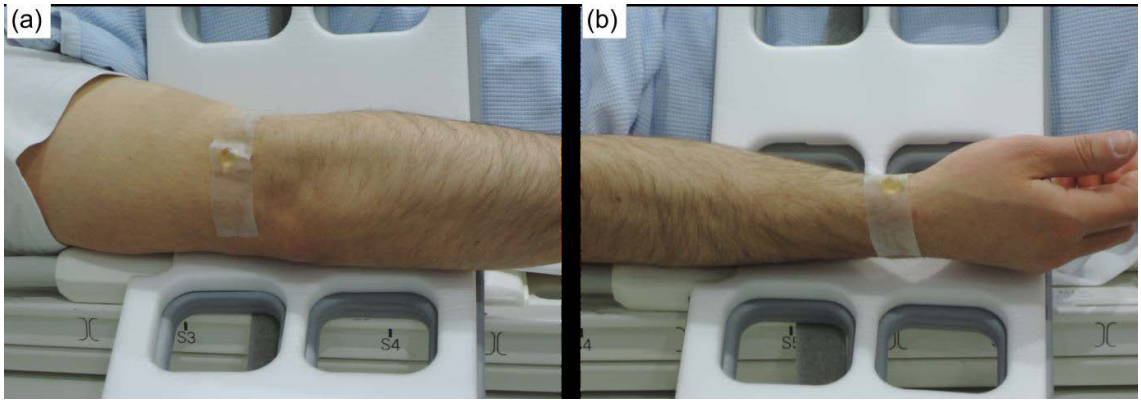

Figure 4.1: Placement of oil capsule for a) upper arm imaging, b) lower arm imaging

Post-Operative Assessment

The vein was identified central to the anastomosis. Diameter and velocity measurements were taken 6cm proximal to the anastomosis, and this process was also repeated for the artery.

4.2.3 MR Imaging

All participants were placed head first and supine into the scanner bore with their arms relaxed by their side. An 8-channel small flex RF coil was placed around the arm region of interest. The participant was positioned slightly off-axis in relation to the scanner bore, in order to ensure that the arm (anatomical area of interest) was as near as possible to the isocentre of the magnetic field.

Morphology Assessment

A 2D gradient echo localiser sequence was used for initial visualisation of the proposed anastomosis area. Following this, a 2D time-of-flight (TOF) MR sequence was applied in an axial oblique orientation at either the upper or lower arm (see table 1) perpendicular to the long bones, and region coverage was maintained at approximately 10-15 cm. Imaging

parameters used were repetition time (TR) and echo time (TE) of 14 ms and 5.8 ms respectively, flip angle (FA) of 18, and a 1.5 mm slice thickness (ST). Images were acquired using a single average over a field of view (FOV) of 140 mm, with an imaging matrix of 512 x 512 pixels (no interpolation), and receiver bandwidth of 165 Hz/pixel. This was followed by a 3D T2* Multi Echo Data Image Combination (MEDIC) sequence (TR/TE: 29/16 ms, FA: 30, slice thickness: 1.06 mm (176 slices in the imaging block), FoV: 136 mm, matrix: 512 x 512 pixels (no interpolation), and receiver bandwidth: 160 Hz/pixel) over the same area.

Velocity Assessment

Through plane blood velocity measurements were obtained in the artery and vein of interest at distal and proximal positions relative to the bifurcation or anastomosis site. A retrospectively ECG gated 2D phase contrast MRA sequence (PC-MRA) was used to derive velocity measurements (TR/TE: 99.7/7.62 ms, FA: 20, FOV 100 mm, matrix 192 x 115 pixels, receiver bandwidth: 440 Hz/pixel, VENC: 10-250 cm/s (depending on whether artery or vein) and 16-64 temporal phases over the cardiac cycle).

4.2.4 Image analysis

The MEDIC, ToF and PC-MRI sequences were exported in DICOM format to an offline computer. Osirix Lite (Pixemo, Switzerland) was used as a database, and for diameter and area measurements. Transverse image slices from the MEDIC and ToF sequences were used for ROI analysis of vessel diameter and area. Diameter measurements were made of the vessel diameter in the major and minor axis for each image slice using electronic calipers in Osirix, and vessel area was plotted as a function of distance from the anastomosis or bifurcation (see figure 4.2). Anatomical landmarks (e.g. bifurcations of other vessels) were used to register adjacent measurements between the two time-points. Trend lines were plotted using a rolling 3-point average.

Semi-automatic segmentation and analysis of the PC-MRI images was undertaken using Segment (Medviso, Sweden). A ROI was drawn around the vessel of interest and automatic propagation of the ROI was processed through all images in the series. Flow and velocity information of blood in the vessel ROI was extracted (see figure 4.3). For comparison with US, the diameters measured by MRI were averaged over a 1cm region approximately 6cm from the anastomosis or oil capsule i.e. consistent with the US imag-

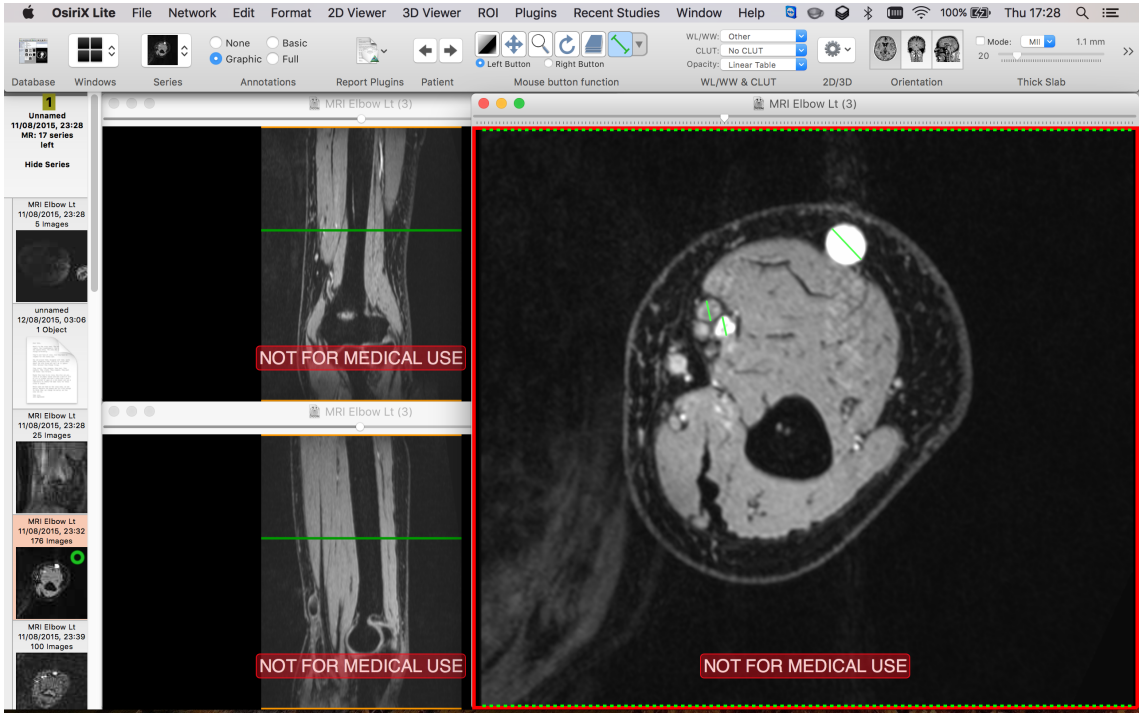

Figure 4.2: Osirix workstation showing 3 perpendicular slices of a patient's AVF from MEDIC images

ing locations.

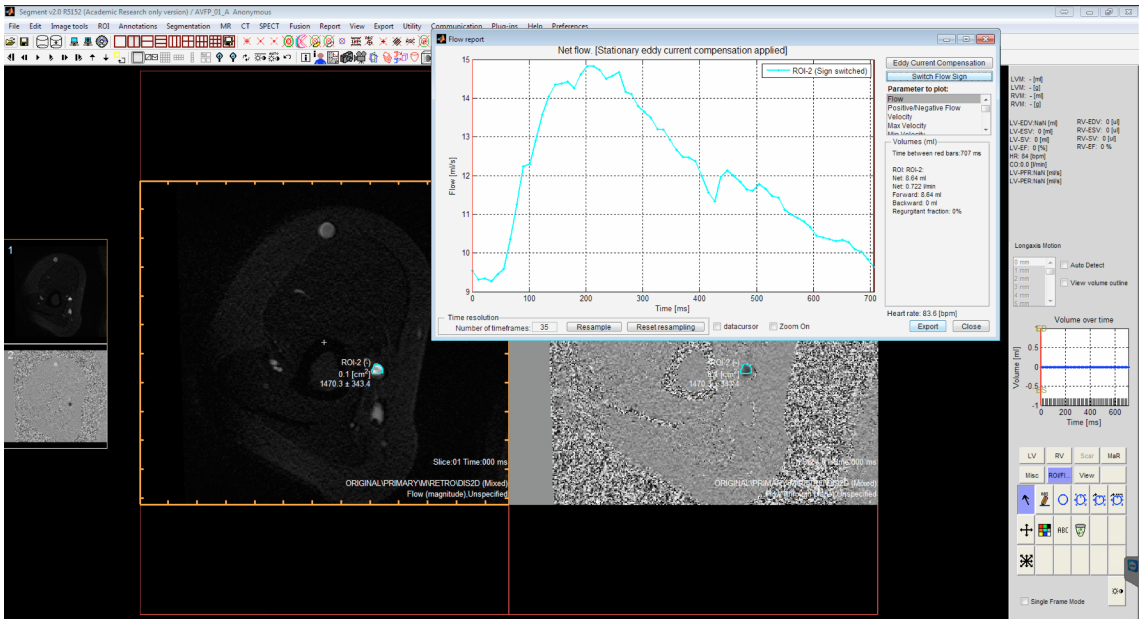

Figure 4.3: Segment workstation showing contour on a patients artery, and corresponding velocity waveform from PC-MRI images

4.2.5 Statistical Analysis

All statistical analysis was conducted using RStudio (RStudio inc, US). All datasets were assessed for normality using the Shapiro-Wilks Normality test. Statistical comparison of means was subsequently performed using a students t-test for normally distributed data, or the Mann-Whitney test for non-normal data. Paired equivalents were used when appropriate. Bland-Altmann style plots were used to visualise agreement between the modalities. Graphs were plotted using Python with the matplotlib and Seaborn packages.

An additional (junior) operator performed repeat measurements of the vessel diameter from MEDIC MRI images. Agreement between two users was assessed using Bland-Altmann plots.

4.2.6 Compliance with Ethical Standards

The study received ethical approval from the East of Scotland Research and Ethics Service (EoSRES). Written informed consent was obtained from all individual participants included in the study.

4.3 Results

4.3.1 Imaging and Surgical Outcomes

Sixteen fully consented participants (table 4.1) were recruited into the study; 10 healthy volunteers (HV1-10) and 6 patients with end-stage renal disease (PRF1-6) previously referred for AVF creation surgery. Three of the PRF participants were indicated for brachio-cephalic AVF creation (PRF1, PRF3, PRF5) and three were indicated for radio-cephalic AVF creation (PRF2, PRF4, PRF6). All participants underwent pre-operative vessel mapping using ultrasound (S200, Siemens, USA), performed by an experienced operator, and magnetic resonance imaging (3T Siemens Magneton Trio-PrismaFIT, Erlagen, Germany) performed by an experienced clinical research team. Pre-operative images from both modalities were obtained on the same day. Post AVF surgery, all PRF participants underwent ultrasound surveillance imaging at 6 weeks. Four of the PRF participants (PRF1, PRF2, PRF3, PRF6) also underwent a single MRI surveillance session, 17 - 26 days after surgery.

	Patients (n = 16)
Age	44 ± 16
Male	
Diabetes	4
Arterial fibrillation	2
Heart failure	1
Upper arm imaging	5
Lower arm imaging	11

Table 4.1: MRI study participants

All 16 participants were scanned successfully using both US and MRI, although initial observation of the images revealed that the following exclusions were required: ToF: one dataset (PRF5) - unreadable due to participant movement; MEDIC: one dataset (HV4) - unreadable due to participant movement; PC-MRI: two datasets (PRF4, HV2) - arterial VENC sub-optimal; US: one dataset (HV6) file data corrupted during storage. Figure 4.4 shows example axial image slices acquired at the radio-cephalic region of the upper arm of a healthy volunteer using (i) T2* MEDIC and (ii) 2D ToF MRA.

Surgically, AVF creation was initially successful for all but one participant (PRF1). In this unsuccessful case it was necessary to abandon the procedure due to calcification of the vessels, although a second procedure was subsequently successful at a more proximal site. Participant PRF6 developed a post-surgical infection at the anastomosis site, but with

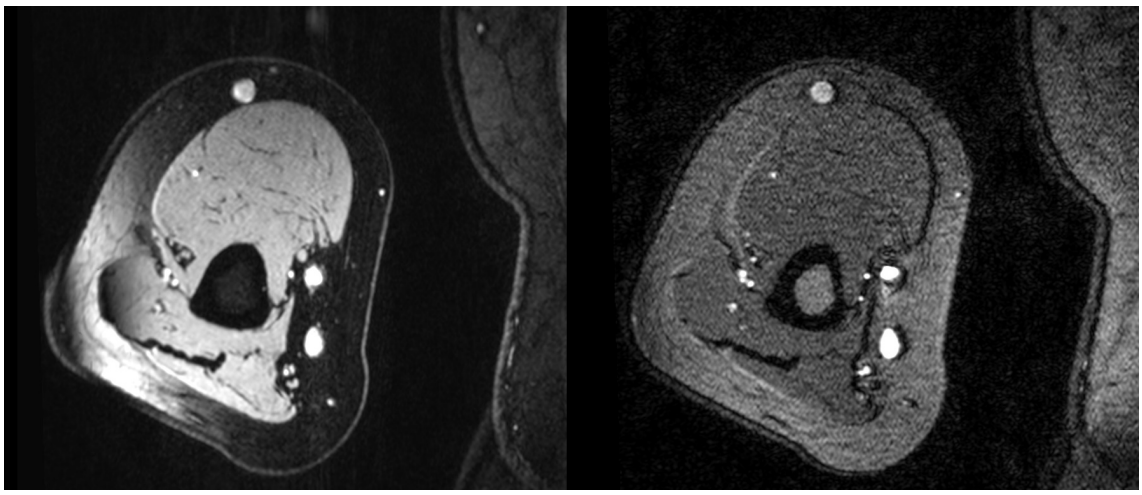

Figure 4.4: example axial image slices acquired at the radio-cephalic region of the upper arm of a healthy volunteer using (i) T2* MEDIC and (ii) 2D ToF MRA.

no long-term complications.

4.3.2 Morphology results 2D TOF v MEDIC v US diameter comparisons

When data acquired using ToF, MEDIC and US were compared (figure 4.5), mean arterial diameters were found to be consistent across all imaging modalities (3.2 $\pm$ 0.7 mm for ToF; 3.4 $\pm$ 0.8 mm for MEDIC; 3.5 $\pm$ 0.7mm for US; $p > 0.05$ for all). However statistical differences were noted when comparing the mean venous diameters measured by ToF (3.5 $\pm$ 1.2 mm) to those measured by both MEDIC (4.4 $\pm$ 1.6 mm) and US (4.6 $\pm$ 1.0mm); $p < 0.05$. Bland-Altman style plots (figure 4.6) demonstrate good agreement between MRI (both MEDIC and ToF) and US for all artery diameters, with mean values close to zero. However, a clear underestimation of venous diameters was observed for data derived from the ToF sequence.

When participants were split into PRF (n=6) and HV groups (n=10), mean arterial diameters were consistent when measured with US (3.5 $\pm$ 1.0 mm for PRF; 3.5 $\pm$ 0.5 mm for HV). However, mean arterial diameters were lower for the PRF cohort relative to the HV cohort when derived from both NCE-MRA sequences (MEDIC: 3.0 $\pm$ 1.0 mm for PRF, 3.8 $\pm$ 0.5mm for HV); (ToF: 2.7 $\pm$ 0.9mm for PRF, 3.5 $\pm$ 0.5mm for HV); $p < 0.05$ for each. For the veins, mean measured diameters were consistently smaller in the PRF cohort relative to the HV cohort, irrespective of whether US or MRI was used (US: 3.9 $\pm$ 1.0 mm for PRF, 5.0 $\pm$ 0.8mm for HV; MEDIC: 3.0 $\pm$ 1.5mm for PRF, 5.3 $\pm$ 0.6mm for HV; ToF 2.6 $\pm$ 0.8 mm for PRF, 4.0 $\pm$ 1.0mm for HV); $p < 0.05$ for all.

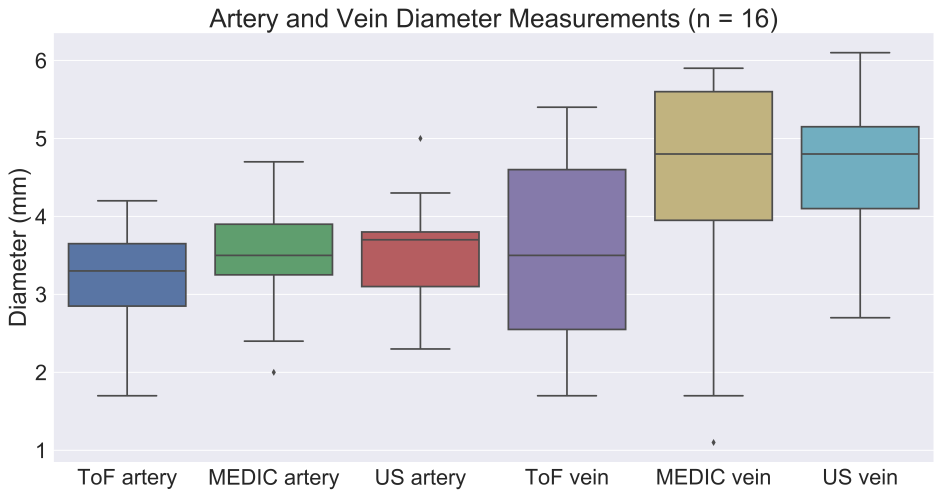

Figure 4.5: Illustrations of arterial and venous diameter measurements - using ToF, MEDIC and US.

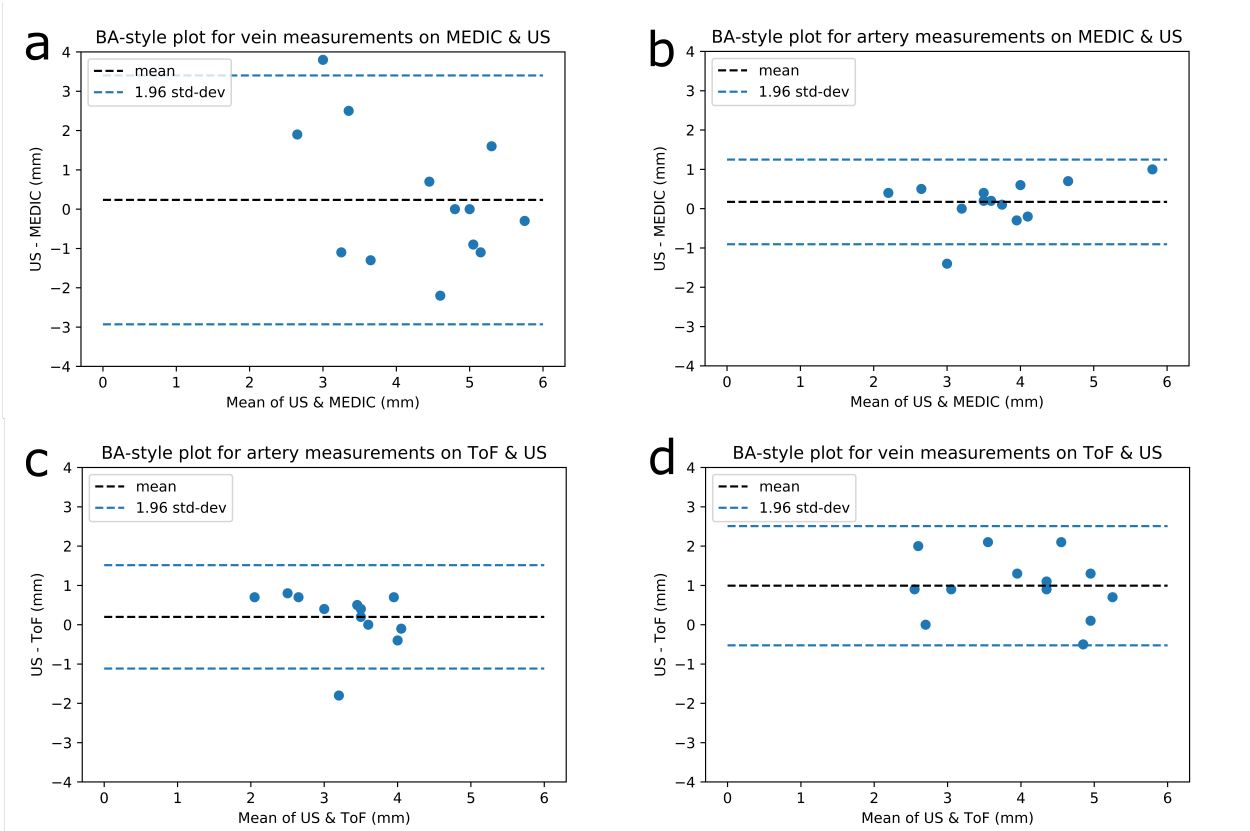

Figure 4.6: Bland-Altmann style plots depicting mean difference between: (a) artery diameter measurements from MEDIC MRI and US; (b) vein diameter measurements on MEDIC MRI and US; (c) artery diameter measurements on ToF MRI and US; (d) vein diameter measurements on ToF MRI and US.

4.3.3 Flow velocity results PC-MRA v US velocity comparisons

For arterial flow velocity measurements, the mean velocities measured by MRI (51.4±17.2 cm/sec) and US (53.2 ± 12.6 cm/sec) were similar ($p > 0.05$). When the data were considered on an individual basis, the bias between the MRI and US observations was 0.54

and the MRI versus US root mean square (RMS) coefficient of variation (CoV) was 11.8 %.

Similarly, when the data were sub-divided into PRF and HV cohorts, the mean velocities measured by MRI and US were still consistent (PC-MRI: 49.8 $\pm$ 25.6 cm/sec for PRF, 52.2 $\pm$ 12/4 cm/sec for HV); and US: 55.0 $\pm$ 7.7 cm/sec for PRF, 52.0 $\pm$ 15/4 cm/sec for HV); $p > 0.05$ for all. These values are displayed graphically in figure 4.7.

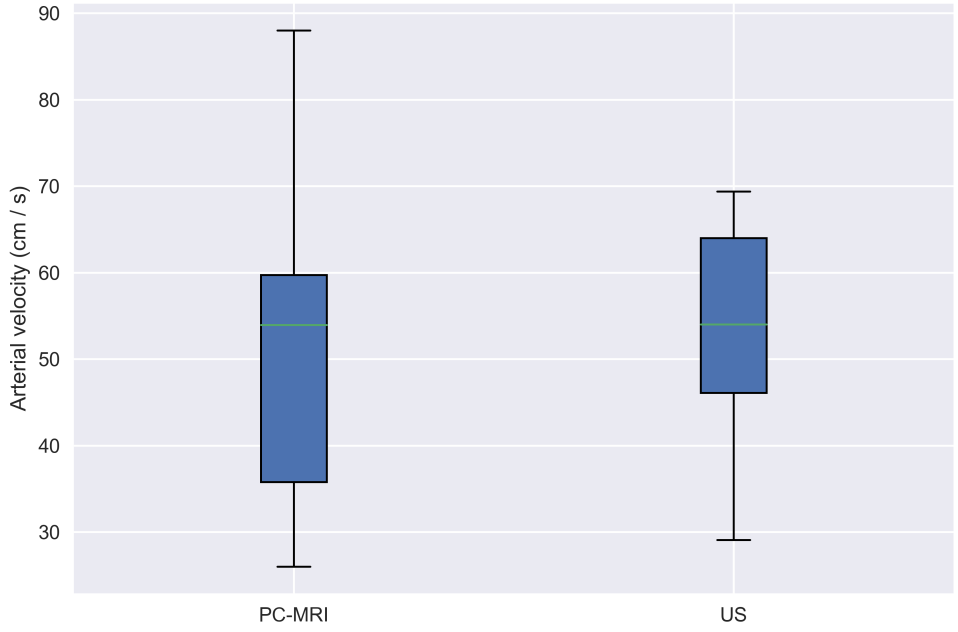

Figure 4.7: Boxplots showing mean blood flow velocity for PC-MRI and US

4.3.4 Pre and post-operative observations of vessel morphology and flow

Pre-operative and post-operative arterial and venous diameter measurements were measured, but statistical testing of these measurements were not attempted since the number of subjects involved was small (n=4). The RMS differences between the post-surgery minus pre-surgery measured vein diameters were 3.2mm (ToF), 3.9mm (MEDIC) and 2.2mm (US), and for the arterial diameters the RMS differences were 1.7mm (ToF), 2.2mm (MEDIC) and 1.3mm (US). Looking in more detail at the vein morphology over the full length of the MR imaging block, all veins studied developed larger cross-sectional areas after surgery relative to their pre-surgical dimensions. However the cross-sectional

area changes were not uniform across the full length of the vein area scanned (see figure 4.8).

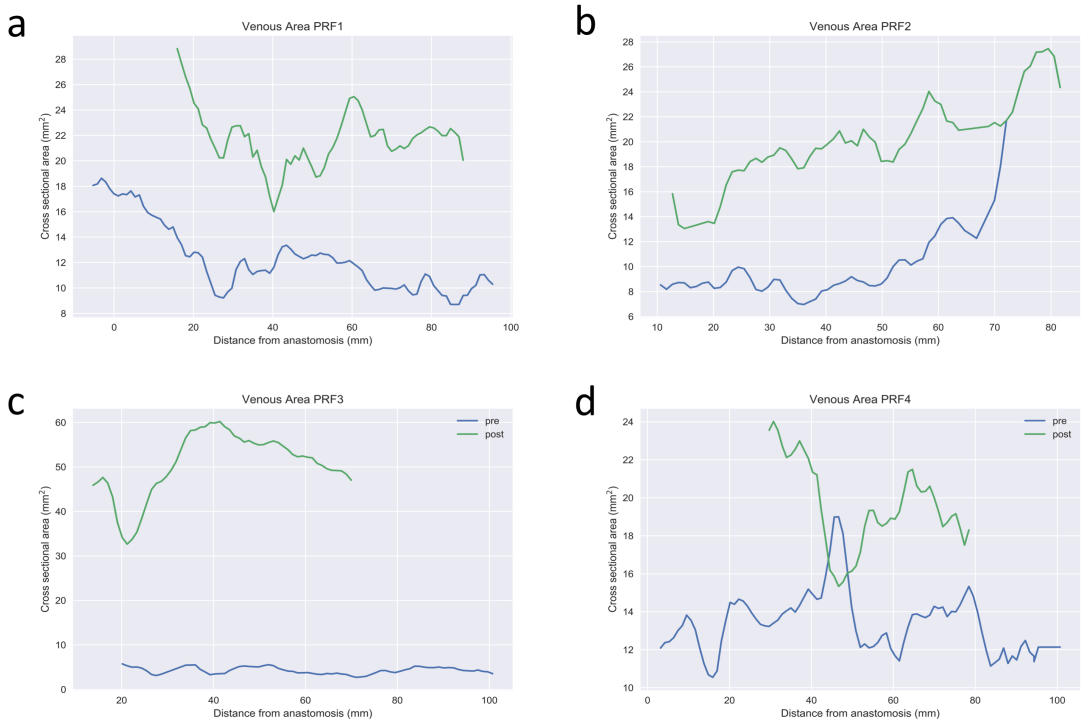

Figure 4.8: Graphs depicting pre and post-operative venous area for participants (a) PRF1; (b) PRF2; (c) PRF3; (d) PRF4. Areas of narrowing are visible in participants PRF3 and PRF4.

Arterial peak velocities were markedly increased after surgery. The RMS differences between the post-surgery minus pre-surgery measured arterial velocities were 164.3 cm/sec (PC-MR) and 183.6 cm/sec (US). Post-operatively the arterial waveforms were altered, with loss of their characteristic tri-phasic pattern (a lack of reverse velocity component and a loss of a clear diastolic peak velocity component).

4.3.5 Repeatability of MRI diameter measurements

Measurements from the MEDIC MRI images were found to be reproducible when assessed by a junior researcher (see figure 4.9). Mean difference for all cases were around zero, with around 10 % standard deviation.

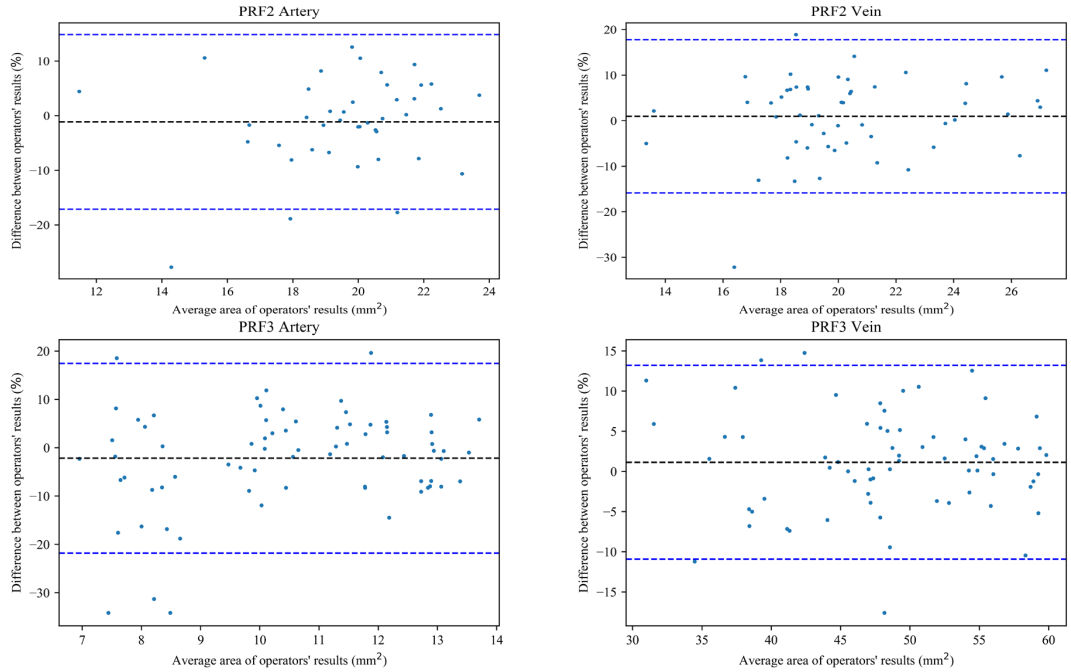

Figure 4.9: Bland-Altmann style plots depicting mean difference between two operators measuring arterial and venous diameter throughout the length of the AVF for two study volunteers.

4.3.6 Imaging features of the TOF and MEDIC MR Sequences for AVF Visualisation

On all pre-surgical images (ToF and MEDIC) the vessel lumen flow signal intensity was hyper-intense, as expected. However on the post-surgical images the vessel lumen was hyper-intense at locations proximal to the anastomosis but the signal was lost within the anastomosis itself. On the ToF images it was not possible to discern the vessel pathway of the anastomosis since the vessel edges were unclear, but on the MEDIC images the vessel edges remained consistently and clearly visible - thus enabling a better view of the stationary structures associated with the anastomosis. Example post-surgical MEDIC images are shown in figure 4.10.

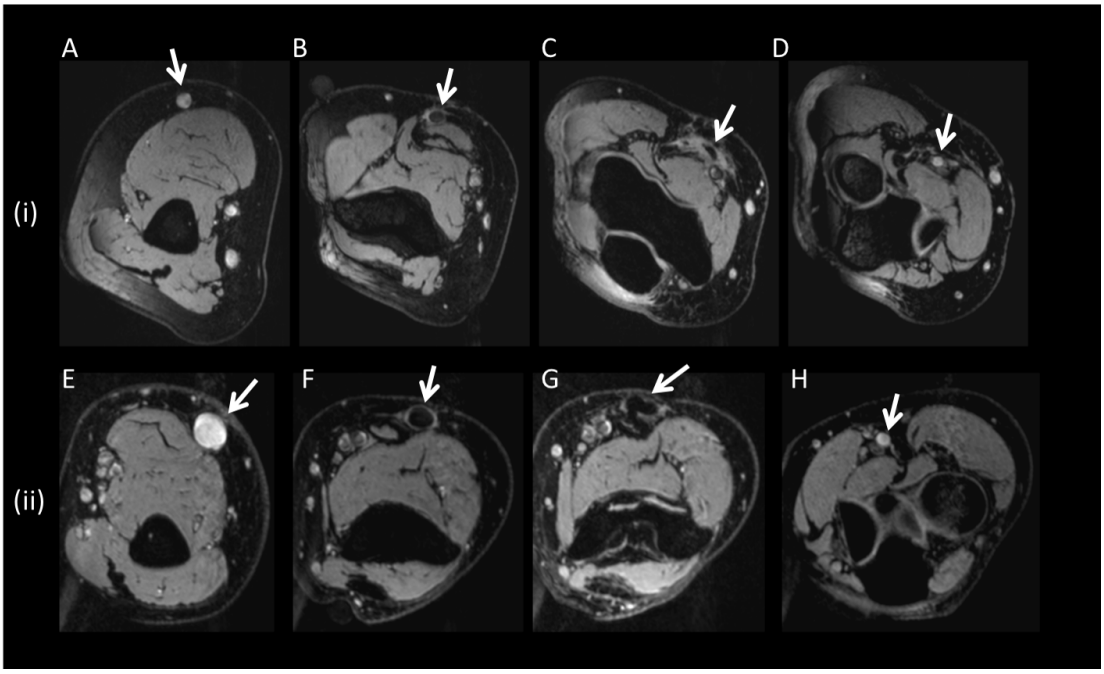

Figure 4.10: Example 3T Gradient-Echo MEDIC MR images of the elbow region of two different participants, (i) and (ii), who each underwent AVF placement. (A) and (E) show examples of high luminal signal intensity in the cephalic veins at a location a few cm proximal to the anastomosis site. The luminal diameter is slightly enlarged in participant (i) and grossly enlarged in participant (ii); (B) and (F) show examples of hypo-intense luminal signal intensity together with hyper-intense vessel edge signal intensity at the approach to the anastomosis site; (C) and (G) each illustrate the flat swing site location of the anastomosis; and (D) and (H) each illustrate the hyper-intense luminal signal intensity in the brachial artery distal to the anastomosis site. The images were obtained 24 days post-surgery for participant (i) and 26 days post-surgery for participant (ii).

4.4 Discussion

In this pilot study, the feasibility of using 3T MRI techniques for the assessment of upper and lower arm blood flow geometries and velocities at potential AVF sites is described. For morphological assessments, the MRI T2* MEDIC technique used compared favourably against the current reference standard of US, with very similar diameters obtained in patients and healthy volunteers. Further, the combined observation of hypo-intense vessel lumen with hyper-intense vessel edges in the vicinity of the anastomosis using MEDIC was a consistent finding in the four examples studied. Further studies are warranted to explore this pattern of contrast behaviour, but initial evidence suggests that it may have the potential to assist with the visualisation of AVF remodelling events. Increased knowledge of the remodelling process of arteriovenous fistulae is required to help improve scientific understanding of AVF failure, and ultimately to facilitate the pre-operative identification of patients whose fistulae may fail to reach maturation. Current guidelines recommend physical examination or US, but these cannot provide the anatomical detail required to increase the knowledge of the remodelling process. The purpose of this work was to explore wider imaging opportunities as an alternative pre-operative assessment to gain extra anatomical information. We utilised two MRI sequences (ToF and MEDIC), alongside US to compare the geometries of arteries and veins in patients with renal failure (n=6) and healthy volunteers (n=10). In a subset of the patients, AVF remodelling was also monitored post-surgery. A comparison was made with US, rather than patient outcome due to the small number of patients recruited into the study, and it was deemed necessary to determine that the modalities were in agreement for vessel diameter measurements before MRI could be considered as a useful tool to measurem these diameters in these patients.

The MEDIC sequence was in agreement with US for all morphological measurements made across the whole group (n=16). However, the ToF sequence underestimated the diameter of the cephalic vein relative to both MEDIC and US. Although the ToF sequence can be useful in detection of stenosis, these results suggest that if the depiction of accurate vessel diameter information is important, then MEDIC would be a better choice. The strong agreement seen between the MEDIC sequence and US confirms that this may be a viable modality for mapping patient vasculature prior to AVF surgery. An additional advantage is that MEDIC was able to depict both the arterial and venous system in the arm in a single session, whereas ToF was unable to depict adequately the venous vessels

in some cases. Importantly, US is recognised by current Kidney Disease Outcomes Quality Initiative (KDOQI) guidelines - thus the agreement between the two modalities also helps to provide an indirect validation of the MEDIC sequence for assessment of vessel morphology. However, it is important to state that the MEDIC sequence is unproven for conventional clinical MR angiography and we would not recommend it for radiological stenosis assessment since formal performance studies (e.g. comparisons with DSA) have not been done. In this research study we have used MEDIC specifically for vessel diameter tracking.

The MEDIC and US morphology measures were generally in good agreement with each other. It is possible that the higher SNR of the 3D MEDIC sequence enabled clearer visualisation of the vessel diameters relative to those of the ToF images. Further, the presence of the higher signal vessel edge detail on MEDIC (clearly seen in the anastamosis regions on the patients) may additionally contribute to the true vessel width not seen on 2D-TOF. From the perspective of US, a possible concern is the fact that tourniquets are routinely used to instigate a level of venous congestion potentially affecting the vein diameters. However, work presented by van Bemmelen et al [178] determined that differences between US diameter measurement values obtained with and without a tourniquet were not significant for either the cephalic or the basilic vein. They concluded that vein diameters are affected by warm water immersion, but not the use of a tourniquet.

The lack of MRI contrast media used in this study completely removes any possibility of nephrogenic systemic fibrosis or contrast induced nephropathy. The MEDIC sequence has the advantage of acquiring the imaging in 3D - thus allowing measurements to be made throughout the length of the vessel, unlike selective measurements from US. Further, the MEDIC does not appear to suffer from through-plane signal losses in quite the same way as ToF. An extension to consider the central vessels would also be feasible as part of a future study. Previous research by Planken et al [136] has reported that contrast enhanced CE-MRI is more accurate than US when comparing diameter measurements made during AVF surgery, but no other similar study has been performed using a NCE-sequence. In our study, the radial artery diameter in the PRF participants as measured by MEDIC was in agreement with literature values measured by US [81]. Vessels used for AVF creation were above the recommended minimum vessel diameters stated in the literature [107, 163, 183].

Our results show that, pre-operatively, the vessels can have a heterogeneous cross-sectional area. The implications of this for AVF maturation requires further study. It is

possible that narrower (but non-stenotic) regions which exist pre-operatively, may be more prone to stenosis development post-AVF creation. Post-operatively, vessels had achieved or were approaching the recommended diameter of 6mm for cannulation. This adds to the sentiment that pre-operative vessel diameters are not the major predictor of maturation that some studies would suggest. Heterogeneous changes in the venous segment of an AVF have been observed before [161, 63]. In this study, we included a pre-operative analysis, enabling us to determine if any areas had undergone a decrease in area. It is possible that the areas of post-operative narrowing observed could be the result of neo-intimal hyperplasia, and that the areas of lower dilation are related to local endothelial dysfunction or abnormal flow patterns. However, this would need to be determined by further studies involving larger cohorts, multiple post-surgical analyses and/or haemodynamic simulations.

Few studies have focussed on the changes that occur in the arterial segment, post AVF creation. Corpataux et al [39] found that the radial artery did not significantly change over a 3-month period. However, we noted large increases in the CSA of the radial arteries studied. The observations noted by us may corroborate the use of MRI for providing additional anatomical data which may form part of the larger picture of AVF-remodelling.

The purpose of this study was not to demonstrate the diagnostic ability of the MRI sequences for AVF stenosis detection, although regions of narrowing were identified in the venous segment of 2 AVFs. One of these participants (PRF3) did develop a stenosis at a later date which was detected by routine US imaging. Further work is needed to determine the pattern of stenosis formation post AVF, and whether MRI may have a role in targeted post-operative stenosis screening.

MRI is rarely used in a clinical setting with ESRD patients due to financial constraints, patient contraindications and concerns over the use of MRI contrast agents. Contraindication rates to MRI imaging of around 10 % in patients with ESRD have been reported previously [47, 134]. Research involving MRI in patients on, or awaiting haemodialysis has also slowed considerably since the occurrence of NSF. Non-contrast enhanced sequences such as black-blood or ToF MRI have been studied previously [161, 63], and the relative limitations of each technique are reported. The MEDIC sequence used in this study (a gradient echo technique with T2* weighting) provides good agreement with US measures, but in common with ToF techniques it also suffers from inflow-related signal losses at the anastomosis. However, the MEDIC sequence does provide good vessel edge detail at the locations in and around the anastomosis, and it is possible that this may prove

to be useful as a surveillance tool to characterise the development of stationary structures such as possible stenosis sites.

This study has several limitations. Firstly, detailed optimisation work was not performed on the ToF sequence to maximise the vessel/background contrast for use at the chosen anatomical location - the vendor default parameters were utilised. The flip angle was slightly lower than one might normally expect, although since we were observing relatively slow flow within the veins the use of a larger flip angle may have resulted in partial saturation of the venous signal. It is difficult to optimise the sequence when both arteries and veins are being observed, although we accept that the negative effect of using a smaller flip angle will be an elevated signal from stationary tissue. Lower flip angles were also necessary in order for the acquisition to stay within acceptable SAR limits on our 3T scanner for the chosen TR. Other experimental complexities included the fact that the anatomy was, by definition, positioned at the periphery of the scanner bore in an area of relatively heterogeneous magnetic field leading to unavoidable regions of inhomogeneous signal intensity. Finally, we were not able to apply fat suppression because doing this would have resulted in a longer sequence TR leading to unacceptably long scan times. The TR was also implemented with consideration of the expected venous flow velocities likely to be present in the healthy volunteers. We estimated that the slowest diastolic blood flow velocities present would be about 10 cm/sec, and using an estimate that the TR would need to be equal or greater than the slice thickness (1.5 mm) divided by the minimum flow velocity (10 cm/sec) to allow full in-flow of unsaturated blood i.e. the TR would need to be a minimum of approximately 15 ms. Our choice of TR 14.5 ms was therefore at the limit in terms of the slowest blood flow velocities likely to be encountered. However since the cardiac cycle was postulated to involve velocities mostly above 10cm/sec, we felt that using this short TR would be the best solution to ensure the shortest scan time - and lower chances of subject motion artefacts. We also used a TE of 5.8ms (the shortest TE to acquire fat/water out of phase images at 3.0T), which was implemented to ensure that the signal from water and fat were out of phase thus helping to minimise stationary background tissue signals a little further.

Other modern MRI pulse sequences are potentially available for non-contrast enhanced visualisation of the vascular system. These include, for example, black blood spin echo sequences (utilising double or triple inversion pulses to null the signal from the vessels), and cardiac gated gradient-echo based sequences that typically use inversion recovery along with a steady state free precession read-out after a systolic inflow period

to allow movement of hyper-intense blood into the imaging plane. Common examples of these are Non Contrast MRA of Arteries and Veins (NATIVE, Siemens), Quiescent Interval Steady State (QISS, Siemens); Balanced Triggered Angiography Non Contrast Enhanced (B-TRANCE, Philips); Inhance Inflow IR (IFIR, GE) and Time Spatial Labeling Inversion Pulse (TimeSLIP, Cannon). These sequences may be useful in the future when it becomes possible to optimise them easily for arteries and veins interchangeably.

In summary, our study has demonstrated that the MEDIC sequence can offer accurate depiction of both the arterial and venous dimensions in healthy volunteers and for patients requiring detailed vessel mapping of AVF sites. This information can be acquired in a single imaging session and does not rely on contrast agent injections, which makes it suitable for imaging wider patient groups with ESRD. This pilot study has demonstrated that non-contrast enhanced MRI can be used to describe vessel morphology and blood flow at anatomical sites associated with AVF surgery - with results comparable to the reference standard of US. Additionally, the pattern of image contrast associated with the MEDIC sequence at the anastomosis site may assist with future studies designed to examine the AVF maturation process without the need for contrast agents. [2]

Notes

[2]This work is currently publish MacDonald, C. J., Gandy, S., Avison, E. C. M., Matthew, S., Ross, R., and Houston, J. G. (2018). Non-contrast MRI methods as a tool for the pre-operative assessment and surveillance of the arterio-venous fistula for haemodialysis. Magnetic Resonance Materials in Physics, Biology and Medicine, 31(6), 735745.

Chapter 5

MRI and CFD Variation

5.1 Introduction

CFD is a well-known tool in engineering, used to assess the flow of fluids *in silico*. This computational method is applied in cardiovascular engineering to predict and analyze blood flow patterns in complex situations, such as cerebral aneurysms, valve prosthesis, stented vessels, and AVFs [117]. Commonly, these studies are performed using 3D geometries segmented from medical images, such as CT and MRI, with or without contrast agent. Patients with renal failure cannot receive Gd-based contrast agents commonly used for MRI [71], so NCE-MRI sequences are used to image blood vessels in these cases. Multiple NCE sequences exist, including the well-known ToF, and newer sequences such as the MEDIC sequence.

The accuracy of CFD in predicting flow dynamics depends on a series of factors including the boundary conditions, turbulence modeling, meshing techniques, researcher experience, and geometrical accuracy. With the increased use of CFD in the assessment and planning of medical devices, the accuracy of the geometries used in simulations is critical to informing design decisions, and assessing disease pathology. Recently, the American Food and Drug Administration (FDA) has begun to consider a good practice to use computational models in the design process of medical devices. The FDA conducted a multi-center study to compare CFD results to an experimental model, and observed a large degree of variability between research groups [167]. Another large study conducted by The International Aneurysm Challenged observed wide variability in CFD results between researchers [177]. Similarly, variations in results have been observed when segmentations from MRI images and CT images are compared, and when imaging of the same participant is undertaken at different time points [172], suggesting that deviations in geometry are an important factor in WSS variation. It is possible different MRI sequences can introduce similar variability into blood vessel segmentation, and, consequently, the CFD analysis.

WSS has been identified as having a significant effect on the development of stenoses in AVFs, and has been studied extensively using CFD. In these studies a number of different MRI sequences have been used in geometry acquisition [29, 63, 50, 161]. Using the AVF as a model for segmentation and CFD, the aim of this study was to examine the differences in geometric and CFD-derived parameters occurring when different MRI sequences (namely MEDIC and ToF) are used for initial imaging.

In order to assess the error introduced by changing MRI sequence, a series of phan-

toms simulating morphological features of the AVF were scanned using both ToF and MEDIC. Geometrical features were quantified along many points to compare MEDIC and ToF, and to profile differences under controlled circumstances. WSS quantities were obtained from patient-specific CFD simulations using geometries from the two MRI sequences. The results from these simulations were compared to demonstrate the differences resulting from a changing in MRI sequence.

5.2 Methods

Section 5.2.1 of the methods section describes those methods which were common for the phantom and the patients. First, the imaging protocol is described, namely the MRI parameters used, and the order of imaging sequences. Second, the segmentation of the vessels, and the process of generating geometrical data is described. Finally, analysis of this geometric data is then described in the context of assessing differences between the two MRI-sequences. Section 5.2.2 describes methods which were unique for the phantom. The phantom manufacture is described, along with the process of analyzing the signal distributions and the effect of the phantom geometry on the signal. Section 5.2.3 describes methods which were unique for the patients . The imaging of the patients is described, followed by the CFD protocol, and the generation/processing of the WSS data.

The patient cohort, and scanning procedure are identical to that of the previous chapter, however to allow the chapter to stand-alone, the procedures are reproduced here.

5.2.1 Common methodology

MRI Imaging

All images were acquired on a 3.0 T PrismaFIT scanner (SIEMENS, Erlangen, Germany) with an 8-channel small flexible array coil. A 2D gradient echo localizer sequence was used for initial visualization of the area of interest. Following this, a 2D ToF MR sequence was applied in an axial oblique orientation and region coverage was maintained at approximately 10 - 15 cm. Imaging parameters used were TR and TE of 14; 5.8 ms respectively, FA of 18°, and a 1.5 mm ST), FOV of 140 mm, with an imaging matrix of 512 x 512 px (no interpolation), and receiver bandwidth of 165 Hz / px. This was followed by a 3D T2* MEDIC sequence (TR/TE: 29 / 16 ms, FA: 30, ST: 1.06 mm (176 slices in the imaging block), FoV: 136 mm, matrix: 512 x 512 px (no interpolation), and receiver bandwidth: 160 Hz / px) over the same area. The MRI sequences had similar voxel sizes, with vox_{ToF} = 0.273 mm and vox_{MEDIC} = 0.266 mm.

Vessel Segmentation

All images were segmented using the sweeping method available on SimVascular (Stanford University, CA, USA), by an experienced cardiovascular engineer with 5+ years experience. Nodes of 3D splines were manually positioned near the center of the vessel for

working as sweeping pathlines. Next, the 3D scans were interpolated onto a sequence of planes perpendicular to the pathlines, where 2D closed-loop splines segmenting the vessel lumen are obtained. Finally, the closed-loop spline segmentations were lofted together to form the 3D tubular models with smooth transition between the segmented planes. These models were exported as finely-spaced stereolithography files for geometry analysis and CFD meshing.

This method has many advantages in contrast to selecting individual voxels, and applying the marching cubes algorithm for obtaining the vessel wall. Voxel segmentation normally require some sort of thresholding, whose accuracy is very sensitive to pixel contrast and noise. In contrast, the 2D closed-loop spline are inherently smooth, the segmentation is not bound to voxel size, and are less sensitive to random noise.

Geometry Analysis

To compare geometric features (primarily model area and spatial projection) between the MRI sequences it was necessary to define an origin point shared between the images. For the phantom models the origin point was defined as the first segment of vessel to enter the phantom box area. For the patient models the origin point was defined as the point at the anastomosis where the vein centerline intersects with the artery centerline for the patient models.

Geometrical features from the segmented models were measured as per published methods [37]. Vessel centrelines in the form of splines were extracted using the maximum inscribed sphere radius method [9]. The distance along the centerlines to the defined origin point s was defined as a topological 1D coordinate system to locate and compare the geometrical features of the vessel. Thus the Cartesian position of any point of the centerline splines was found from the distance along the centerline as $\boldsymbol{\gamma}(s) = (x(s), y(s), z(s))$, where the distance coordinate s was obtained from a line integral of $\boldsymbol{\gamma}$ using any arbitrary parametric coordinate. The vessel cross-sectional area $A = A(s)$ was obtained by integrating slices of the geometrical models perpendicular to the centerline.

Agreement between MEDIC and ToF phantom images was assessed using Bland-Altmann methodology [19]. For each area measurement, the mean and difference between the model areas were calculated. This was done for the full length of the straight phantoms, and for a length of 5 cm centered on the curve center for the curved phantoms.

Measured parameters such as area were also interpreted numerically through the use

of an error metric which was essentially defined as the summed difference of the parameter, divided by its average

$$E_f = \frac{2}{n} \sum_{i=1}^{n} \left| \frac{f_{\mathrm{T},i} - f_{\mathrm{M},i}}{f_{\mathrm{T},i} + f_{\mathrm{M},i}} \right| , \tag{5.1}$$

where n is the number of sampled data, and f_{T} and f_{M} are any quantity f obtained from the ToF and MEDIC images, respectively. E_f takes a value of zero for identical measurements, and increases as the error between the measurements increases.

5.2.2 Phantom Methods

Phantom Preparation

Two phantom setups were manufactured, a straight tube aligned with the MRI scanner z-axis, and a loop swing. The first setup consisted of an open acrylic box, with a couple of supporting structures to a plastic tube with its inlet and outlet points on the opposite walls of the box. Three phantoms of this type were manufactured, with tube diameters (D) 2; 3; 5 mm. The inlet of the tubing on one side wall of the box was connected to a water source and a pulsatile flow pump (Cole Parmer, Masterflex Digital Pump System, Germany). Each phantom was imaged with water flowing at flow rates (Q) of both 0.5; 1.0 L / min. With water density $\rho = 1e^3 kg/m^3$ and dynamic viscosity $\mu = 1e^{-3} Pa/s$, the Reynolds number

$$\mathit{Re} = \frac{4}{\pi} \frac{\rho\, Q}{\mu\, D} \tag{5.2}$$

of the phantoms range in 2,100–10,600, indicating that the flow conditions are either transitional or turbulent.

The second phantom setup consisted of an open acrylic box with both inlet and outlet points of a tube of 5 mm in diameter positioned on the same wall. In this case, three plastic cylinders were glued into the phantom body, two of which acted as supporting structures, and the most distal one as a wrapping post (curve-H), as in figure 5.1. This setup was then repeated with the tubing wrapped around the center cylinders (curve-L), with the effect of reducing the curvature. The effect of this was to change the 'sharpness' of the curve. All phantoms were filled with a small amount of water in order to prime the scanner.

All phantoms were placed into the scanner bore with the center of the phantom aligned with the scanner isocenter.

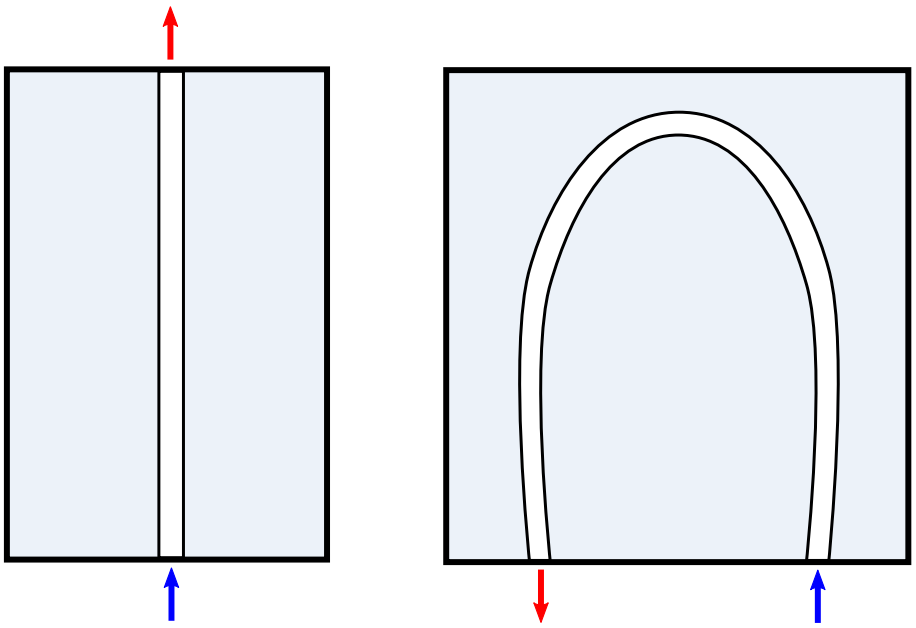

Figure 5.1: Schematic of the straight (left) and curved (right) phantom setups.

Phantom Signal Analysis

In order to profile each imaging sequence, signal intensity measurements were taken using FIJI (figi.sc) [157]. Circular RoIs were used to measure signal from the flowing water, background and stationary water sources in the image. This was done manually for each slice in the series. Signal intensity values were normalized using a min-max normalization algorithm available in scikit-learn [132]. Signal distributions were visualized graphically using the "Seaborn" and "matplotlib" libraries in Python 2.7.

The STL model for the curved phantom was used to assess correlations between the signal intensity to the flow angle relative to the magnetic field direction in the curved phantom. Tangent unit vectors $\hat{\boldsymbol{t}} = \mathrm{d}\boldsymbol{\gamma}/\mathrm{d}s$ were sampled at intervals $\Delta s = 1mm$ along the centerline. The metric

$$\Gamma = \hat{\boldsymbol{t}} \cdot \hat{\boldsymbol{B}}_0 \tag{5.3}$$

defined by the dot product between Γ and the B0 (z-axis) unit vector was calculated for each instance in order to assess the effect of flow-direction. Γ takes values of 0 for flow parallel to B0, and values of 1 for flow perpendicular to B0. Correlations between Γ and the signal intensity were assessed graphically, and with Spearman's correlation statistic. Similarly, correlations between signal intensity and the first spatial derivative of Γ were assessed:

$$\Gamma' = \frac{d\hat{\boldsymbol{t}}}{ds} \cdot \hat{\boldsymbol{B}}_0 \tag{5.4}$$

5.2.3 Patient Methods

Patient Preparation and Imaging

Four patient volunteers with end-stage renal failure who had been referred for AVF creation surgery were recruited into this study from our institution. All volunteers provided informed written consent, and ethical approval was obtained. Two of the patients were indicated for brachio-cephalic AVF creation (PRF1, PRF3) and two were indicated for radio-cephalic AVF creation (PRF2, PRF4). Post AVF surgery, all patients underwent an MRI surveillance session, 17–26 days after surgery.

All volunteers were placed head first and supine into the bore with their arms relaxed by their side. An 8-channel phased array RF coil was placed around the arm of interest. The patient was positioned slightly off-axis in relation to the scanner bore, in order to ensure that the arm (anatomical area of interest) was as near as possible to the innocenter of the magnet. The site of the anastomosis was identified by palpable thrill and was marked by positioning an cod liver oil capsule on the skin adjacent to the site.

Volunteers had one additional sequence added to their protocol. A phase-contrast (PC) MRI was performed, both proximally and distally to the anastomosis, in order to measure the patient-specific flow rates at each branch of the AVF. Imaging parameters used were TR/TE: 99.7 / 7.62 ms, FA: 20°, FOV 100 mm, matrix 192×115, receiver bandwidth: 440 Hz/pixel, VENC: 10 -250 cm s (depending on whether artery or vein) and 16–64 temporal phases over the cardiac cycle. Velocity wave-forms for the blood flow were produced by semi-automated segmentation on Segment (Medviso, Switzerland). The principle of mass conservation is not precisely obeyed throughout the entire pulse time, when the flow rates through all exits of the AVF are summed. This happens for apparently three reasons: instrument error, pulse variability from the times when the proximal and distal scans were made, and blood vessel compliance.

CFD

The CFD meshing and processing were both performed with HELYX v.2.5 (Engys, UK) by an experienced cardiovascular engineer with 5+ years experience. A hexahedra-dominant octree algorithm was used for meshing, where the STL files from the image segmentation were used to define the mesh geometry. The mesh surface was divided by four patches: wall, proximal artery, distal artery, and proximal vein; at which the boundary conditions were applied. Most cells had sides of 250 um, and a inflation prism layer of five cells from

50 - 125 um covered the wall patch. The walls were considered rigid, and the boundary conditions of all exits of the fistula were specified according to the patient-specific flow rate pulses obtained from the PC-MRI scans. In order to avoid the error introduced by the difference between scanning the pulse at the proximal and distal sections, only the flow rates of the proximal section were used, and the distal flow rate was obtained from the the principle of mass conservation. In the case where a distal vein was present, the distal arterial pulse was also used, and the distal vein flow rate was estimated by the principle of mass conservation. The pulses were applied with parabolic velocity profile onto circular patches. Blood was considered a Newtonian fluid with dynamic viscosity $\mu = 3.5e^{-3} Pa\ s$ and density $\rho = 1.06e^{3} kg/m^{3}$, and flow condition was laminar. A large eddy simulation was run to validate the laminar flow hypothesis.

Since it is believed that WSS has significant influence in the patency of AVF by its role in the genesis of intimal hyperplasia [145], both time-averaged WSS

$$\mathit{TAWSS} := \frac{1}{T} \int_{t_0}^{t_0+T} \boldsymbol{\tau}_w \, dt \, , \tag{5.5}$$

and oscillatory shear index (OSI)

$$\mathit{OSI} := \frac{1}{2} \left(1 - \frac{\left\| \int_{t_0}^{t_0+T} \boldsymbol{\tau}_w \, dt \right\|}{\int_{t_0}^{t_0+T} \left\| \boldsymbol{\tau}_w \right\| \, dt} \right) \tag{5.6}$$

were used in the analysis. In Eqs. 5.5 and 5.6, $\boldsymbol{\tau}_w$ is the WSS tensor, T is the pulse period, and t_0 is a point in time. The *OSI* shows whether the $\boldsymbol{\tau}_w \hat{\boldsymbol{n}}$ vector oscillates on a single pulse orientation ($\mathit{OSI} = 0.0$) or oscillating between positive and negative orientations ($\mathit{OSI} = 0.5$) during the pulse period, where $\hat{\boldsymbol{n}}$ is the surface normal vector. Time averaged quantities were measured in the third pulse (i.e., $t_0 \equiv 2T$) of the simulation in order to remove flow-dependent effects.

5.3 Results

5.3.1 Phantom Signal Analysis

The curved phantoms suffered from a signal loss artefact near the curve centre on MEDIC. A number of features of the signal distribution were common to all phantom cases (see figure 5.2):

- The signal from flowing water was similar for both sequences.
- Signal from the water used to prime the scanner was higher on the MEDIC than the ToF.
- Background noise was higher for the ToF image series.

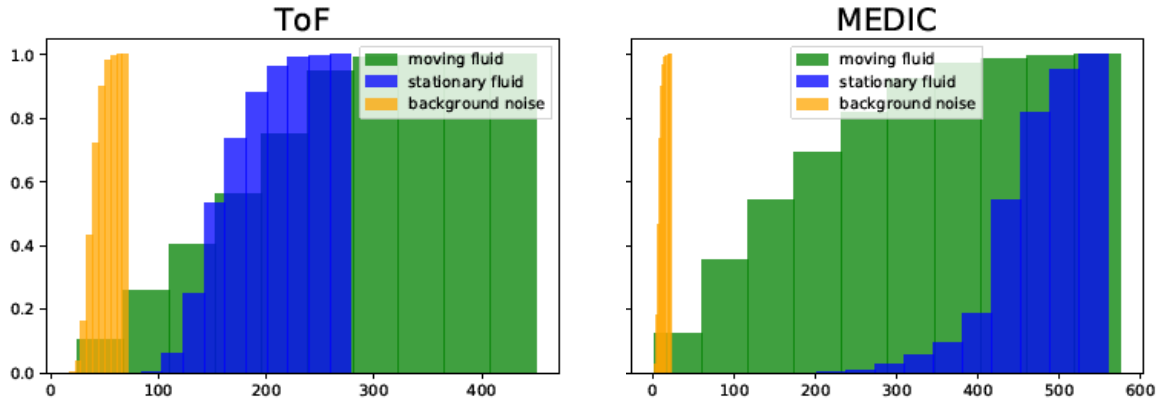

Figure 5.2: Histograms for MEDIC and ToF signal distributions. Noise is lower on MEDIC, and stationary water signal lower on ToF. Flowing water signal is similar for both sequences.

Flow direction data was generated from the 2 curved phantoms as described, and is visualized in figure 5.3. Signal intensity was plotted alongside Γ, and no clear trend was observed. When the signal intensity was plotted alongside the first derivative, Γ', a consistent negative correlation was observed for the MEDIC sequence, but not the ToF. The signal intensity of the MEDIC exhibited a strong negative correlation with Γ', for both phantom geometries, as assessed with Spearman's correlation coefficient (curve-L, $r = -0.89$, $p < 0.05$; curve-H, $r = -0.85$, $p < 0.05$). No such observation was observed consistently on the ToF images. This is visualised in figure 5.4. The cross-sectional area error metric E_A for the phantom can be seen in table 5.1.

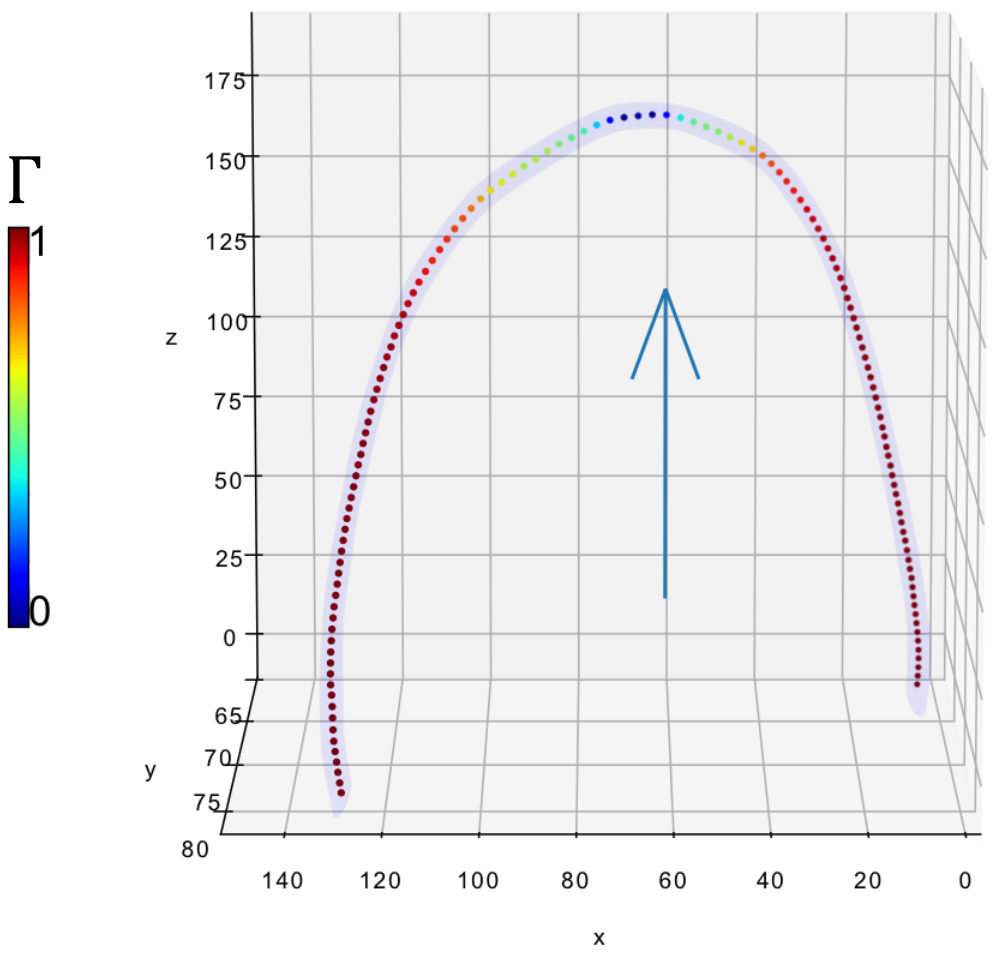

Figure 5.3: 3D visualization of curve-H phantom, showing the sampled points along the vessel colour-coded to the values of Γ. As expected, Γ takes a value of zero when flow is at a right angle to B0 (blue arrow).

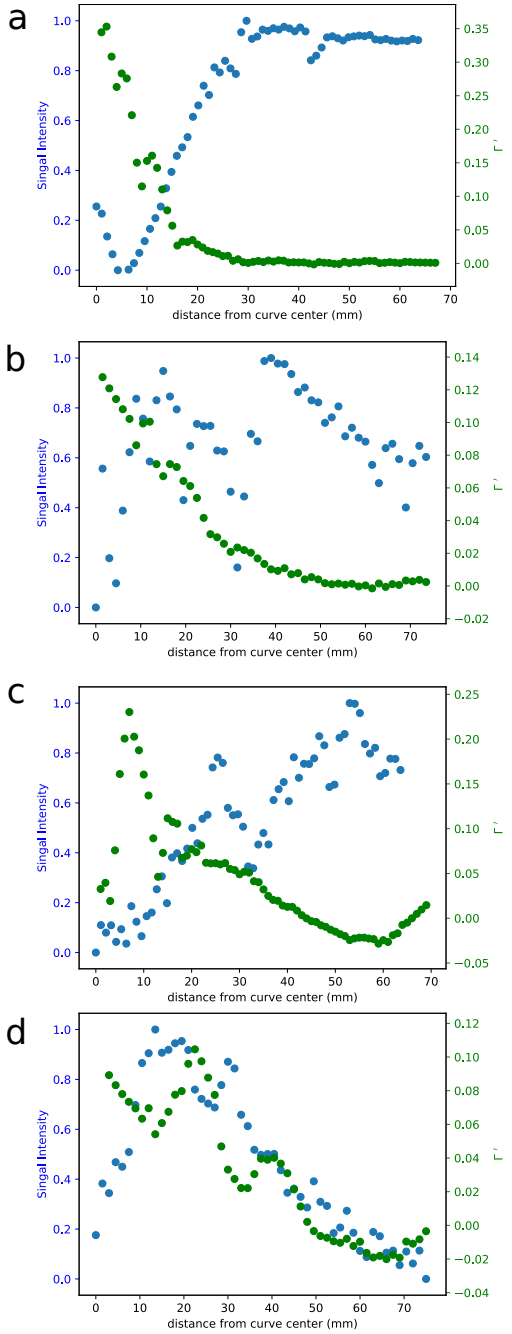

Figure 5.4: Signal dependency on rate of change of flow direction for: (a) curve-H MEDIC, $r = -0.85$, $p < 0.05$; (b) curve-H ToF, $r = -0.85$, $p < 0.05$; (c) curve-L MEDIC, $r = -0.89$, $p < 0.05$; (d) curve-L ToF, $r = 0.47$, $p < 0.05$;

Phantom	E_A (-)	Mean Difference in Diameter (mm)
Straight, 5 mm	0.04	-0.02 $\pm$ 0.12
Straight, 3 mm	0.20	-0.3 $\pm$ 0.14
Straight, 2 mm	0.22	-0.26 $\pm$ 0.16
Curved-H, 5 mm	0.03	0.00 $\pm$ 0.20
Curved-L, 5 mm	0.10	0.20 $\pm$ 0.60

Table 5.1: Error analysis between MEDIC and ToF sequences for phantom STL measurements at a flow rate of 1L / min

Bland-altmann analysis revealed that for the straight phantoms, mean differences were between 0 – 13 % for all cases. Differences between the imaging sequences increased as the vessel radius decreased, but no other clear trend was obvious. Bland-altmann plots for these phantom geometries can be seen in figure 5.5 a. A larger degree of variability was observed when the flow rate was changed as can be visualised in figure 5.5 b.

For the curved phantoms, the largest deviation was seen at the centre of the curve. Bland-altmann plots for these phantom geometries can be seen in figure 5.5 c. Values for E_A, along with mean differences in radii for the phantom cases are reported in Table 5.1.

5.3.2 Patient Analysis

Segmentation using both MEDIC and ToF sequences was possible for all MRI series. Nevertheless, the 3D segmentations of the same patients were not completely identical when comparing the MEDIC and ToF sequences. For example, and in agreement with the previous chapter, the depiction of arterial area was generally larger for the MEDIC, although the lumen area, shape and curvature were variable throughout the length of all vessels studied. The segmentation end points were at different positions, because the FoV of the two sequences were not over a precisely shared volume. Signal drop-out was observed in the area near the anastomosis for both ToF and MEDIC, meaning that segmentation was reliant on interpretation at this point. All these variations impact the flow dynamics in the CFD study.

Area variability directly interferes with the hydrodynamics of internal flows, but the order of this influence also depends on other flow features. By looking at figures 5.7 and 5.8, it is evident that the sequences produce different WSS distributions, but that the main features are in roughly the same area. Depending on the sequence studied, one may draw different conclusions about the distribution of WSS in the artery of patient PRF1, as seen in figure 5.7 a. TAWSS does not show how evenly distributed WSS was during the pulse period, or any other dynamic characteristic of this quantity.

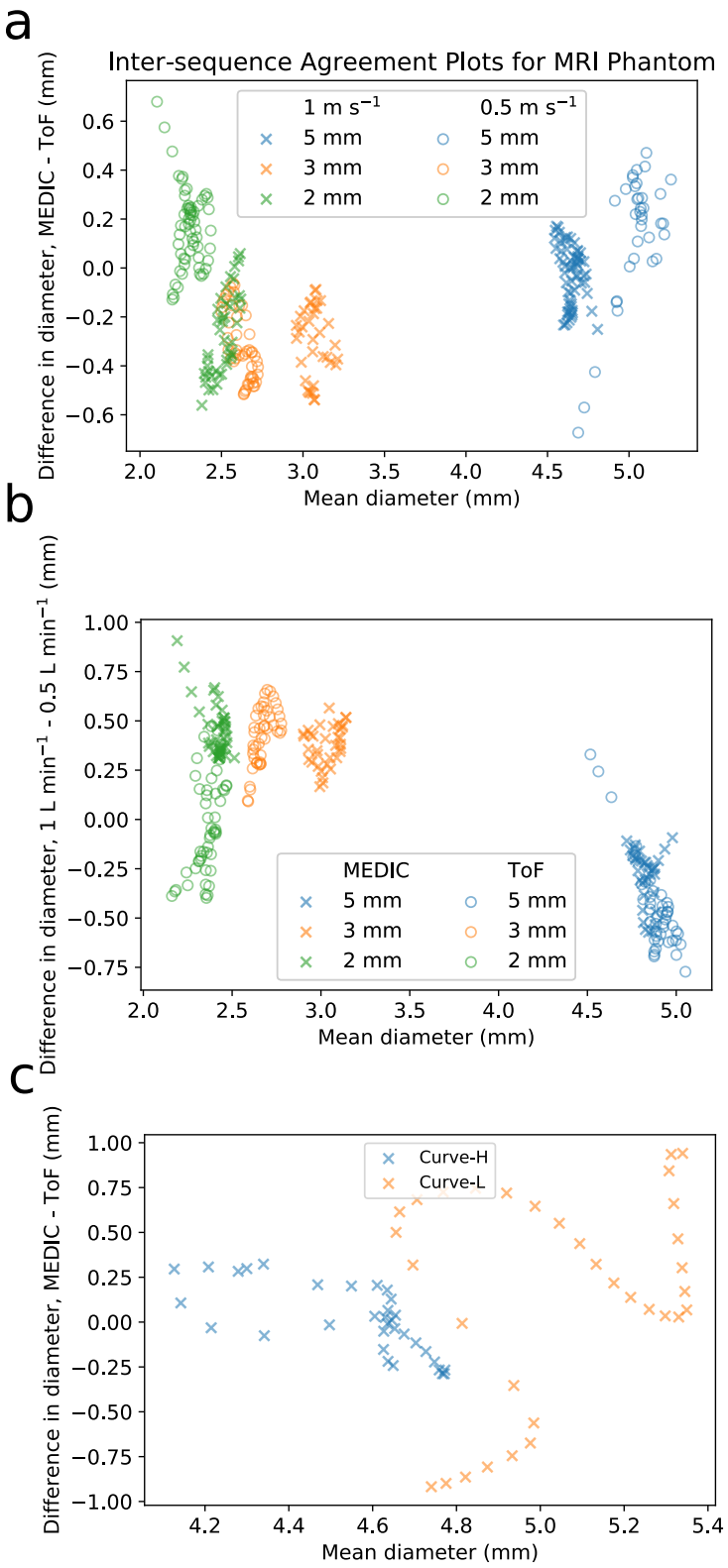

Figure 5.5: Bland-Altmann plots for all phantom cases, showing differences in the measurement on the y-axis, and mean value on the x-axis. (a) Agreement between MEDIC and ToF sequences, (b) Agreement between high and low flow, (c) Agreement between high and low-curve.

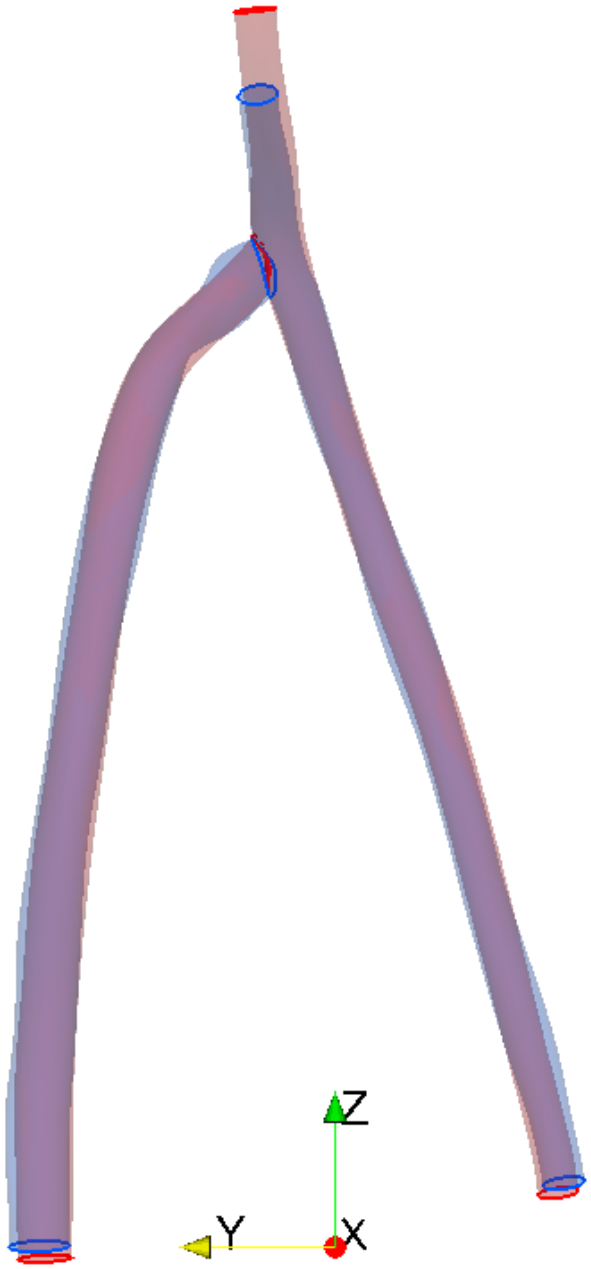

Figure 5.6: Overlapping segmentations of the MEDIC (blue) and ToF (red) images of patient AVF1.

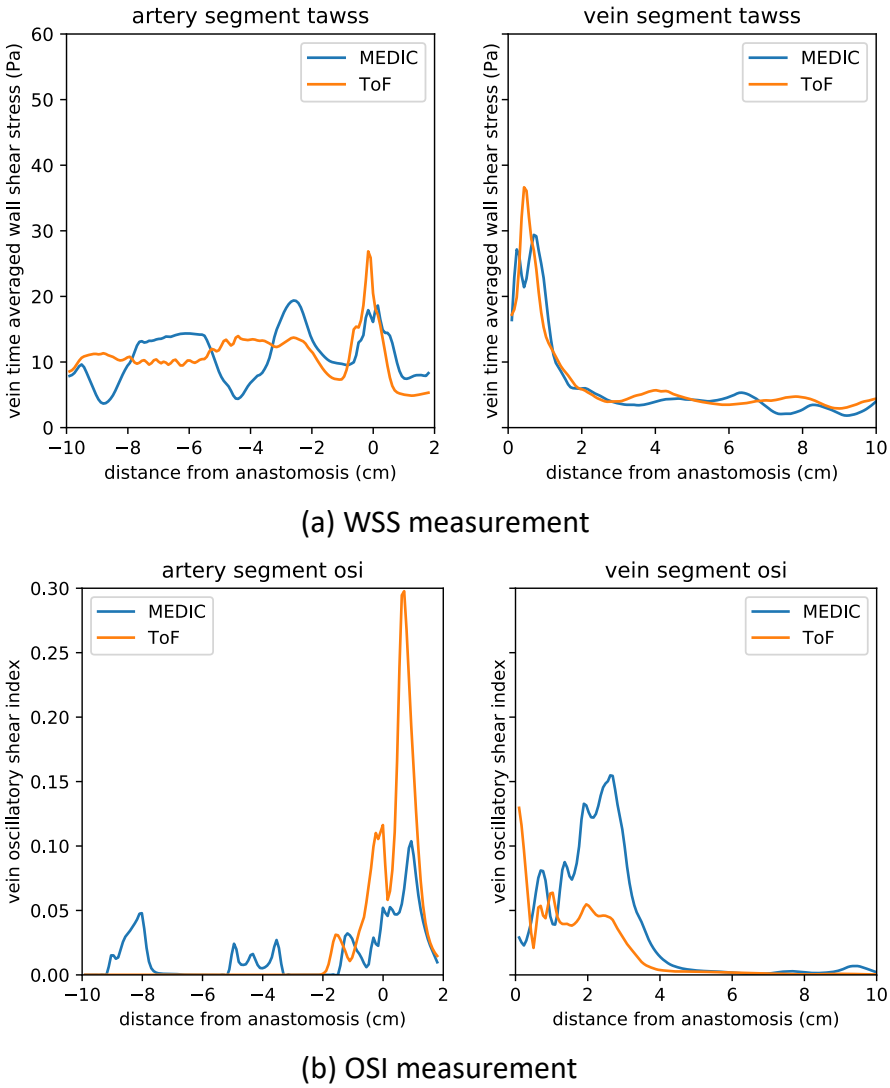

Figure 5.7: (a) WSS measurements and (b) OSI measurements for patient PRF1

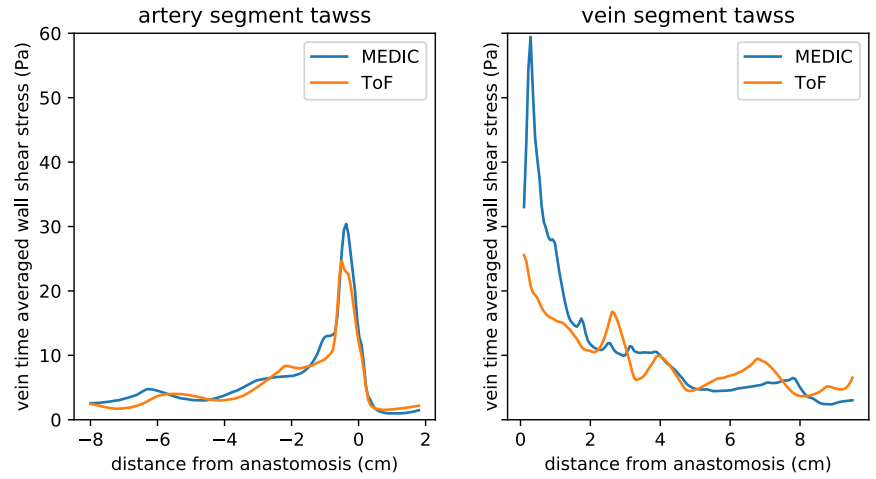

(a) WSS measurement

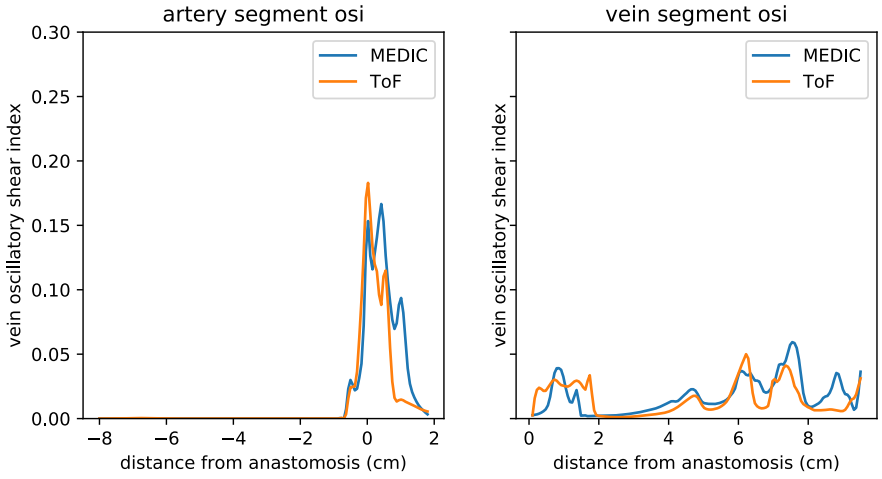

(b) OSI measurement

Figure 5.8: (a) WSS measurements and (b) OSI measurements for patient PRF2

Vessel	Patient	E_A	E_{TAWSS}	E_{OSI}
Artery	PRF1	0.14	0.37	1.39
	PRF2	0.09	0.25	0.73
	PRF3	0.17	0.43	1.29
	PRF4	0.22	0.44	1.23
Vein	PRF1	0.17	0.25	0.84
	PRF2	0.13	0.32	0.61
	PRF3	0.28	0.37	0.65
	PRF4	0.15	0.34	0.97

Table 5.2: Error analysis for patient data.

The OSI shows how strongly the direction of WSS forces changes during the pulse cycle due to flow reversal or varying flow direction. In general, the regions of high OSI do not correlate with regions of high TAWSS. In figure 5.9, it is possible to compare the spatial distribution of OSI for both MEDIC and ToF sequences of patient PRF1. As the only difference in those simulations is the vessel geometry, it is evident how sensitive OSI is to variations in geometry. Intermittent flow separations happen at different positions, such as on the posterior and anterior vessel walls of the MEDIC and ToF sequences respectively. In general, MEDIC showed more regions of high OSI than ToF, because the geometry from higher-resolution MEDIC showed a more variable cross-sectional area than that from ToF. E_f values for all patient cases, including area, WSS and OSI can be seen in table 5.2 and figure 5.10.

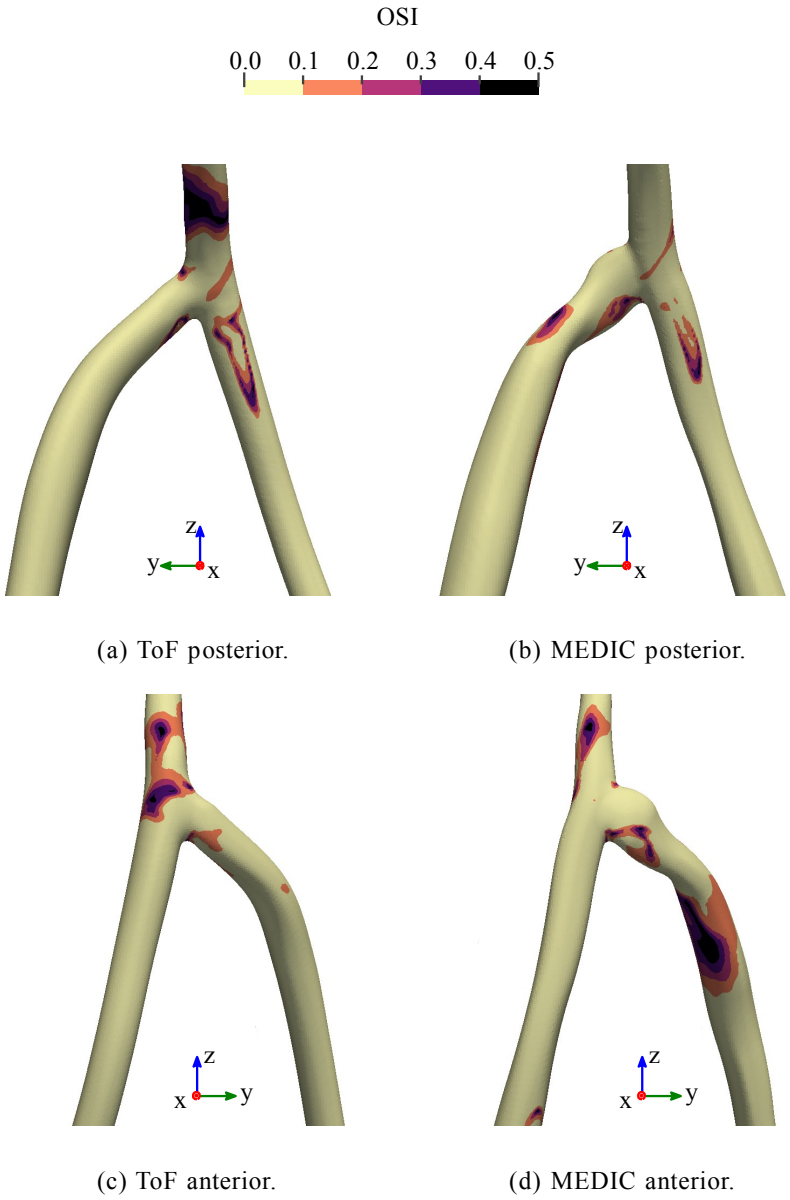

(a) ToF posterior.

(b) MEDIC posterior.

(c) ToF anterior.

(d) MEDIC anterior.

Figure 5.9: Oscillatory shear index of the third pulse of patient PRF1.

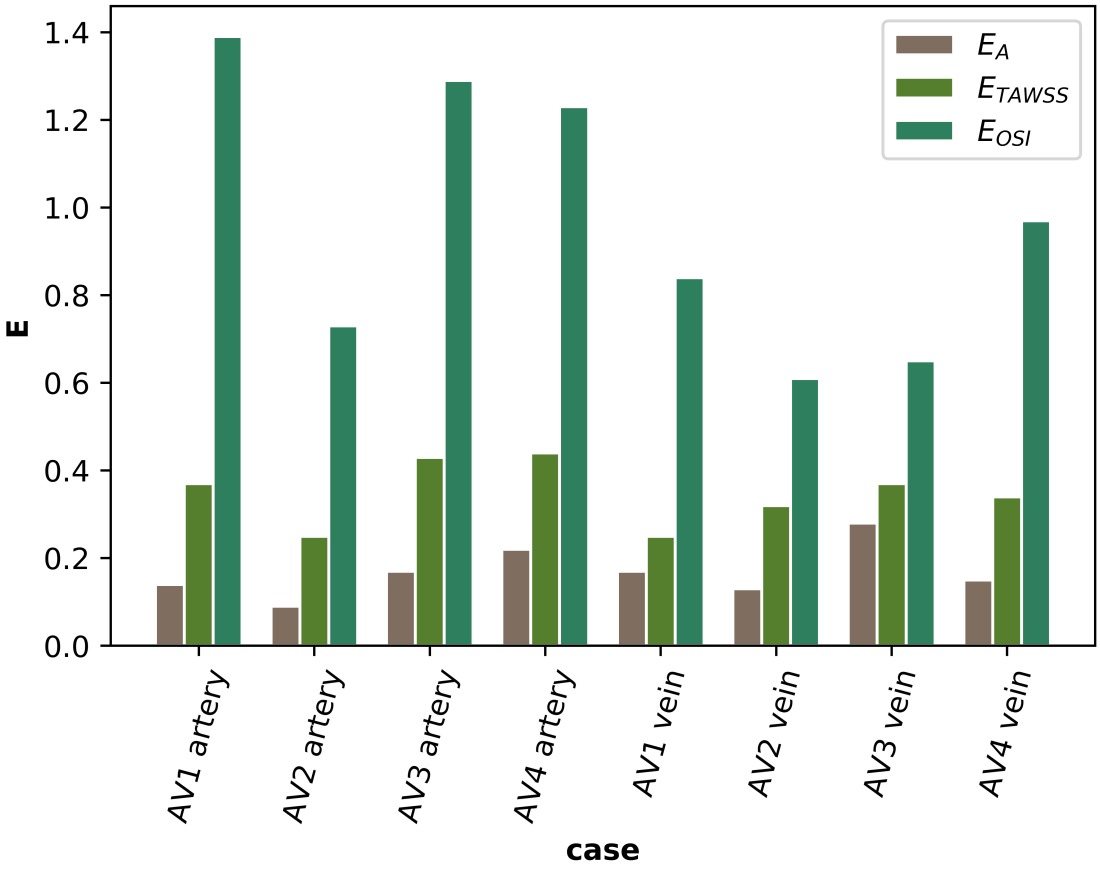

Figure 5.10: Error analysis for patient STL and CFD measurements

5.4 Discussion

In this study we have demonstrated that the choice of MRI sequence can lead to subtle but important differences in segmented model geometry. The differences are of varying magnitude throughout the length of the vessel, suggesting that local effects are causing the observed differences in CFD results. The effect of this area variation caused significant disagreement between the CFD results from the two MRI sequences.

The anastomosis of the AVF introduces challenges for MR imaging, and signal dropout was observed in all the anastomoses studied. Flow recirculation at the anastomosis is reported in simulations of AVFs [49], and it is likely that this effect could be a major cause of spin dephasing [175] resulting in signal loss at the anastomosis. Due to the orientation of the swing site, flow is no longer confined along the z-axis of the B0 field, effectively reducing the velocity of any incoming spins relative to the B0 field, which can be another cause of signal loss. AVF flow has been demonstrated to be turbulent [145], and this is the cause of the signature "thrill" of the AVF. Turbulent flow can undergo spin dephasing causing MR signal heterogeneities, however, turbulent flow was observed in the phantoms, and did not decrease the MRI signal. These problems may act together to lower signal at the swing site and anastomosis, making this region particularly difficult to segment and heavily reliant on operator interpretation, an under-reported aspect in most CFD based studies of AVFs.

The signal distributions of the MEDIC and ToF sequences were analyzed using a series of phantoms, and no difference was observed in the signal intensity profiles from the vessels. However, the ToF sequence was intrinsically more noisy, and the MEDIC produced a higher signal from stationary water used to prime the scanner. An analogous geometry to the curved swing-site segment of the AVF was created using two curved phantoms. Next, the effect of an off-axis flow on signal intensity measurements for the two different curves was assessed. This led to the observation that for the MEDIC sequence, the signal intensity was inversely proportional to the rate of change of the flow-direction (as assessed by Γ'), which may be a reason for the observed signal dropout in the patient images. Signal loss in the curved phantom was not apparent on the ToF images, but both sequences exhibited signal loss on the patient images at the swing-site, suggesting that local flow effects at the anastomosis may have more effect than flow-direction effects as represented by Γ (Eq. 5.4).

The area disagreement E_A between the straight phantoms increased as the tube di-

ameter was decreased, which would be expected as the size of the phantom reduces and approaches the resolution of the scanner. The error was also increased in the curved phantoms as compared with the straight phantoms of the same diameter. Increased disagreement was observed when the flow velocity was changed, which is likely due to the use of "out-of-the-box" sequences. A main benefit of "out-of-the-box" sequences is the ability to image vessels with both high and low-velocity flows in one sitting. However, optimization of the sequences could be performed to find the parameters which give the truest geometric depiction for each flow velocity, or to identify the parameters which reduce the error between the velocities.

These geometric errors propagate into larger errors for parameters derived from CFD. The error metric E_{WSS} was larger than E_A for every patient vessel studied (table 5.2 and Fig. 5.10). Wall shear stress and cross-sectional area are inversely related through a straight vessel, as given by the Darcy-Weisbach equation

$$\tau_w = \frac{f_D}{8}\rho\left(\frac{Q}{A}\right)^2 , \tag{5.7}$$

where f_D is an empirical friction factor, ρ is fluid density, Q is flow rate, and A is area. In the laminar regime, the relation of WSS and area is weaker ($\tau_w \propto A^{-1.5}$), because the friction factor is inversely proportional to the Reynolds number (Re), $f_D = 64/\mathit{Re}$. However, in the turbulent regime, the friction factor does not scale with *Re*, but it rather depends more on the roughness of the vessel, which leads to a second-order inverse relationship between WSS and area ($\tau_w \propto A^{-2}$). Hence, it is important that accurate measurements of vessel area are obtained for accurate estimation of WSS. As OSI is derived from WSS, and depends on more non-linear effects, such as flow separations, E_{OSI} was significantly larger than E_A and E_{WSS} for all cases studied.

This study has a number of limitations. One user segmented the geometries from all MR image sets, so it was not possible to assess variability between operators. This is well covered in the literature and was not the purpose of our study. We did not compare our results to an experimental model, such as in the FDA-sponsored study [167].

No comparison was made with any black-blood sequences or other modalities such as CT, which are also used in to create 3D models for CFD studies of AVFs. Black-blood MRI has been shown to yield good results when measuring vessel parameters for intracranial vessels [10]. Similarly to this work, authors signify that sequence parameters affect wall measurements and sharpness of the vessel wall boarders, which require optimization

prior to commencing the study. Black blood MRA should in theory help with measurements of rapidly flowing or turbulent blood, which may yield low signal due to loss of spins phase-coherence and in-flow effects. Use of black-blood techniques in lumen measurements of AVFs and CFD modeling of wall shear stress has been demonstrated [63]. Another emerging method not considered in this study is 4D flow MRI. In addition to morphological information, the technique has been shown to non-invasively characterize physiological properties, such as velocity, flow volume, wall shear stress, pressure gradients, streamlines and flow path lines in cerebral arteriovenous malformations [31]. 4D flow MRI has been shown to currently underestimate WSS values in intracranial arteries, but with good estimate of WSS distribution when compared to CFD methods [169].

In conclusion, we have demonstrated that different MRI sequences do not give reproducible results when considering CFD studies of AVFs. The results from this study should be taken into consideration when planning patient specific CFD studies. Comparisons with known results from experiment should be performed to fully understand the effect of changing MRI sequence for these studies, and to determine which sequences provide geometries closest to the ground-truth.

Chapter 6

Conclusions, impact, and future work

6.1 Conclusions

The main purpose of this thesis was to identify additional risk-factors for AVF failure in order to aid in clinical decision making, aid in patient counseling towards the risk of failure, and ultimately increase long-term patency. In attempt to identify these factors, blood-borne biomarkers, new ultrasound and MRI methods were studied.

Chapter 2 aimed to determine if pre-operative serological markers, and known risk-factors were predicative of AVF outcome in a single centre, retrospective study, as well as provide up to date patency rates for the local cohort. Pre-operative levels of ferritin and phosphate were identified as independent risk-factors for AVF failure in a small retrospective study. Known risk-factors such as age and gender were not significantly related to the outcome in this study. Diabetes was not identified as a marker during logistic regression modeling, but its inclusion as a variable in the KNN model with ferritin and phosphate categorised over 70 % of test patients correctly. Primary AVF failure in this group was around 30 % at 1-year, in line with literature values. A very high primary assisted patency of over 90 % was observed, demonstrating the benefits of post-operative US surveillance.

Chapter 3 aimed to determine if pre-operative measurements of arterial elasticity and strain could act as novel risk-factors for AVF failure. Neither SWE nor VVI measurements were predicative of the clinical success or failure of the AVF, but both were shown to have potential in peripheral vascular sonography. Alongside this, a marked decrease in arterial stiffness of the brachial artery was observed following AVF creation.

Chapter 4 aimed to determine if 3T MRI was a feasible imaging platform for these patients, and described a small pilot study involving MEDIC MR imaging of AVFs in

order to test the technique in the central vessels in the future. MEDIC showed good agreement with US, an ability to profile the cross-sectional area of the vessels at a high resolution, and lumen edge depiction at the anastomosis, indicating that it may find benefit as part of a patient's workup prior to AVF creation.

Finally, chapter 5 used these same MR images to demonstrate a degree of variability in CFD simulations, indicating that one cannot freely change MRI sequence and expect identical results in these simulations.

6.2 Impact

The inflammatory markers CRP and albumin have been studied previously, with mixed results. This work found no relation between CRP, albumin, and the outcome of the AVF, adding to the negative result literature. The relationship observed between ferritin and phosphate on AVF outcome has not been observed previously. However, one study does not provide a guarantee it will be observed in other cohorts awaiting AVF creation, but should be followed up.

The lack of establishing additional risk-factors from US, using novel markers of arterial stiffness, reflects the difficulty previous researchers have experienced in this field. Arterial stiffness has previously demonstrated no relationship to AVF outcome, although only a handful of studies have searched for such a correlation. This work adds to the body of negative results. However, this work does demonstrate the value of the SWE technique in vascular ultrasound, and adds to the literature supporting its use, particularly in assessments of arterial stiffness. The observation that larger arteries result in larger arterial AVF segments should come as no surprise, and supports previous research that larger vessels should be used for AVF creation where possible.

The demonstrated feasibility of NCE-MRI (re)opens an additional avenue for the study of AVFs. It is possible that the additional spatial resolution and anatomical data may prove useful in clinical planning for certain types of patients, or may prove useful in detecting possible high-risk areas for stenosis development. However, the specific patient groups who may benefit from this imaging are still to be determined.

6.3 Future work

This thesis leaves specific opportunities for further study:

Chapter 2 leaves the possibility of further study regarding serological markers. Further studies should investigate the effect of ferritin and phosphate, determining values to act as cut-off for increased risk, ideally in a prospective study. Following this, work could be performed to determine the mechanisms by which they can cause AVF failure.

Chapter 3 leaves possibilities for following-up the demonstrated US methods. The decreased SWV in the brachial artery is an interesting observation, and histological study to determine what is its cause could be performed. It would also be interesting to determine the effect of varying blood-pressure on SWV measurements for similarly sized arteries. Further trials could be performed using SWE, now that is has been demonstrated to be a robust method. Larger cohort studies, with longer followup of patients awaiting AVF creation could be undertaken to determine if SWE can act as a risk-factor for AVF failure.

Further work could be performed to determine the limits of the VVI package, as previous research indicates that assessment of the carotid seems feasible, but the brachial artery introduced difficulties. The observation of irregular velocity profiles has been observed in previous patient cohorts. However, in this study irregular profiles were observed in healthy volunteers. Further research should assess if this phenomenon is merely a probe movement artefact, or a genuine finding.

Chapter 4 has demonstrated the feasibility of 3T MRI in this cohort. Now that the MEDIC MRI sequence has shown good agreement with US, further clinical study could be undertaken to determine it's ability to detect or predict stenosis. An extension to the central vessels should be considered high priority, in order to obtain a non-invasive imaging modality for use in this patient cohort. Perhaps the use of non-contrast enhanced MRI sequences can restart the MRI based study of AVFs, which has slowed since the association of Gd based contrast with nephrogenic systemic fibrosis.

Previous work in CFD has demonstrated that imaging modalities are not wholly interchangeable, and the work in chapter 6 demonstrates that MRI sequences are not wholly interchangeable. Further work is required to determine which MRI sequence provides geometries closes to the ground truth, and that provide results that agree with experiments. Following this, the magnitude of error compared to experiment could be determined, allowing selection of the best sequence for imaging.

In this typically aged group with a high-level of co-morbidities, a multi-factorial method may be more beneficial. Further research incorporating large cohorts, long followup, and results from imaging, serological biomarkers, and existing comorbidities/risk-factors would be interesting. Such an outlook may be the eventual method which identifies

a reliable risk-factor, eventually allowing primary patency rates to increase.

Bibliography

[1] A. I. Adler, R. J. Stevens, S. E. Manley, R. W. Bilous, C. A. Cull, and R. R. Holman. Development and progression of nephropathy in type 2 diabetes: The United Kingdom Prospective Diabetes Study (UKPDS 64). *Kidney Int.*, 63(1):225–232, 2003.

[2] D. Akin, S. Ozmen, and R. Kaya. A novel factor for primary arteriovenous fistula failure: hyperinsulinism. *Ren. Fail.*, pages 1–4, jul 2016.

[3] A. A. Al-Jaishi, M. J. Oliver, S. M. Thomas, C. E. Lok, J. C. Zhang, A. X. Garg, S. D. Kosa, R. R. Quinn, and L. M. Moist. Patency rates of the arteriovenous fistula for hemodialysis: A systematic review and meta-analysis. *Am. J. Kidney Dis.*, 63(3):464–478, 2014.

[4] H. Alley, C. D. Owens, W. J. Gasper, and S. M. Grenon. Ultrasound assessment of endothelial-dependent flow-mediated vasodilation of the brachial artery in clinical research. *J. Vis. Exp.*, (92):e52070, jan 2014.

[5] M. Allon, T. Greene, L. M. Dember, J. A. Vita, A. K. Cheung, N. M. Hamburg, P. B. Imrey, J. S. Kaufman, M. L. Robbin, Y.-T. Y.-T. Shiu, C. M. Terry, H. R. Umphrey, H. I. Feldman, and Hemodialysis Fistula Maturation Study Group. Association between Preoperative Vascular Function and Postoperative Arteriovenous Fistula Development. *J. Am. Soc. Nephrol.*, may 2016.

[6] M. Allon, M. E. Lockhart, R. Z. Lilly, M. H. Gallichio, C. J. Young, J. Barker, M. H. Deierhoi, and M. L. Robbin. Effect of preoperative sonographic mapping on vascular access outcomes in hemodialysis patients. *Kidney Int.*, 60(5):2013–2020, nov 2001.

[7] J. Almasri, M. Alsawas, M. Mainou, R. A. Mustafa, Z. Wang, K. Woo, D. L. Cull, and M. H. Murad. Outcomes of vascular access for hemodialysis: A systematic review and meta-analysis. *J. Vasc. Surg.*, 64(1):236–243, jul 2016.

[8] H. S. An, J. S. Baek, G. B. Kim, Y. A. Lee, M. K. Song, B. S. Kwon, E. J. Bae, and C. I. Noh. Impaired Vascular Function of the Aorta in Adolescents with Turner Syndrome. *Pediatr. Cardiol.*, 38(1):20–26, 2017.

[9] L. Antiga, B. Ene-Iordache, and A. Remuzzi. Computational geometry for patient-specific reconstruction and meshing of blood vessels from mr and ct angiography. *IEEE transactions on medical imaging*, 22(5):674–684, 2003.

[10] L. Antiga, B. Wasserman, and D. Steinman. On the overestimation of early wall thickening at the carotid bulb by black blood mri, with implications for coronary and vulnerable plaque imaging. *Magnetic Resonance in Medicine*, 60(5):1020–1028, 2008.

[11] S. Aoun, J. Blacher, M. E. Safar, and J. J. Mourad. Diabetes mellitus and renal failure: effects on large artery stiffness. *J. Hum. Hypertens.*, 15(10):693–700, oct 2001.

[12] I. Aragoncillo, S. Abad, S. Caldés, Y. Amézquita, A. Vega, A. Cirugeda, C. Moratilla, J. Ibeas, R. Roca-Tey, C. Fernández, N. Macías, B. Quiroga, A. Blanco, M. Villaverde, C. Ruiz, B. Martín, A. M. Ruiz, J. Ampuero, F. de Alvaro, and J. M. López-Gómez. Adding access blood flow surveillance reduces thrombosis and improves arteriovenous fistula patency: a randomized controlled trial. *J. Vasc. Access*, 18(4):352–358, jul 2017.

[13] A. P. Avolio, S. G. Chen, R. P. Wang, C. L. Zhang, M. F. Li, and M. F. O'Rourke. Effects of aging on changing arterial compliance and left ventricular load in a northern Chinese urban community. *Circulation*, 68(1):50–58, 1983.

[14] P. Bachleda, P. Utikal, M. Kocher, M. Cerna, J. Fialova, and L. Kalinova. Arteriovenous graft for hemodialysis, graft venous anastomosis closure current state of knowledge. Minireview. *Biomed. Pap.*, 159(1):27–30, jun 2015.

[15] K. Bashar, M. Clarke – Moloney, P. E. Burke, E. G. Kavanagh, S. R. Walsh, M. Clarke - Moloney, P. E. Burke, E. G. Kavanagh, and S. R. Walsh. The role

of venous diameter in predicting arteriovenous fistula maturation: When not to expect an AVF to mature according to pre-operative vein diameter measurements? A best evidence topic. *Int. J. Surg.*, 15:95–99, mar 2015.

[16] G. A. Beathard, P. Arnold, J. Jackson, and T. Litchfield. Aggressive treatment of early fistula failure. *Kidney Int.*, 64(4):1487–94, oct 2003.

[17] M. A. Bilgic, H. Yilmaz, A. Bozkurt, H. T. Celik, I. C. Bilgic, O. M. Gurel, I. Kirbas, N. Bavbek, and A. Akcay. Relationship of late arteriovenous fistula stenosis with soluble E-selectin and soluble EPCR in chronic hemodialysis patients with arteriovenous fistula. *Clin. Exp. Nephrol.*, 2015.

[18] J. Blacher, A. P. Guerin, B. Pannier, S. J. Marchais, and G. M. London. Arterial calcifications, arterial stiffness, and cardiovascular risk in end-stage renal disease. *Hypertension*, 38(4):938–942, 2001.

[19] J. M. Bland and D. G. Altman. Statistical methods for assessing agreement between two methods of clinical measurement. *Lancet*, i:307–310, 1986.

[20] A. Bode and J. Tordoir. Vascular access for hemodialysis therapy. *Studies in Computational Intelligence*, 404:235–303, 01 2013.

[21] A. S. Bode, J. Leermakers, J. W. Kroon, P. Brands, R. N. Planken, and J. H. M. Tordoir. Determination of brachial artery stiffness prior to vascular access creation: reproducibility of pulse wave velocity assessment. *Nephrol. Dial. Transplant*, 27(6):2370–6, jun 2012.

[22] K. Bojakowski, M. Dzabic, E. Kurzejamska, G. Styczynski, P. Andziak, Z. Gaciong, C. Söderberg-Nauclér, and P. Religa. A high red blood cell distribution width predicts failure of arteriovenous fistula. *PLoS One*, 7(5):e36482, jan 2012.

[23] A. M. Boyce, T. H. Shawker, S. C. Hill, P. L. Choyke, M. C. Hill, R. James, N. A. Yovetich, M. T. Collins, and R. I. Gafni. Ultrasound is superior to computed tomography for assessment of medullary nephrocalcinosis in hypoparathyroidism. *The Journal of clinical endocrinology and metabolism*, 98(3):989–994, 03 2013.

[24] M. J. Brescia, J. E. Cimino, K. Appel, and B. J. Hurwich. Chronic Hemodialysis Using Venipuncture and a Surgically Created Arteriovenous Fistula. *N. Engl. J. Med.*, 275(20):1089–1092, nov 1966.

[25] M. Briet, P. Boutouyrie, S. Laurent, and G. M. London. Arterial stiffness and pulse pressure in CKD and ESRD. *Kidney Int.*, 82(4):388–400, 2012.

[26] L. D. Browne, K. Bashar, P. Griffin, E. G. Kavanagh, S. R. Walsh, and M. T. Walsh. The Role of Shear Stress in Arteriovenous Fistula Maturation and Failure: A Systematic Review. *PLoS One*, 10(12):e0145795, 2015.

[27] J. D. Cameron, C. J. Bulpitt, E. S. Pinto, and C. Rajkumar. The aging of elastic and muscular arteries: A comparison of diabetic and nondiabetic subjects. *Diabetes Care*, 26(7):2133–2138, 2003.

[28] F. Candan, G. Yildiz, and M. Kayataş. Role of the VEGF 936 gene polymorphism and VEGF-A levels in the late-term arteriovenous fistula thrombosis in patients undergoing hemodialysis. *Int. Urol. Nephrol.*, 46(9):1815–1823, sep 2014.

[29] G. T. Carroll, T. M. McGloughlin, P. E. Burke, M. Egan, F. Wallis, and M. T. Walsh. Wall Shear Stresses Remain Elevated in Mature Arteriovenous Fistulas: A Case Study. *J. Biomech. Eng.*, 133(2):021003, feb 2011.

[30] M. Cecelja and P. Chowienczyk. Role of arterial stiffness in cardiovascular disease. *JRSM Cardiovasc. Dis.*, 1(4):1–10, jul 2012.

[31] W. Chang, M. W. Loecher, Y. Wu, D. B. Niemann, B. Ciske, B. Aagaard-Kienitz, S. Kecskemeti, K. M. Johnson, O. Wieben, C. Mistretta, and P. Turski. Hemodynamic changes in patients with arteriovenous malformations assessed using high-resolution 3D radial phase-contrast MR angiography. *AJNR. Am. J. Neuroradiol.*, 33:1565–72, 2012.

[32] T.-C. Chen, C.-Y. Wang, C.-Y. Hsu, C.-H. Wu, C.-C. Kuo, K.-C. Wang, C.-C. Yang, M.-T. Wu, F.-R. Chuang, and C.-T. Lee. Free p -Cresol Sulfate Is Associated with Survival and Function of Vascular Access in Chronic Hemodialysis Patients. *Kidney Blood Press Res*, 35:583–588, 2012.

[33] K. S. Cheng, C. R. Baker, G. Hamilton, A. P. Hoeks, and A. M. Seifalian. Arterial elastic properties and cardiovascular risk/event. *Eur. J. Vasc. Endovasc. Surg.*, 24(5):383–397, 2002.

[34] S.-C. Chien, C.-Y. Chen, C.-F. Lin, and H.-I. Yeh. Critical appraisal of the role of serum albumin in cardiovascular disease. *Biomark. Res.*, 5(1):31, 2017.

[35] J. A. Chirinos. Arterial stiffness: Basic concepts and measurement techniques. *J. Cardiovasc. Transl. Res.*, 2012.

[36] I. J. Cho, C. Y. Shim, W. I. Yang, S. A. Kim, H. J. Chang, Y. Jang, N. Chung, and J. W. Ha. Assessment of Mechanical Properties of Common Carotid Artery in Takayasu's Arteritis Using Velocity Vector Imaging. *Circ. J.*, 74(7):1465–1470, 2010.

[37] G. Choi, C. P. Cheng, N. M. Wilson, and C. A. Taylor. Methods for quantifying three-dimensional deformation of arteries due to pulsatile and nonpulsatile forces: Implications for the design of stents and stent grafts. *Annals of Biomedical Engineering*, 37(1):14–33, 2009.

[38] C.-Y. Y. Chou, H.-L. L. Kuo, Y.-F. F. Yung, Y.-L. L. Liu, and C.-C. C. Huang. C-reactive protein predicts vascular access thrombosis in hemodialysis patients. *Blood Purif.*, 24(4):342–346, aug 2006.

[39] J.-M. Corpataux, E. Haesler, P. Silacci, H. B. Ris, and D. Hayoz. Low-pressure environment and remodelling of the forearm vein in Brescia-Cimino haemodialysis access. *Nephrol. Dial. Transplant*, 17(6):1057–62, jun 2002.

[40] M. C. Corretti, T. J. Anderson, E. J. Benjamin, D. Celermajer, F. Charbonneau, M. A. Creager, J. Deanfield, H. Drexler, M. Gerhard-Herman, D. Herrington, P. Vallance, J. Vita, and R. Vogel. Guidelines for the ultrasound assessment of endothelial-dependent flow-mediated vasodilation of the brachial artery. *J. Am. Coll. Cardiol.*, 39(2):257–265, jan 2002.

[41] M. Couade, M. Pernot, C. Prada, E. Messas, J. Emmerich, P. Bruneval, A. Criton, M. Fink, and M. Tanter. Quantitative Assessment of Arterial Wall Biomechanical Properties Using Shear Wave Imaging. *Ultrasound Med. Biol.*, 36(10):1662–1676, 2010.

[42] V. CT, R. Klein, M. SE, and K. BK. The risk of cardiovascular disease mortality associated with microalbuminuria and gross proteinuria in persons with older-onset diabetes mellitus. *Arch. Intern. Med.*, 160(8):1093–1100, apr 2000.

[43] L. A. Dageforde, K. A. Harms, I. D. Feurer, and D. Shaffer. Increased minimum vein diameter on preoperative mapping with duplex ultrasound is associated with

arteriovenous fistula maturation and secondary patency. *J. Vasc. Surg.*, 61(1):170–176, jan 2015.

[44] R. Dammers, J. H. M. Tordoir, J. P. Kooman, R. J. T. J. Welten, J. M. M. Hameleers, P. J. E. H. M. Kitslaar, and A. P. G. Hoeks. The effect of flow changes on the arterial system proximal to an arteriovenous fistula for hemodialysis. *Ultrasound Med. Biol.*, 31(10):1327–1333, oct 2005.

[45] L. M. Dember, P. B. Imrey, M.-A. Duess, N. M. Hamburg, B. Larive, M. Radeva, J. Himmelfarb, L. W. Kraiss, J. W. Kusek, P. Roy-Chaudhury, C. M. Terry, M. A. Vazquez, W. Vongpatanasin, G. J. Beck, and J. A. Vita. Vascular Function at Baseline in the Hemodialysis Fistula Maturation Study. *J Am Heart Assoc*, 5(7):e00322, 2016.

[46] B. Dixon. Why don't fistulas mature? *Kidney Int.*, 70(8):1413–1422, oct 2006.

[47] C. Doelman, L. E. Duijm, Y. S. Liem, C. L. Froger, A. V. Tielbeek, A. B. Donkers-van Rossum, P. W. Cuypers, P. Douwes-Draaijer, J. Buth, and H. C. van den Bosch. Stenosis detection in failing hemodialysis access fistulas and grafts: Comparison of color Doppler ultrasonography, contrast-enhanced magnetic resonance angiography, and digital subtraction angiography. *J. Vasc. Surg.*, 42(4):739–746, oct 2005.

[48] M. El-Abbadi and C. M. Giachelli. Arteriosclerosis, calcium phosphate deposition and cardiovascular disease in uremia: current concepts at the bench. *Current Opinion in Nephrology and Hypertension*, 14(6), 2005.

[49] B. Ene-Iordache, L. Cattaneo, G. Dubini, and A. Remuzzi. Effect of anastomosis angle on the localization of disturbed flow in 'side-to-end' fistulae for haemodialysis access. *Nephrol. Dial. Transplant.*, 28(4):997–1005, 2013.

[50] B. Ene-Iordache and A. Remuzzi. Disturbed flow in radial-cephalic arteriovenous fistulae for haemodialysis: Low and oscillating shear stress locates the sites of stenosis. *Nephrol. Dial. Transplant.*, 27(1):358–368, 2012.

[51] A. Farber, P. B. Imrey, T. S. Huber, J. M. Kaufman, L. W. Kraiss, B. Larive, L. Li, and H. I. Feldman. Multiple preoperative and intraoperative factors predict early fistula thrombosis in the Hemodialysis Fistula Maturation Study. *J. Vasc. Surg.*, 63(1):163–170.e6, 2016.

[52] G. Ferraioli, C. Tinelli, B. Dal Bello, M. Zicchetti, G. Filice, and C. Filice. Accuracy of real-time shear wave elastography for assessing liver fibrosis in chronic hepatitis C: A pilot study. *Hepatology*, 56(6):2125–2133, 2012.

[53] C. S. Fox, K. Matsushita, M. Woodward, H. J. Bilo, J. Chalmers, H. J. L. Heerspink, B. J. Lee, R. M. Perkins, P. Rossing, T. Sairenchi, M. Tonelli, J. A. Vassalotti, K. Yamagishi, J. Coresh, P. E. de Jong, C.-P. Wen, and R. G. Nelson. Associations of kidney disease measures with mortality and end-stage renal disease in individuals with and without diabetes: a meta-analysis. *Lancet*, 380(9854):1662–1673, nov 2012.

[54] A.-S. Garnier and M. Briet. Arterial Stiffness and Chronic Kidney Disease. *Pulse*, 3(3-4):229–241, mar 2016.

[55] G. S. Georgiadis, D. G. Charalampidis, C. Argyriou, E. I. Georgakarakos, and M. K. Lazarides. The Necessity for Routine Pre-operative Ultrasound Mapping Before Arteriovenous Fistula Creation: A Meta-analysis. *Eur. J. Vasc. Endovasc. Surg.*, 49(5):600–5, may 2015.

[56] M. Ginsburg, J. M. Lorenz, S. P. Zivin, S. Zangan, and D. Martinez. A practical review of the use of stents for the maintenance of hemodialysis access. *Seminars in interventional radiology*, 32(2):217–224, 06 2015.

[57] A. J. Gonzalez, K. M. Casey, B. J. Drinkwine, and J. S. Weiss. Series of Noncontrast Time-of-Flight Magnetic Resonance Angiographies to Identify Problems with Arteriovenous Fistula Maturation. *Ann. Vasc. Surg.*, 30:93–9, jan 2016.

[58] C. M. Gullion, D. S. Keith, G. A. Nichols, and D. H. Smith. Impact of Comorbidities on Mortality in Managed Care Patients With CKD. *Am. J. Kidney Dis.*, 48(2):212–220, 2006.

[59] N. J. Haddad, S. V. Cleef, and A. K. Agarwal. Central Venous Catheters in Dialysis: The Good, the Bad and the Ugly. *Open Urol. Nephrol. J.*, 1(5):12–18, 2012.

[60] M. Hammes. Importance of the Endothelium in Arteriovenous Fistula Outcomes. *Am. J. Nephrol.*, 60637:426–427, 2016.

[61] A. Han, S.-K. Min, M.-S. Kim, K. W. Joo, J. Kim, J. Ha, J. Lee, and S.-i. Min. A Prospective, Randomized Trial of Routine Duplex Ultrasound Surveillance on

Arteriovenous Fistula Maturation. *Clin. J. Am. Soc. Nephrol.*, 11(10):1817–1824, oct 2016.

[62] S. Harada, M. Yamakido, M. Yalniz, Ç. Özbaşli, J. L. Teruel, G. F. Juarez, R. Marcen, J. Nogueira, J. Ortuño, F. Akçiçek, A. Başçi, K. Yelden, I. Çoker, D. Mees, Y. Taniguchi, N. Yorioka, H. Oda, T. Masaki, and K. Usui. Magnetic Resonance Angiography as a Technique for the Visualization of Hemodialysis Shunts. *Nephron*, 73(1):73–78, 1996.

[63] Y. He, C. M. Terry, C. Nguyen, S. A. Berceli, Y.-T. T. E. Shiu, and A. K. Cheung. Serial analysis of lumen geometry and hemodynamics in human arteriovenous fistula for hemodialysis using magnetic resonance imaging and computational fluid dynamics. *J. Biomech.*, 46(1):165–9, jan 2013.

[64] T. Hod, R. N. DeSilva, B. K. Patibandla, Y. Vin, R. S. Brown, and A. S. Goldfarb-Rumyantzev. Factors predicting failure of AV "fistula first" policy in the elderly. *Hemodial. Int.*, 18(2):507–515, apr 2014.

[65] D. W. Hosmer, T. Hosmer, S. L. E. Cessie, and S. Lemeshow. A COMPARISON OF GOODNESS-OF-FIT TESTS FOR THE LOGISTIC REGRESSION MODEL. *Stat. Med*, 16(May 1995):965–980, 1997.

[66] P. Hovind, L. Tarnow, P. Rossing, M. Graae, I. Torp, C. Binder, and H.-H. Parving. Predictors for the development of microalbuminuria and macroalbuminuria in patients with type 1 diabetes: inception cohort study. *BMJ*, 328(7448):1105, may 2004.

[67] B. Hu, J. Shao, and M. Palta. Pseudo R2 in longistic regression model. *Stat. Sin.*, 16:847–860, 2006.

[68] T. S. Huber, J. W. Carter, R. L. Carter, and J. M. Seeger. Patency of autogenous and polytetrafluoroethylene upper extremity arteriovenous hemodialysis accesses: a systematic review. *J. Vasc. Surg.*, 38(5):1005–11, nov 2003.

[69] M. Jesky, A. Lambert, A. C. Burden, and P. Cockwell. The impact of chronic kidney disease and cardiovascular comorbidity on mortality in a multiethnic population: A retrospective cohort study. *BMJ Open*, 3(12):1–12, 2013.

[70] W. Jin, G. Zhang, H. Liu, H. Zhang, B. Li, and X. Zhu. Non-contrast-enhanced MR angiography for detecting arteriovenous fistula dysfunction in haemodialysis patients. *Clin. Radiol.*, 70(8):852–857, aug 2015.

[71] E. Kanal, A. J. Barkovich, C. Bell, J. P. Borgstede, W. G. Bradley, J. W. Froelich, T. Gilk, J. R. Gimbel, J. Gosbee, E. Kuhni-Kaminski, J. W. Lester, J. Nyenhuis, Y. Parag, D. J. Schaefer, E. A. Sebek-Scoumis, J. Weinreb, L. A. Zaremba, P. Wilcox, L. Lucey, and N. Sass. ACR Guidance Document for Safe MR Practices: 2007. *Am. J. Roentgenol.*, 188(6):1447–1474, jun 2007.

[72] M. A. Kaygin, U. Halici, A. Aydin, O. Dag, D. N. Binici, H. K. Limandal, Ü. Arslan, A. Kiymaz, N. Kahraman, S. Calik, A. I. Savur, and B. Erkut. The relationship between arteriovenous fistula success and inflammation. *Ren. Fail.*, 30(8):20–24, 2013.

[73] J. Kendrick and M. Chonchol. The role of phosphorus in the development and progression of vascular calcification. *American Journal of Kidney Diseases*, 58(5):826 – 834, 2011.

[74] M. F. Kheda, L. E. Brenner, M. J. Patel, J. J. Wynn, J. J. White, L. M. Prisant, S. A. Jones, and W. D. Paulson. Influence of arterial elasticity and vessel dilatation on arteriovenous fistula maturation: a prospective cohort study. *Nephrol. Dial. Transplant*, 25(2):525–31, feb 2010.

[75] H.-H. Kim, Y. H. Choi, S.-H. Suh, J. S. Lee, Y. H. Jung, and Y. H. So. Arteriovenous Graft Modeling and Hemodynamic Interpretation. *Open J. Fluid Dyn.*, 02(04):324–330, 2012.

[76] H.-R. Kim, H.-K. Kim, and D.-J. Oh. Serum osteoprotegerin level is associated with degree of arteriovenous fistula stenosis in patients with hemodialysis. *Clin. Nephrol.*, 80(11):322–327, nov 2013.

[77] K. H. Kim, J. C. Park, H. J. Yoon, N. S. Yoon, Y. J. Hong, H. W. Park, J. H. Kim, Y. Ahn, M. H. Jeong, J. G. Cho, and J. C. Kang. Usefulness of Aortic Strain Analysis by Velocity Vector Imaging as a New Echocardiographic Measure of Arterial Stiffness. *J. Am. Soc. Echocardiogr.*, 22(12):1382–1388, dec 2009.

[78] H. Kitagawa, T. Kishi, R. Saito, S. Tomokazu, K. Noguchi, and N. Sunohara. [MR venography using the 3D-MEDIC (multi echo data imaging combination) sequence

for lower extremities]. *Nihon Hoshasen Gijutsu Gakkai Zasshi*, 64(2):277–285, 2008.

[79] A. Kordzadeh, J. Chung, and Y. P. Panayiotopoulos. Cephalic vein and radial artery diameter in formation of radiocephalic arteriovenous fistula: A systematic review. *J. Vasc. Access*, 16(6):506–511, 2015.

[80] S. Korsheed, M. T. Eldehni, S. G. John, R. J. Fluck, and C. W. McIntyre. Effects of arteriovenous fistula formation on arterial stiffness and cardiovascular performance and function. *Nephrol. Dial. Transplant*, 26(10):3296–302, oct 2011.

[81] E. Korten, I. M. Toonder, Y. C. Schrama, W. C. J. Hop, A. C. van der Ham, and C. H. A. Wittens. Dialysis fistulae patency and preoperative diameter ultrasound measurements. *Eur. J. Vasc. Endovasc. Surg.*, 33(4):467–71, apr 2007.

[82] D. Kruger. Neo-intimal hyperplasia, diabetes and endovascular injury : review article. *Cardiovasc. J. Afr.*, 23(9):507–511, 2012.

[83] D. N. Ku, D. P. Giddens, C. K. Zarins, and S. Glagov. Pulsatile Flow and Atherosclerosis in the Human Carotid Bifurcation Positive Correlation between Plaque Location and Low and Oscillating Shear Stress. *Arter. Thromb Vasc Biol*, 5(3):293–302, 1985.

[84] Y. M. Ku, Y. O. Kim, J. I. Kim, Y. J. Choi, S. A. Yoon, Y. S. Kim, S. W. Song, C. W. Yang, Y. S. Kim, Y. S. Chang, and B. K. Bang. Ultrasonographic measurement of intima-media thickness of radial artery in pre-dialysis uraemic patients: Comparison with histological examination. *Nephrol. Dial. Transplant.*, 21(3):715–720, 2006.

[85] M. Kumwenda, S. Mitra, and C. Reid. CLINICAL PRACTICE GUIDELINE VASCULAR ACCESS FOR HAEMODIALYSIS UK Renal Association 6th Edition. Technical report, 2015.

[86] J. P. Laissy, D. Menegazzo, M. P. Debray, A. Loshkajian, B. Viron, F. Mignon, and E. Schouman-Claeys. Failing arteriovenous hemodialysis fistulas: assessment with magnetic resonance angiography. *Invest. Radiol.*, 34(3):218–24, mar 1999.

[87] T. A. Lang, D. G. Altman Principal, T. Lang Communications, and T. International Director. Basic Statistical Reporting for Articles Published in Biomedical Jour-

nals: The “ Statistical Analyses and Methods in the Published Literature ” or The SAMPL Guidelines “. *Int J Nurs Stud.*, 52(1):5–9, 2015.

[88] K. N. Larson, A. L. Gagnon, M. D. Darling, J. W. Patterson, and T. G. Cropley. Nephrogenic Systemic Fibrosis Manifesting a Decade After Exposure to Gadolinium. *JAMA dermatology*, 151(10):1117–20, oct 2015.

[89] M. Larsson, P. Verbrugghe, M. Smoljkić, J. Verhoeven, B. Heyde, N. Famaey, P. Herijgers, and J. D'hooge. Strain assessment in the carotid artery wall using ultrasound speckle tracking: validation in a sheep model. *Phys. Med. Biol.*, 60(3):1107–23, feb 2015.

[90] M. K. Lazarides, G. S. Georgiadis, G. A. Antoniou, and D. N. Staramos. A meta-analysis of dialysis access outcome in elderly patients. *J. Vasc. Surg.*, 45(2):420–426.e2, 2007.

[91] T. Lee and N. U. Haq. New Developments in Our Understanding of Neointimal Hyperplasia. *Adv. Chronic Kidney Dis.*, 22(6):431–437, 2015.

[92] V. Y.-f. Leung, J. Shen, V. W.-s. Wong, J. Abrigo, G. L.-h. Wong, A. M.-l. Chim, S. H.-t. Chu, A. W.-h. Chan, P. C.-l. Choi, A. T. Ahuja, H. L.-y. Chan, and W. C.-w. Chu. Quantitative Elastography of Liver Fibrosis and Spleen Stiffness in Chronic Hepatitis B Carriers: Comparison of Shear-Wave Elastography and Transient Elastography with Liver Biopsy Correlation. *Radiology*, 269(3):910–918, 2013.

[93] A. S. Levey and J. Coresh. Chronic kidney disease. *Lancet*, 379(9811):165–180, 2012.

[94] G.-Y. Li, Q. He, G. Xu, L. Jia, J. Luo, and Y. Cao. An ultrasound elastography method to determine the local stiffness of arteries with guided circumferential waves. *Journal of Biomechanics*, 51:97–104, 2016.

[95] Z. Li, L. Du, F. Wang, and X. Luo. Assessment of the arterial stiffness in patients with acute ischemic stroke using longitudinal elasticity modulus measurements obtained with Shear Wave Elastography. *Med Ultrason*, 18(2):182–189, 2016.

[96] E. Linden, W. Cai, J. C. He, C. Xue, Z. Li, J. Winston, H. Vlassara, and J. Uribarri. Endothelial dysfunction in patients with chronic kidney disease results from advanced glycation end products (AGE)-mediated inhibition of endothelial nitric

oxide synthase through RAGE activation. *Clin. J. Am. Soc. Nephrol.*, 3(3):691–8, may 2008.

[97] T. Liyanage, T. Ninomiya, V. Jha, B. Neal, H. M. Patrice, I. Okpechi, M. hui Zhao, J. Lv, A. X. Garg, J. Knight, A. Rodgers, M. Gallagher, S. Kotwal, A. Cass, and V. Perkovic. Worldwide access to treatment for end-stage kidney disease: a systematic review. *The Lancet*, 385(9981):1975 – 1982, 2015.

[98] C. Lomonte, F. Casucci, M. Antonelli, B. Giammaria, N. Losurdo, G. Marchio, and C. Basile. Is There a Place for Duplex Screening of the Brachial Artery in the Maturation of Arteriovenous Fistulas? *Semin. Dial.*, 18(3):243–246, jun 2005.

[99] G. M. London, S. J. Marchais, A. P. Guérin, and F. Métivier. Arteriosclerosis, vascular calcifications and cardiovascular disease in uremia. *Current Opinion in Nephrology and Hypertension*, 14(6), 2005.

[100] X. J. Ma, Y. Y. Duan, L. J. Yuan, T. S. Cao, Y. Wang, H. G. Yang, and S. Chen. Quantitative assessment of maternal common carotid artery mechanics using velocity vector imaging in pre-eclampsia. *Eur. J. Obstet. Gynecol. Reprod. Biol.*, 160(1):30–34, 2012.

[101] J. M. MacRae, S. Ahmed, B. Hemmelgarn, Y. Sun, B.-J. Martin, I. Roifman, and T. Anderson. Role of vascular function in predicting arteriovenous fistula outcomes: an observational pilot study. *Can. J. kidney Heal. Dis.*, 2(1):19, jan 2015.

[102] A. Marks. *Outcomes and epidemiology of chronic kidney disease: the first Grampian laboratory outcomes morbidity and mortality study (GLOMMS-I)*. Aberdeen University Press, 2014.

[103] A. Masengu, J. B. Hanko, and A. P. Maxwell. Arterial stiffness and arteriovenous fistula failure of maturation. *J. Vasc. Access*, 17(6):477–482, 2016.

[104] C. R. May, D. T. Eton, K. Boehmer, K. Gallacher, K. Hunt, S. MacDonald, F. S. Mair, C. M. May, V. M. Montori, A. Richardson, A. E. Rogers, and N. Shippee. Rethinking the patient: Using Burden of Treatment Theory to understand the changing dynamics of illness. *BMC Health Serv. Res.*, 14(1):1–11, 2014.

[105] I. D. Maya, J. C. O'Neal, C. J. Young, J. Barker-Finkel, and M. Allon. Outcomes of brachiocephalic fistulas, transposed brachiobasilic fistulas, and upper arm grafts. *Clin. J. Am. Soc. Nephrol.*, 4(1):86–92, jan 2009.

[106] D. G. McGrogan, A. P. Maxwell, A. Z. Khawaja, and N. G. Inston. Current tools for prediction of arteriovenous fistula outcomes. *Clin. Kidney J.*, 8(3):282–289, 2015.

[107] R. R. Mendes, M. A. Farber, W. A. Marston, L. C. Dinwiddie, B. A. Keagy, and S. J. Burnham. Prediction of wrist arteriovenous fistula maturation with preoperative vein mapping with ultrasonography. *J. Vasc. Surg.*, 36(3):460–463, 2002.

[108] D. Menegazzo, J. P. Laissy, A. Dürrbach, M. P. Debray, B. Messin, V. Delmas, F. Mignon, and E. Schouman-Claeys. Hemodialysis access fistula creation: preoperative assessment with MR venography and comparison with conventional venography. *Radiology*, 209(3):723–728, dec 1998.

[109] J. Meng, Z. X. Li, W. Jiang, C. Xu, Y. C. Li, J. Huang, and Q. M. Sun. Relationship of Serum ADMA With pulmonary hypertension in patients on hemodialysis. *Dial. Transplant.*, 39(6):242–246, jun 2010.

[110] E. Messas, M. Pernot, and M. Couade. Arterial wall elasticity: State of the art and future prospects. *Diagn. Interv. Imaging*, 94(5):561–569, 2013.

[111] J. A. Milburn, I. Ford, N. J. Mutch, N. Fluck, and J. Brittenden. Thrombin-Anti-Thrombin Levels and Patency of Arterio-Venous Fistula in Patients Undergoing Haemodialysis Compared to Healthy Volunteers: A Prospective Analysis. *PLoS One*, 2013.

[112] C. D. Miller, M. L. Robbin, and M. Allon. Gender differences in outcomes of arteriovenous fistulas in hemodialysis patients. *Kidney Int.*, 63(1):346–52, jan 2003.

[113] G. F. Mitchell. Effects of central arterial aging on the structure and function of the peripheral vasculature: implications for end-organ damage. *J. Appl. Physiol.*, 105(5):1652–1660, 2008.

[114] G. F. Mitchell, H. Parise, E. J. Benjamin, M. G. Larson, M. J. Keyes, J. A. Vita, R. S. Vasan, and D. Levy. Changes in arterial stiffness and wave reflection with

advancing age in healthy men and women: The Framingham Heart Study. *Hypertension*, 43(6):1239–1245, 2004.

[115] J.-Y. Moon, H. M. Lee, S.-H. Lee, T.-W. Lee, C.-G. Ihm, Y.-I. Jo, S.-W. Han, and S.-G. Shin. Hyperphosphatemia is associated with patency loss of arteriovenous fistula after 1 year of hemodialysis. *Kidney Research and Clinical Practice*, 34(1):41 – 46, 2015.

[116] M. Morena, J. Y. Bosc, I. Jaussent, A. M. Dupuy, N. Terrier, H. Leray-Moragues, J. L. Flavier, F. Maurice, C. Delcourt, J. P. Cristol, and B. Canaud. The role of mineral metabolism and inflammation on dialysis vascular access failure. *J Vasc Access*, 7(2):77–82, Apr-Jun 2006.

[117] P. D. Morris, A. Narracott, H. von Tengg-Kobligk, D. A. Silva Soto, S. Hsiao, A. Lungu, P. Evans, N. W. Bressloff, P. V. Lawford, D. R. Hose, and J. P. Gunn. Computational fluid dynamics modelling in cardiovascular medicine. *Heart*, 102(1):18–28, jan 2016.

[118] S. K. Morton, A. J. Rodríguez, D. R. Morris, A. P. Bhandari, J. V. Moxon, and J. Golledge. A Systematic Review and Meta-Analysis of Circulating Biomarkers Associated with Failure of Arteriovenous Fistulae for Haemodialysis. *PLoS One*, 11(7):e0159963, jul 2016.

[119] J. J. Mourad, X. Girerd, P. Boutouyrie, S. Laurent, M. Safar, and G. London. Increased stiffness of radial artery wall material in end-stage renal disease. *Hypertens.*, 30(6):1425–30, dec 1997.

[120] M. Muller, J. L. Gennisson, T. Deffieux, M. Tanter, and M. Fink. Quantitative Viscoelasticity Mapping of Human Liver Using Supersonic Shear Imaging: Preliminary In Vivo Feasability Study. *Ultrasound Med. Biol.*, 35(2):219–229, 2009.

[121] E. A. Murphy, R. A. Ross, R. G. Jones, S. J. Gandy, N. Aristokleous, M. Salsano, J. R. Weir-McCall, S. Matthew, and J. G. Houston. Imaging in Vascular Access. *Cardiovasc. Eng. Technol.*, 8(3):255–272, sep 2017.

[122] J. Nakata, H. Io, T. Watanabe, Y. Sasaki, Y. Makita, T. Aoki, H. Yanagawa, R. Kanda, and Y. Tomino. Impact of preoperative ultrasonography findings on the patency rate of vascular access in Japanese hemodialysis patients. *Springerplus*, 5(1):462, dec 2016.

[123] A. B. Nayak, A. Luhar, M. Hanudel, B. Gales, T. R. Hall, J. P. Finn, I. B. Salusky, and J. Zaritsky. High-resolution, whole-body vascular imaging with ferumoxytol as an alternative to gadolinium agents in a pediatric chronic kidney disease cohort. *Pediatr. Nephrol.*, 30(3):515–521, 2014.

[124] B. Nikolic. Hemodialysis Fistula Interventions: Diagnostic and Treatment Challenges and Technical Considerations. *Tech. Vasc. Interv. Radiol.*, 2008.

[125] L.-F. Olsson, R. Odselius, E. Ribbe, and J. r. Hegbrant. Evidence of calcium phosphate depositions in stenotic arteriovenous fistulas. *American Journal of Kidney Diseases*, 38(2):377–383, 2019/05/04 2001.

[126] A. Ortiz, Z. A. Massy, D. Fliser, B. Lindholm, A. Wiecek, A. Martínez-Castelao, A. Covic, D. Goldsmith, G. Süleymanlar, G. M. London, and C. Zoccali. Clinical usefulness of novel prognostic biomarkers in patients on hemodialysis. *Nat. Rev. Nephrol.*, 8:141, nov 2011.

[127] A. Otero González, A. Iglesias Forneiro, M. J. Camba Caride, C. Pérez Melón, M. P. Borrajo Prol, E. Novoa Fernández, I. G. Arenas Moncaleano, S. Uribe Moya, and F. Lagoa Labrador. Survival for haemodialysis vs. peritoneal dialysis and technique transference: Experience in Ourense, Spain, from 1976 to 2012. *Nefrologia*, 35(6):562–566, 2015.

[128] C. D. Owens, N. Wake, J. M. Kim, D. Hentschel, M. S. Conte, and A. Schanzer. Endothelial function predicts positive arterial-venous fistula remodeling in subjects with stage IV and V chronic kidney disease. *J. Vasc. Access*, 11(4):329–34, jan 2010.

[129] T. G. Papaioannou and C. Stefanadis. Vascular wall shear stress: basic principles and methods. *Hell. J Cardiol*, 46(1):9–15, 2005.

[130] J. Parmar, M. Aslam, and N. Standfield. Pre-operative Radial Arterial Diameter Predicts Early Failure of Arteriovenous Fistula (AVF) for Haemodialysis. *Eur. J. Vasc. Endovasc. Surg.*, 33(1):113–115, jan 2007.

[131] S. T. Patel, J. Hughes, and J. L. Mills. Failure of arteriovenous fistula maturation: an unintended consequence of exceeding dialysis outcome quality Initiative guidelines for hemodialysis access. *J. Vasc. Surg.*, 38(3):439–45; discussion 445, sep 2003.

[132] F. Pedregosa, G. Varoquaux, A. Gramfort, V. Michel, B. Thirion, O. Grisel, M. Blondel, P. Prettenhofer, R. Weiss, V. Dubourg, J. Vanderplas, A. Passos, D. Cournapeau, M. Brucher, M. Perrot, and É. Duchesnay. Scikit-learn: Machine Learning in Python. *J. Mach. Learn. Res.*, 12:2825–2830, 2012.

[133] J. A. Pietryga, M. D. Little, and M. L. Robbin. Sonography of Arteriovenous Fistulas and Grafts. *Semin. Dial.*, 30(4):309–318, 2017.

[134] C. Pinto, R. Hickey, T. J. Carroll, K. Sato, K. Dill, R. a. Omary, R. Kroeker, O. Simonetti, and J. C. Carr. Time-resolved MR angiography with generalized autocalibrating partially parallel acquisition and time-resolved echo-sharing angiographic technique for hemodialysis arteriovenous fistulas and grafts. *J. Vasc. Interv. Radiol.*, 17(6):1003–9, 2006.

[135] R. L. Pisoni, E. W. Young, D. M. Dykstra, R. N. Greenwood, E. Hecking, B. Gillespie, R. A. Wolfe, D. A. Goodkin, and P. J. Held. Vascular access use in Europe and the United States: results from the DOPPS. *Kidney Int*, 61(0085-2538):305–316, 2002.

[136] N. R. Planken, J. H. Tordoir, L. E. Duijm, H. C. Bosch, F. M. van der Sande, J. P. Kooman, M. W. Haan, T. Leiner, H. C. van den Bosch, F. M. van der Sande, J. P. Kooman, M. W. de Haan, and T. Leiner. Magnetic resonance angiographic assessment of upper extremity vessels prior to vascular access surgery: Feasibility and accuracy. *Eur. Radiol.*, 18(1):158–167, jan 2008.

[137] R. N. Planken, T. Leiner, R. J. Nijenhuis, L. E. Duijm, P. W. Cuypers, P. Douwes-Draaijer, F. M. Van der Sande, A. G. Kessels, and J. H. Tordoir. Contrast-enhanced magnetic resonance angiography findings prior to hemodialysis vascular access creation: a prospective analysis. *J. Vasc. Access*, 9(4):269–277, oct 2008.

[138] M. Podgórski, P. Grzelak, M. Kaczmarska, M. Polguj, M. Łukaszewski, and L. Stefańczyk. Feasibility of two-dimensional speckle tracking in evaluation of arterial stiffness: Comparison with pulse wave velocity and conventional sonographic markers of atherosclerosis. *Vascular*, 26(1):63–69, feb 2018.

[139] S. B. Prenner and J. A. Chirinos. Arterial stiffness in diabetes mellitus, 2015.

[140] C. Purcell, M. Tennant, and J. McGeachie. Neo-intimal hyperplasia in vascular grafts and its implications for autologous arterial grafting. *Ann. R. Coll. Surg. Engl.*, 79(3):164–8, may 1997.

[141] K. B. Quencer and M. Arici. Arteriovenous Fistulas and Their Characteristic Sites of Stenosis. *AJR. Am. J. Roentgenol.*, 205(4):726–34, oct 2015.

[142] D. K. Rajan, S. Bunston, S. Misra, R. Pinto, and C. E. Lok. Dysfunctional Autogenous Hemodialysis Fistulas: Outcomes after Angioplasty—Are There Clinical Predictors of Patency? *Radiology*, 232(2):508–515, 2004.

[143] D. K. Rajan, T. W. I. Clark, N. K. Patel, S. W. Stavropoulos, and M. E. Simons. Prevalence and treatment of cephalic arch stenosis in dysfunctional autogenous hemodialysis fistulas. *J. Vasc. Interv. Radiol.*, 14(5):567–573, may 2003.

[144] K. V. Ramnarine, J. W. Garrard, B. Kanber, S. Nduwayo, T. C. Hartshorne, and T. G. Robinson. Shear wave elastography imaging of carotid plaques: feasible, reproducible and of clinical potential. *Cardiovasc. Ultrasound*, 12(1):49, dec 2014.

[145] A. Remuzzi, M. Bozzetto, and P. Brambilla. Is shear stress the key factor for AVF maturation? *J. Vasc. Access*, 18(Suppl 1):S10–S14, 2017.

[146] a. Remuzzi, B. Ene-Iordache, L. Mosconi, S. Bruno, A. Anghileri, L. Antiga, and G. Remuzzi. Radial artery wall shear stress evaluation in patients with arteriovenous fistula for hemodialysis access. *Biorheology*, 40(1-3):423–430, 2003.

[147] U. renal registry. 20th annual report of the renal association. *Nephron*, 139, 2018.

[148] P. M. Ridker, N. Rifai, L. Rose, J. E. Buring, and N. R. Cook. Comparison of C-Reactive Protein and Low-Density Lipoprotein Cholesterol Levels in the Prediction of First Cardiovascular Events. *N. Engl. J. Med.*, 347(20):1557–1565, nov 2002.

[149] M. Robbin, M. Gallichio, M. Deierhoi, C. Young, T. Weber, and M. Allon. US vascular mapping before hemodialysis access placement. *Radiology*, 217(1):83–88, oct 2000.

[150] M. L. Robbin, T. Greene, A. K. Cheung, M. Allon, S. A. Berceli, J. S. Kaufman, M. Allen, P. B. Imrey, M. K. Radeva, H. R. Umphrey, and C. J. Young. Arteriovenous Fistula Development in the First 6 Weeks after Creation 1. *Radiology*, 000(0):1–10, 2016.

[151] J. A. Rodriguez, L. Armadans, E. Ferrer, A. Olmos, S. Codina, J. Borrellas, and L. Piera. The function of permanent vascular access. *Nephrol. Dial. Transplant.*, pages 402–408, 2000.

[152] P. Rooijens, J. Tordoir, T. Stijnen, J. Burgmans, A. Smet de, and T. Yo. Radiocephalic Wrist Arteriovenous Fistula for Hemodialysis: Meta-analysis Indicates a High Primary Failure Rate. *Eur. J. Vasc. Endovasc. Surg.*, 28(6):583–589, 2004.

[153] T. C. Rothuizen, C. Wong, P. H. A. Quax, A. J. van Zonneveld, T. J. Rabelink, and J. I. Rotmans. Arteriovenous access failure: more than just intimal hyperplasia? *Nephrol. Dial. Transplant*, 28(5):1085–92, may 2013.

[154] P. Sahasrabudhe, T. Dighe, N. Panse, S. Deshpande, A. Jadhav, and S. Londhe. Prospective long-term study of patency and outcomes of 505 arteriovenous fistulas in patients with chronic renal failure: Authors experience and review of literature. *Indian J. Plast. Surg.*, 47(3):362–9, 2013.

[155] W. L. Salzer. Peritoneal dialysis-related peritonitis: challenges and solutions. *Int. J. Nephrol. Renovasc. Dis.*, Volume 11:173–186, jun 2018.

[156] A. F. Schild, E. Perez, E. Gillaspie, C. Seaver, J. Livingstone, and A. Thibonnier. Arteriovenous fistulae vs. arteriovenous grafts: a retrospective review of 1,700 consecutive vascular access cases. *J. Vasc. Access*, 9(4):231–5, 2008.

[157] J. Schindelin, I. Arganda-Carreras, E. Frise, V. Kaynig, M. Longair, T. Pietzsch, S. Preibisch, C. Rueden, S. Saalfeld, B. Schmid, J. Y. Tinevez, D. J. White, V. Hartenstein, K. Eliceiri, P. Tomancak, and A. Cardona. Fiji: An open-source platform for biological-image analysis. *Nat. Methods*, 9(7):676–682, 2012.

[158] J. A. Shakarchi and N. Inston. Early cannulation grafts for haemodialysis: An updated systematic review. *The Journal of Vascular Access*, 20(2):123–127, 2019. PMID: 29843554.

[159] S. Shenoy. Innovative Surgical Approaches to Maximize Arteriovenous Fistula Creation. *Semin. Vasc. Surg.*, 20(3):141–147, 2007.

[160] L. Sibal, S. C. Agarwal, P. D. Home, and R. H. Boger. The Role of Asymmetric Dimethylarginine (ADMA) in Endothelial Dysfunction and Cardiovascular Disease. *Curr. Cardiol. Rev.*, 6(2):82–90, may 2010.

[161] M. Sigovan, V. Rayz, W. Gasper, H. F. Alley, C. D. Owens, and D. Saloner. Vascular Remodeling in Autogenous Arterio-Venous Fistulas by MRI and CFD. *Ann. Biomed. Eng.*, 41(4):657–668, apr 2013.

[162] R. M. Sigrist, J. Liau, A. E. Kaffas, M. C. Chammas, and J. K. Willmann. Ultrasound elastography: Review of techniques and clinical applications. *Theranostics*, 7(5):1303–1329, 2017.

[163] M. B. Silva, Jr, R. W. Hobson II, P. J. Pappas, Z. Jamil, C. T. Araki, M. C. Goldberg, G. Gwertzman, and F. T. Padberg, Jr. A strategy for increasing use of autogenous hemodialysis access procedures: Impact of preoperative noninvasive evaluation. *J. Vasc. Surg.*, 27(2):302–308, feb 1998.

[164] I. S. Song, W. S. Yang, S. B. Kim, J.-h. Lee, T.-w. Kwon, and J. S. Park. Association of plasma fibrinogen concentration with vascular access failure in hemodialysis patients. *Nephrol. Dial. Transplant.*, 14:137–141, 1999.

[165] SRR. Scottish Renal Registry Annual Report. Technical report, 2018.

[166] K. B. Stevenson, E. L. Hannah, C. A. Lowder, M. J. Adcox, R. L. Davidson, M. C. Mallea, N. Narasimhan, and J. P. Wagnild. Epidemiology of hemodialysis vascular access infections from longitudinal infection surveillance data: Predicting the impact of NKF-DOQI clinical practice guidelines for vascular access. *Am. J. Kidney Dis.*, 39(3):549–555, 2002.

[167] S. F. C. Stewart, P. Hariharan, E. G. Paterson, G. W. Burgreen, V. Reddy, S. W. Day, M. Giarra, K. B. Manning, S. Deutsch, M. R. Berman, M. R. Myers, and R. A. Malinauskas. Results of FDA's First Interlaboratory Computational Study of a Nozzle with a Sudden Contraction and Conical Diffuser. *Cardiovasc. Eng. Technol.*, 4(4):374–391, dec 2013.

[168] S. Svedlund and L.-M. Gan. Longitudinal wall motion of the common carotid artery can be assessed by velocity vector imaging. *Clin. Physiol. Funct. Imaging*, 31(1):32–8, jan 2011.

[169] J. Szajer and K. Ho-Shon. A comparison of 4d flow mri-derived wall shear stress with computational fluid dynamics methods for intracranial aneurysms and carotid bifurcations — a review. *Magnetic Resonance Imaging*, 48:62 – 69, 2018.

[170] N. Tessitore, G. Lipari, A. Poli, V. Bedogna, E. Baggio, C. Loschiavo, G. Mansueto, and A. Lupo. Can blood flow surveillance and pre-emptive repair of subclinical stenosis prolong the useful life of arteriovenous fistulae? A randomized controlled study. *Nephrol. Dial. Transplant.*, 19(9):2325–2333, 2004.

[171] D. H. J. Thijssen, M. A. Black, K. E. Pyke, J. Padilla, G. Atkinson, R. A. Harris, B. Parker, M. E. Widlansky, M. E. Tschakovsky, and D. J. Green. Assessment of flow-mediated dilation in humans: a methodological and physiological guideline. *Am. J. Physiol. Heart Circ. Physiol.*, 300(1):H2–12, jan 2011.

[172] J. B. Thomas, J. S. Milner, B. K. Rutt, and D. A. Steinman. Reproducibility of image-based computational fluid dynamics models of the human carotid bifurcation. *Ann. Biomed. Eng.*, 31(2):132–41, feb 2003.

[173] Y. Tomiyama, K. Yoshinaga, S. Fujii, N. Ochi, M. Inoue, M. Nishida, K. Aziki, T. Horie, C. Katoh, and N. Tamaki. Accurate quantitative measurements of brachial artery cross-sectional vascular area and vascular volume elastic modulus using automated oscillometric measurements: Comparison with brachial artery ultrasound. *Hypertens. Res.*, 38(7):478–484, 2015.

[174] M. Tonelli, M. James, N. Wiebe, K. Jindal, and B. Hemmelgarn. Ultrasound Monitoring to Detect Access Stenosis in Hemodialysis Patients: A Systematic Review. *Am. J. Kidney Dis.*, 2008.

[175] J. Tsuruda, D. Saloner, and D. Norman. Artifacts associated with MR neuroangiography. *Am. J. Neuroradiol.*, 13(5):1411–1422, 1992.

[176] L. Turmel-Rodrigues and C. J. Renaud. *Diagnostic and Interventional Radiology of Arteriovenous Accesses for Hemodialysis*. Springer Paris, Paris, 2013.

[177] K. Valen-Sendstad, A. W. Bergersen, Y. Shimogonya, L. Goubergrits, J. Bruening, J. Pallares, S. Cito, S. Piskin, K. Pekkan, A. J. Geers, I. Larrabide, S. Rapaka, V. Mihalef, W. Fu, A. Qiao, K. Jain, S. Roller, K.-A. Mardal, R. Kamakoti, T. Spirka, N. Ashton, A. Revell, N. Aristokleous, J. G. Houston, M. Tsuji, F. Ishida, P. G. Menon, L. D. Browne, S. Broderick, M. Shojima, S. Koizumi, M. Barbour, A. Aliseda, H. G. Morales, T. Lefèvre, S. Hodis, Y. M. Al-Smadi, J. S. Tran, A. L. Marsden, S. Vaippummadhom, G. A. Einstein, A. G. Brown, K. Debus, K. Niizuma, S. Rashad, S.-i. Sugiyama, M. Owais Khan, A. R. Updegrove, S. C. Shad-

den, B. M. W. Cornelissen, C. B. L. M. Majoie, P. Berg, S. Saalfield, K. Kono, and D. A. Steinman. Real-World Variability in the Prediction of Intracranial Aneurysm Wall Shear Stress: The 2015 International Aneurysm CFD Challenge. *Cardiovasc. Eng. Technol.*, 2018.

[178] P. S. Van Bemmelen, P. Kelly, and J. Blebea. Improvement in the visualization of superficial arm veins being evaluated for access and bypass. *J. Vasc. Surg.*, 2005.

[179] J. J. Van Der Heijden-Spek, J. A. Staessen, R. H. Fagard, A. P. Hoeks, H. a. Boudier, L. M. Van Bortel, H. A. Struijker Boudier, and L. M. Van Bortel. Effect of age on brachial artery wall properties differs from the aorta and is gender dependent: A population study. *Hypertension*, 35(2):637–642, 2000.

[180] A. Velasco, C. Ono, K. Nugent, P. Tarwater, and A. Kumar. Ultrasonic evaluation of the radial artery diameter in a local population from Texas. *J. Invasive Cardiol.*, 24(7):339–41, 2012.

[181] B. Waldum-Grevbo, T. Leivestad, A. V. ReisÃter, and I. Os. Impact of initial dialysis modality on mortality: A propensity-matched study. *BMC Nephrol.*, 16(1):1–8, 2015.

[182] A. R. Weale, P. Bevis, W. D. Neary, S. Boyes, J. D. Morgan, P. A. Lear, and D. C. Mitchell. Radiocephalic and brachiocephalic arteriovenous fistula outcomes in the elderly. *J. Vasc. Surg.*, 47(1):144–50, jan 2008.

[183] V. Wong, R. Ward, J. Taylor, S. Selvakumar, T. V. How, and a. Bakran. Factors associated with early failure of arteriovenous fistulae for haemodialysis access. *Eur. J. Vasc. Endovasc. Surg.*, 12(2):207–13, 1996.

[184] C.-C. Wu, S.-C. Wen, C.-W. Yang, S.-Y. Pu, K.-C. Tsai, and J.-W. Chen. Plasma ADMA Predicts Restenosis of Arteriovenous Fistula. *J. Am. Soc. Nephrol.*, 20(1):213–222, 2009.

[185] W. I. Yang, C. Y. Shim, W. D. Bang, C. M. Oh, H. J. Chang, N. Chung, and J. W. Ha. Asynchronous arterial systolic expansion as a marker of vascular aging: Assessment of the carotid artery with velocity vector imaging. *J. Hypertens.*, 29(12):2404–2412, 2011.

[186] M. I. Yilmaz, M. Saglam, K. Caglar, E. Cakir, A. Sonmez, T. Ozgurtas, A. Aydin, T. Eyileten, O. Ozcan, C. Acikel, M. Tasar, G. Genctoy, K. Erbil, A. Vural, and C. Zoccali. The determinants of endothelial dysfunction in CKD: oxidative stress and asymmetric dimethylarginine. *Am. J. Kidney Dis.*, 47(1):42–50, jan 2006.

[187] J. S. Yudkin, C. D. A. Stehouwer, J. J. Emeis, and S. W. Coppack. C-Reactive Protein in Healthy Subjects: Associations With Obesity, Insulin Resistance, and Endothelial Dysfunction. *Arterioscler. Thromb. Vasc. Biol.*, 19(4), 1999.

[188] M. K. Zadeh, S. Mohammadipour, and Z. Omrani. Correlation between CRP and early failure of arteriovenous fistula (AVF). *Med. J. Islam. Repub. Iran*, 2015.

[189] C. K. Zarins, D. P. Giddens, B. K. Bharadvaj, V. S. Sottiurai, R. F. Mabon, S. Glagov, S. Gladov, and S. Glagov. Carotid Bifurcation Atherosclerosis: Quantative Correlation of Plaque Localization with Flow Velocity Profiles and Wall Shear Stress. *Circ. Res.*, 53(4):502–514, oct 1983.

[190] A. Zarjou, V. Jeney, P. Arosio, M. Poli, P. Antal-Szalmás, A. Agarwal, G. Balla, and J. Balla. Ferritin prevents calcification and osteoblastic differentiation of vascular smooth muscle cells. *Journal of the American Society of Nephrology*, 20(6):1254–1263, 2009.

[191] P. Zhang, R. Guo, Z. Li, D. Xiao, L. Ma, P. Huang, and C. Wang. Effect of smoking on common carotid artery wall elasticity evaluated by echo tracking technique. *Ultrasound Med. Biol.*, 40(3):643–9, mar 2014.

Appendix

List of Journal Publications and Conferences Presentations/Posters

Chapter 1

The current state of MR in vascular access imaging

Presentation, UKRC, Manchester, Jun 2017

C Macdonald, R Ross, JG Houston

The current state of MR in vascular access imaging

Poster, VAS, Ljubljana, April 2017

C Macdonald, R Ross, JG Houston

Velocity vector imaging, shear wave elastography and flow mediated dilation as potential predictors of arterio-venous fistula outcome

Poster, SUG, Glasgow, Mar 2017

C Macdonald, R Ross, JG Houston

Chapter 2

Blood-borne markers and medications: Effect on VA outcome

Presentation, VAS, Ljubljana, April 2017

C Macdonald, R Ross, JG Houston

Chapter 3

C. MacDonald, R.Ross, J.G. Houston

Shear wave velocity measurements of the brachial artery in a population with end-stage renal disease

Biomedical Physic and Engineering Express, Aug 2018

https://doi.org/10.1088/2057-1976/aad8a3

SWE and VVI as Predictors of AVF Outcomes: Preliminary Results

Presentation, Institute of Physice and Engineering and Medicine, Epsom Sept 2017

C Macdonald, R Ross, JG Houston

Chapter 4

MRI as a tool for pre and post-operative assessment of arterio-venous fistulas

Plenary Presentation, Sinapse ASM, Edinburgh, Jun 2017

C Macdonald, R Ross, JG Houston

Medic sequence as a non-contrast alterantive in the assessment of the cephalic and basillic veins and the brachial artery.

Poster, SINAPSE ASM, Stirling, Jun 2016

C Macdonald, R Ross, S Matthew, S Gandy, JG Houston

Chapter 5

Experimental assessment of MEDIC and ToF imaging accuracy

Poster, MRA Soc, Glasgow, Aug 2018

C Macdonald, R Hellmuth, L Priba, R Ross, JG Houston

Ethical Approvals

TAyside medical Science Centre
Residency Block Level 3
George Pirie Way
Ninewells Hospital and Medical School
Dundee DD1 9SY

Professor Graeme Houston
Chair of Clinical Imaging
University of Dundee
Clinical Radiology
Centre for Cardiovascular & Lung Biology
Division of Medical Sciences
Ninewells Hospital & Medical School
Dundee DD1 9SY

Date: 20 December 2016
Your Ref:
Our Ref: **DL/14/ES/1074**
Enquiries to: Mrs Diane Leonard
Direct Line: 01382 383871
Email: diane.leonard@nhs.net

Dear Professor Houston

Study title: **Development of hemodynamic solutions in Renal Dialysis Venous Access Failure. ReDVA: A CFD sub study.**
REC reference: **14/ES/1074**
Amendment number: **AM03 (For REC Reference Only)**
Amendment date: **30 November 2016**
IRAS project ID: **162107**

The above amendment was reviewed held on 20 December 2016 by the Sub-Committee in correspondence.

Ethical opinion

The members of the Committee taking part in the review gave a favourable ethical opinion of the amendment on the basis described in the notice of amendment form and supporting documentation.

Approved documents

The documents reviewed and approved at the meeting were:

Document	Version	Date
Notice of Substantial Amendment (non-CTIMP)	AM03	30 November 2016
Other [Changes to original IRAS form]		08 December 2016
Other [Email Clarification]		05 December 2016
Other [Participant Leaflet ReDVA MRI SM Tracked]	1	07 November 2016
Other [Cover email with Summary of Changes]		09 December 2016
Other [NHS REC Form]		12 December 2016
Participant consent form	1.0	07 November 2016
Participant information sheet (PIS) [AVF US PIS Tracked]	1.0	07 November 2016
Research protocol or project proposal	3	07 November 2016

Membership of the Committee

The members of the Committee who took part in the review are listed on the attached sheet.

Working with NHS Care Organisations

Sponsors should ensure that they notify the R&D office for the relevant NHS care organisation of this amendment in line with the terms detailed in the categorisation email issued by the lead nation for the study.

Statement of compliance

The Committee is constituted in accordance with the Governance Arrangements for Research Ethics Committees and complies fully with the Standard Operating Procedures for Research Ethics Committees in the UK.

We are pleased to welcome researchers and R & D staff at our Research Ethics Committee members' training days – see details at http://www.hra.nhs.uk/hra-training/

14/ES/1074:	**Please quote this number on all correspondence**

Yours sincerely

for Dr Robert Rea
Chair

E-mail: eosres.tayside@nhs.net

Enclosures: List of names and professions of members who took part in the review

Copy to: NHS Tayside R&D Office
TASC

East of Scotland Research Ethics Service REC 1

Attendance at Sub-Committee of the REC meeting on 20 December 2016

Committee Members:

Name	Profession	Present	Notes
Dr Robert Rea	Business Development Manager	Yes	Chair
Mrs Katherine Coll	Trial Manager	Yes	

Also in attendance:

Name	Position (or reason for attending)
Mrs Diane Leonard	Assistant Co-ordinator

Information Governance
Maryfield House South
Mains Loan
Dundee
DD4 7BT
01382 740074
Fax Number
www.nhstayside.scot.nhs.uk

Shona Matthew
Research Assistant
Clinical Radiology
Ninewells Hospital
Dundee
DD1 9SY

Date	19 January 2017
Your Ref	
Our Ref	IGTCAL3497
Enquiries to	Mr Joseph Donnelly
Extension	70249
Direct Line	
Email	joseph.donnelly@nhs.net

Dear Shona

CALDICOTT APPROVAL – Nhs Tayside Haemodialysis Patient Data Timeline in the Outcome of Vascular Access Patency

Proposal Sponsor: Prof. Graeme Houston, Consultant Radiologist, NHS Tayside

Data User(s): Shona Matthew, Research Assistant, University of Dundee/NHS Tayside
Dr Rose Ross, Clinical Specialist Sonographer, NHS Tayside
Dr Marco Salsano, Clinical fellow Radiology, NHS Tayside
Dr Drew Henderson, Consultant, Renal Services NHS Tayside
Conor MacDonald, PhD Student, University of Dundee

Caldicott approval is given for you to create patient timelines using anonymised and identifiable data held within the Scottish Renal Registry, interventional radiology and MRI databases, vascular lab databases, HIC databases, the GoDARTS database and eMED. This retrospective data will have been obtained during clinical or research appointments, both pre and post renal failure and pre and post vascular access surgery,as described in your application and supporting information.

It is noted that eMED data will be processed according to existing HIC SOPs and all subsequent data will be anonymised for analysis.

disability confident EMPLOYER

PRINTED ON RECYCLED PAPER

Thank you for your co-operation in providing us with the information requested by us in this process.
Please contact me should any queries arise from the application of this approval.

Yours sincerely

Joe Donnelly

Joe Donnelly
Information Governance Officer – CHI, Caldicott & Data Protection

Copy to: Prof. Graeme Houston, Consultant Radiologist, NHS Tayside
Dr Rose Ross, Clinical Specialist Sonographer, NHS Tayside
Dr Marco Salsano, Clinical fellow Radiology, NHS Tayside
Dr Drew Henderson, Consultant, Renal Services NHS Tayside
Conor MacDonald, PhD Student, University of Dundee